KERNFORSCHUNGSANLAGE JÜLICH GmbH
Institut für Reaktorwerkstoffe

FRACTURE CRITERION FOR BRITTLE MATERIALS BASED ON STATISTICAL CELLS OF FINITE VOLUME

by

H. Cords
G. Kraus
G. Kleist
R. Zimmermann

Jül - Spez - 359
June 1986
ISSN 0343-7639

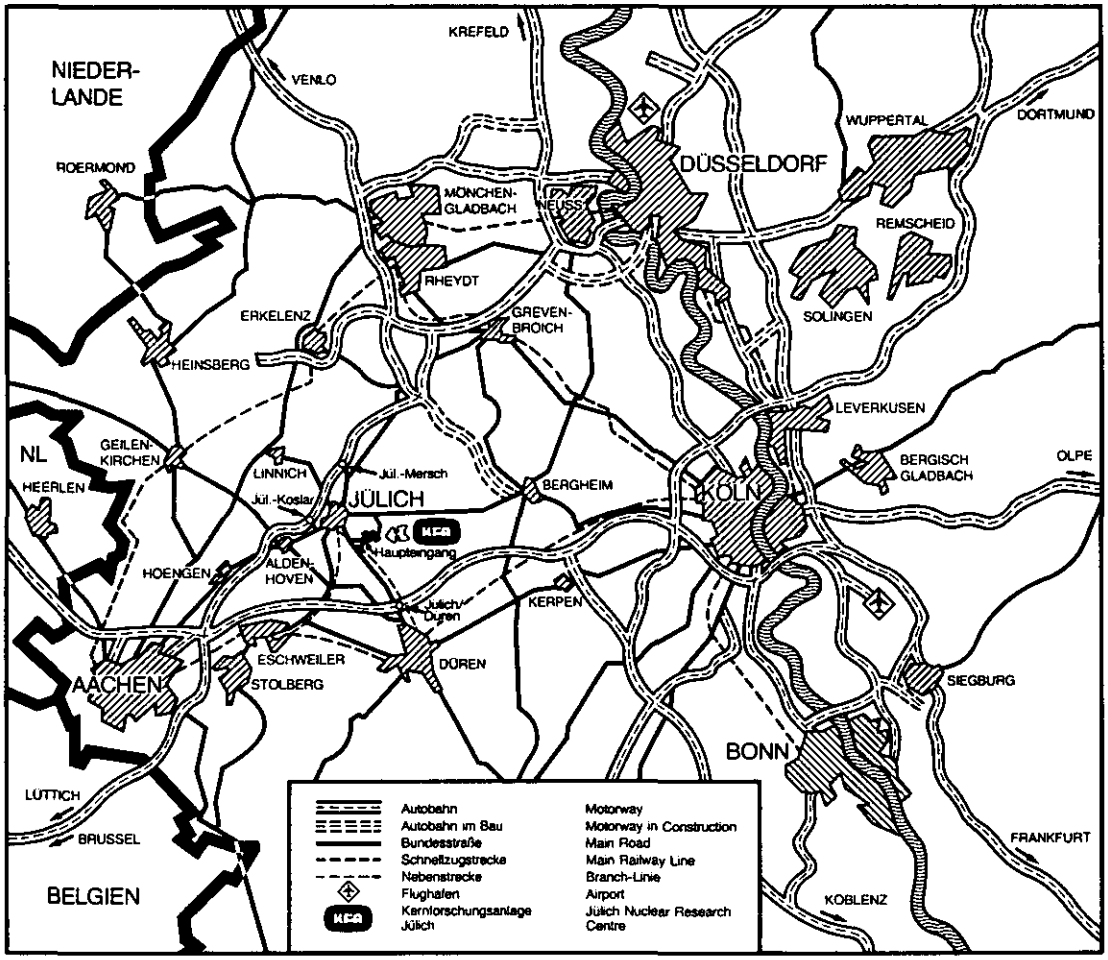

Als Manuskript gedruckt

Spezielle Berichte der Kernforschungsanlage Jülich – Nr. 359

Institut für Reaktorwerkstoffe Jül - Spez - 359

Zu beziehen durch: ZENTRALBIBLIOTHEK der Kernforschungsanlage Jülich GmbH
Postfach 1913 · D-5170 Jülich (Bundesrepublik Deutschland)
Telefon: 02461/610 · Telex: 833556-0 kf d

FRACTURE CRITERION FOR BRITTLE MATERIALS BASED ON FINITE STATISTICAL CELLS

by

H. Cords
G. Kraus*
G. Kleist
R. Zimmermann

*Fa. SIGRI GmbH
D-8901 Meitingen

FRACTURE CRITERION FOR BRITTLE MATERIALS BASED ON STATISTICAL CELLS OF FINITE VOLUME

by
H. Cords
G. Kraus
G. Kleist
R. Zimmermann

ABSTRACT

An analytical consideration of the Weibull Statistical Analysis of brittle materials established the necessity of including one additional material constant for a more comprehensive description of the failure behaviour. The Weibull analysis is restricted to infinitesimal volume elements in consequence of the differential calculus applied. It was found that infinitesimally small elements are in conflict with the basic statistical assumption and that the differential calculus is not needed in fact since nowadays most of the stress analyses are based on finite element calculations, and these are most suitable for a subsequent statistical analysis of strength. The size of a finite statistical cell has been introduced as the third material parameter. It should represent the minimum volume containing all statistical features of the material such as distribution of pores, flaws and grains.

The new approach also contains a unique treatment of failure under multiaxial stresses. The quantity responsible for failure under multiaxial stresses is introduced as a modified strain energy.

Sixteen different tensile specimens including CT-specimens have been investigated experimentally and analyzed with the probabilistic fracture criterion. As a result it can be stated that the failure rates of all types of specimens made from three different grades of graphite are predictable. The accuracy of the prediction is one standard deviation.

BRUCHKRITERIUM FÜR SPRÖDE WERKSTOFFE MIT BERÜCKSICHTIGUNG ENDLICHEN VOLUMENS STATISTISCHER EINHEITEN

von
H. Cords
G. Kraus
G. Kleist
R. Zimmermann

KURZFASSUNG

Das Verfahren von Weibull zur statistischen Analyse von spröden Werkstoffen wurde einer Neubetrachtung unterworfen, die ergab, daß für eine mit dem Experiment besser übereinstimmende Beschreibung des Materialversagens eine zusätzliche Materialkonstante der Theorie beigefügt werden muß. Weibull hatte seine Methode auf infinitesimal kleine Volumenelemente beschränkt, da nur mit dieser Einschränkung die Gleichungen mit Methoden der Infinitesimalrechnung gelöst werden konnten. In der vorliegenden Arbeit wird gezeigt, daß ein infinitesimal kleines Materialvolumen im Widerspruch mit einer in der Statistik üblichen grundlegenden Voraussetzung steht. Heute ist es möglich, die Spannungsanalyse mit einer Finite-Element-Rechnung auszuführen. Die Methode eignet sich vorzüglich für eine nachfolgende statistische Festigkeitsanalyse auf der Basis eines endlichen Volumens. Die Größe des endlichen Elements für statistische Berechnungen wurde als dritter Materialparameter eingeführt. Er ist ein Maß für das kleinste Volumen, das alle statistischen Eigenschaften des Materials enthält wie z.B. die Größenverteilungen von Poren, Rissen und Körnern.

Der Ansatz enthält auch eine neuartige Behandlung des Versagens unter einem mehrachsigen Spannungszustand.

Sechzehn verschiedene Probentypen einschließlich der Bruchmechanikproben vom Typ "Compact Tension" wurden experimentell untersucht und mit dem probabilistischen Versagenskriterium analysiert. Die Untersuchungen, die ausschießlich den Werkstoff Graphit betreffen, ergaben, daß die Versagensraten aller betrachteten Probentypen für drei verschiedene Graphitsorten vorhergesagt werden können. Die Vorhersagegenauigkeit beträgt eine Standardabweichung.

Contents

		page
1.	Introduction	1
2.	The Statistical Subsystems	5
3.	The Probability Distribution	7
4.	The Fracture Criterion	11
5.	Multi-Axial Strength	18
5.1.	Introduction to Problems of Multi-Axial Strength	18
5.2.	Symmetries for Triaxial Strength	21
5.3.	The Predominantely Tensile Region of the Fracture Surface	22
5.4.	Discussion of a Gobal Solution	24
6.	Influence of Size	30
6.1.	The Strength-Density Correlation	30
6.2.	Uniaxial Tensile Strength as a Function of Volume	32
7.	Experiments for Geometrical Independence of the Fracture Criterion	35
7.1.	Geometries and Graphite Grades	35
7.2.	Experimental Results	36
7.3.	Fracture Analysis	36
7.4.	Results of the Fracture Analysis	37
8.	Summary and Conclusion	41
8.1.	Introduction of a Statistical Cell	41
8.2.	Definition of the Statistical Properties as Related to the Cell	42
8.3.	Volume Correction of the Risk Function	44
8.4.	Application of the Theory to Experiments Further Improvements	45
	Appendix	

1. Introduction

The mechanical strength of brittle materials shows considerable scatter due to inhomogeneities inherent in their submicroscopic and microscopic structure. Specifically, the structural components are atoms, crystallites and grains and matrix material as well as different phases or impurities. The atomic binding forces provide the strength, however defects such as vacancies, impurity atoms, stacking faults, dislocations in crystallites and voids, pores and microcracks between and within the grains weaken the structure. Also the anisotropic behaviour of crystallites gives rise to a complex internal stress distribution. Not only the strength is statistically distributed, but other bulk quantities, for example, Young's modulus and density which may be correlated to the strength, show a scatter in the measured data thus indicating that large scale inhomogeneities are present. The great variety of structural constituents introduces the possiblility of several modes of material failure.

Application of the statistical theory means essentially that a system is divided into subsystems which are assumed to be statistically independent of each other. Then, distribution functions have to be assumed empirically to describe the statistical behaviour of the subsystems. The product of probability distributions of the subsystems results in probability function of the total system. Both Weibull /1/ and Freudenthal /2/ applied the statistical theory in this manner. A precise statement identifiying the nature of the statistical subsystems and an unequivocal description of the physical meaning of the term "statistical independence" of the subsystems is not given. In consequence application and interpretation of this method are at least confusing.

There is a simple reason why the size of the subsystem is of prime importance. In the present case the subsystems are

obtained by subdivision of a piece of a material with a volume V into sections with a volume ΔV. The parts have a surface area in common through which an interaction is possible. Each interaction implies statistical dependence of the subsystems. The surface to volume ratio of the subsystems should be chosen as small as possible favouring large subsystems. On the other hand it is advantageous to use volumes as small as possible. The infinitesimally small elements of volume are not possible because not only the interaction through the surface would be greatest but also the subsystem which contains no inhomogeneities has lost its statistical meaning so that no basic probability distribution can be defined. Thus the volume has to be of finite dimensions and its size should be rigorously defined.

In literature particularly in the paper of Freudenthal /2/ the finite size of the volume which should include a number of inhomogeneities is discussed. Nevertheless in applications in any case the differential and integral calculus is used, for instance, in calculating the total risk. In this way, an infinitesimally small element of volume is advocated and the problem of defining the size of a finite element is circumvented. The line of reasoning used to justify the differential calculus starts with the stress calculation. The theory of elasticity is formulated as a set of differential equations. As a prerequisite of stress calculation one has to assume that the material is homogeneous. As far as the stress calculation is concerned the assumed homogeneity does not lead to serious implications except in one case. Neuber /3/ pointed out that considering an inhomogeneous material the stresses at reentrant corners would not be as large as calculated.

He suggests that a finite difference procedure should be applied, especially in connection with stress concentrations in order to have realistic stress values.

The obvious advantages of the differential calculus have then been expanded towards the statistical analysis of strength although the procedure is basically incompatible with the requirements of the statistical theory, as the theory of elasticity requires a homogeneous material while the statistical theory refers to exactly the opposite, an inhomogeneous material.

In the present publication we adopt the following point of view: The stress calculations should be performed under the assumption of homogeneity. In the subsequent analysis of strength the resultant stresses have to be critically assessed:

- Firstly, the calculated stresses are meaningless if referred to the stressed body at a local position. Due to inhomogeneities e.g. flaws, microcracks etc., the local stress distribution is, in fact, a superposition of closely spaced stress concentrations. The calculated value can be considered at best to be an average value of the locally fluctuating stress distribution.

- Secondly, there are inelastic processes which proceed at a relatively low level of stress and will increase at higher stress levels. The material is strained without a corresponding linear increase in stress due to the generation of additional, subcritical microcracks. Thus the stress distribution within a brittle material is smoothed.

Consequently, considering the lack of significance of the stress peaks within a finite statistical cell the elastic stresses should be averaged locally in order to simulate the smoothing effect of the inelastic processes. The characteristic spread of the local mean can be chosen to be of the same size as the element of volume used for the statistical analysis.

Taking into account the inelastic effects, we refer to papers by Kraus and Semmler /4/ and Rödig et al /5/. These authors support the statement that in graphite elastic energy is dissipated at a level of stress which is low compared to the ultimate tensile strength. Performing the averaging process means in essence applying the ideas of Neuber /3/.

The statistical fracture criterion based on a finite element partitioning of the structure has been described by the authors in two earlier papers /6, 7/. The present publication is in support of the earlier work. New aspects and new experiments are described, in particular, the influence of multiaxial stresses and the failure probability are studied.

2. The Statistical Subsystems

It has been already explained that a finite element of volume has to be chosen as small as possible to resolve the strength properties of relatively small structural components, and at the same time as large as possible to satisfy the condition of statistical independence. Statistical independence means that each element will fracture independently of other elements. It is not permissible, for instance, that one stiffer element carries the load of a neighbouring element. The elements have to be chosen sufficiently large to ensure that neighbouring elements have equal stiffness on the average. An ideal example in this respect is the chain. The subsystem i.e. the links of the chain are shaped and stressed identically. The links are in point contact excluding interactions. After determining the distribution function for fracture of the links the distribution function for the chain can be calculated.

In a continuous body it is difficult, to define microscopic subsystems by the size of a grain or selected components of the matrix. The problem is to find a distribution function for the occurrence of cleavage or intergranular fracture. If both types of subsystems are anticipated to contribute simultaneously, the relative abundances have to be found. The distribution functions should refer to the stresses obtained by calculation using the theory of elasticity together with the assumption for homogeneity.
Such a procedure cannot be devised without a considerable amount of additional research. Therefore the element of volume should be large enough to contain all possible statistical events which can be envisaged. It has to include both grains and matrix material in consequence of the two effects mentioned. Furthermore, if stress concentrations at flaws play an important role in the fracture mechanism, the subsystem should include a spectrum of flaws being representative in size and shape for the material in general. In

other words the element of volume has to be sufficiently large to contain a piece of material from which bulk properties such as density, Young's modulus and strength can be deduced experimentally. For a more specific definition of the size it is referred to in section 4.

In the earlier work on graphite /6, 7/ it was found that the element of volume should have a typical size of 1 cm^3 for a graphite being manufactured from grains with an average size of 1 mm. The shape of the element should be as compact as possible to ensure independence. For compactness, a spherical shape has advantages but for complete dissection of a large specimen, a cube is more appropriate.

3. The Probability Distribution

Freudenthal /2/ uses the probability of non-occurence of an event as

$$P_i = \exp\left[-(c \cdot \Delta V)\right] \qquad (1)$$

Weibull /1/ employed the empirical function $c = \frac{1}{V} \cdot (\sigma/\sigma_{ut})^m$ where σ is the calculated stress which has to be applied locally. σ_{ut} can be any value of stress to make the exponential term dimensionless. It is convenient to choose the ultimate tensile strength for σ_{ut}. Similarly, the constant V shall compensate the dimensions of the element of volume introduced by ΔV such that the exponent in Eq.(1) is a number. As long as the stress distribution σ is uniaxial and homogeneous, the basic distribution function P can be applied when considering a finite element in volume. To include the properties of a function σ varying with space coordinates, one has to consider differences in stress within one statistical cell. As has been shown the calculated stresses do not represent the true stress distribution due to the assumed homogeneity of the material. At best the stresses can be regarded as an average stress over a representative volume. For the determination of an integral quantity responsible for the failure behaviour of one element of volume which is stressed with a gradient, it does not seem unreasonable to use an average value of stress. The averaging process not only provides an integral value of risk for the given load conditions of the element but also smoothes the stress distribution allowing for inelastic effects /3/.

The problem of defining an integral quantity for given load conditions emerges again when multi-axial stresses are considered. The assumption concerning the probability distribution function made so far have been developed in order to meet the experimental results. Weibull's heuristic assumption in Eq.(1) that the risk $\frac{1}{V} \cdot (\sigma/\sigma_{ut})^m \cdot \Delta V$ is proportional to the m-th power of the stresses

has been tested successfully. The method of executing a so-called Weibull plot is well established, and it would be of great disadvantage to ignore this fact. Therefore a quantity responsible for the fracture of an element under multi-axial stress should include the features already discussed for uniaxial and constant stresses. The prevailing objective to render a direct description of experimental results yields to an approach which is different from the function Weibull adopted for multi-axial stresses. He only allowed tensile, normal stresses to contribute to fracture. The assumption is in agreement with some experiments performed to determine the fracture surface /8/.

For a practicable fracture criterion, it seems however more promising to rely directly upon a phenomenological description of the measured fracture surface. A detailed mathematical description of the fracture surface is given in Section 5, where a quantity k^2 is defined. According to more recent review articles (Brocklehurst /9/ and Dukes /8/) the modified maximum strain energy provides a reasonably good description of most of the experimental data. This has been taken as the basis of the new phenomenological description of the fracture surface. The quantity k^2 equals the value k_c^2 for critical configurations within the space spanned by the three principal stresses. Special points in that space are the intersections of the surface with the principal axes. At these locations and for tensile stresses the critical value k_c is in fact identical with σ_{ut} (for simplicity it is assumed, that the value for the modulus of elasticity E = 1).

It follows:

$$P_i = \exp\left[- \left(\frac{\bar{k}_i^2}{k_c^2} \right)^{\frac{m}{2}} \cdot \ln 2 \right] \qquad (2)$$

with

$$\overline{k^2} = \frac{1}{\Delta V} \cdot \int_{\Delta V} k^2 \, d\, V \qquad (2a)$$

In Eq.(2) there is no explicit dependency on volume as V was chosen to be equal to ΔV. It was also assumed that the size of each volume is ΔV. This assumption is not necessary but the equations become simpler. The ln2-term ensures that for load conditions on the fracture surface, i.e. $\overline{k^2} = k_c^2$, the probability P_i assumes the value 1/2 and on the fracture surface there is equal probability for fracture and non-fracture.

Eq.(2) has to be considered as a first attempt to describe the statistical behaviour of a small piece of brittle material with the volume ΔV. The function P_i may be tested by multi-axial stress experiments. Setting up Weibull plots, the material parameter m may be obtained. In view of possible deficiencies of Eq.(2) it is however not recommended to use the so-obtained value of m for the prediction of fracture of a large component. It is safer to follow the procedure described in Section 4.

Possible deficiencies could be due to the fact that the assumption of statistical independence is not completely valid /10/. As the elements are interconnected by surfaces, the statistical behaviour is depending on the size of the surface. For this reason it may become necessary to use different types of distribution functions for elements on the surface, at the corners or in the interior of a larger component. In fact, a single test element has no interacting surface, but when incorporated into a large structure it could be influenced by its neighbours to a certain degree.

Another feature can easily be introduced in Eq.(2). At very low values of k^2, the probability for non-fracture P_i would be little less than 1 but the probability of fracture is not zero. Depending on m this uncertainty may impose severe restrictions for the industrial components designer. He has to proof-test the component before putting it into service. In this case it can be demonstrated that for a particular component there is no probability of fracture for values of k^2 smaller than a certain value k_o^2 . Depending on the stress distribution during the proof test k_o^2 is different for each element. In order to calculate the probability for non-fracture of the proof tested component P_i is artificially set 1 if $k^2 < k_o^2$.

4. The Fracture Criterion

The elemental probability distribution Eq.(2) is used to calculate the probability P for failure of a large component including n statistical cells.

$$P = 1 - \exp\left[- \frac{\ln 2}{k_c^m} \sum_{i=1}^{n} \left(\overline{k_i^2} \right)^{\frac{m}{2}} \right] \qquad (3)$$

Following Weibull's terminology /1/ the sum in the exponent is called the total risk of rupture,

$$R = \sum_{i=1}^{n} \left(\overline{k_i^2} \right)^{\frac{m}{2}} \qquad (4)$$

If the risk R equals k_c^m P will be 1/2. This risk is called the critical risk R_c

$$R_c = k_c^m \qquad (5)$$

In other words, if k_c is identical with the uniaxial tensile strength, the critical risk R_c is the m-th power of the uniaxial tensile strength (Weibull's approach).

According to Eq.(3), the same failure rates can be expected for different components if the probabilities P are equal. The component can therefore be compared with a test specimen which need not be necessarily small. In particular, two components can be compared with each other at a value P = 1/2. This implies that the sum

$$R = \sum_{i=1}^{n} \left(\overline{k_i^2} \right)^{\frac{m}{2}} = R_c \qquad (6)$$

is a constant for all geometries and all load cases if the components are critically stressed.

The summation performed in Eq.(6) increases proportionally with respect to the number of elements n if all elements are loaded equally. This assumption is not always valid and therefore it is useful to substitute Eq.(6) by

$$R_c = \left[f(V_{eff})\right] \cdot \left[\frac{1}{n_{eff}} \cdot \sum_{i=1}^{n} \left(\overline{k_i^2}\right)^{\frac{m}{2}}\right] \qquad (7)$$

The suffix "eff" indicates that in the case of stress gradients only parts of the total volume are stressed, while the other parts are nearly free of stresses. The number of statistical cells n, which contributes to V_{eff} is called n_{eff}. A definition of both quantities is given subsequently. The two expressions Eq.(6) and Eq.(7) are identical for $f(V_{eff}) = n_{eff}$. Eq.(7) provides two advantages over Eq.(6):

- Firstly in a conceptual consideration the risk can be regarded as the product of two independent factors. Since the numeral n in the summation term counts the elements with individual volume V the factor $f(V_{eff})$ represents the dependency of strength on volume. The second factor in Eq.(7) depends entirely on the type of stress distribution imposed on the specimen, i.e. the geometry and load conditions. In effect, the second factor in Eq.(7) represents the average risk of all elemental risks.

- Secondly, for $f(V_{eff}) = n_{eff}$ the volume dependency turns out to be the same as in Weibull's theory /1/. This dependency results in pessimistic probabilities for very large volumes /11/. The separate factor $f(V_{eff}) \neq n_{eff}$ makes it possible to correct for this effect by an empirically found function $f(V_{eff})$ such that R_c is indeed a constant against variations in volume.

For medium sized components with a constant stress distribution, the function is expected to be in fact linearly dependent on n. Deviations are found for larger volumes and very small volumes. In order to evaluate $f(V_{eff})$ we suggest the study of the strength of uniaxial test specimens as a function of size. In this case the effective volume, V_{eff} can be replaced by the total volume V. The risks of the specimen of volume $V = n \cdot \Delta V$ and that of volume ΔV can be compared, by means of Eqs.(7)

$$f(V) \cdot \frac{1}{n} \cdot \sum_{i=1}^{n} \left[\sigma_{ut}\ (V)\right]^{\frac{m}{2}} = f(\Delta V) \cdot \frac{1}{1} \cdot \sum^{1} \left[\sigma_{ut}\ (\Delta V)\right]^{\frac{m}{2}} \qquad (7a)$$

$$f(V) \cdot \sigma_{ut}^{m}\ (V) = f(\Delta V) \cdot \sigma_{ut}^{m}\ (\Delta V) \qquad (7b)$$

$$f(V) = \left[\sigma_{ut}\ (\Delta V)\ /\ \sigma_{ut}\ (V)\right]^{m} \qquad (8)$$

Eq.(8) follows if the normalizing condition $f(\Delta V) = 1$ is applied:
In Eqs.(8) $\sigma_{ut}(V)$ is the measured strength of an uniaxial tensile specimen with a large volume V and $\sigma_{ut}(V)$ is that of a specimen with the smallest admissible volume ΔV. The two strengths usually are different from each other as the experiments show. In order to obtain a true material constant i.e. a critical risk R_c which is independent of the size of the specimen it has to be required that Eq.(7a) and subsequently Eq.(8) is valid.
Eq.(8) can be used to determine f(V) experimentally.

The comparison provides an expression for f(V), i.e. Eq.(8). A more explicit, analytical expression for the function f(V) including numerical results is shown in Section 6.

In order to employ the function f(V) for arbitrary stress distributions the effective volume V_{eff} has to be defined. It can be anticipated in a special case that an element of volume added to the

total volume does not enhance the probability of fracture if the related, elemental probability of fracture,

$$P_i = 1 - \overline{P_i} \tag{9}$$

is very low. In this case we suggest the use of the reduced volume V_{eff} instead of V in Eq.(8). Prior to an exact definition of the effective volume we have to define the effective number of elements n_{eff} contributing to the volume in which fracture predominantly occurs.

$$n_{eff} = 2 \cdot \left(\sum_{i=1}^{n} i \cdot P_i \Big/ \sum_{i=1}^{n} P_i \right) - 1 \tag{10}$$

with

$$P_{i+1} \leq P_i \quad \text{for all} \quad i = 1, 2, \ldots n$$

The definition can be tested for its usefulness. For this purpose a specimen is assumed which is equally loaded with stresses with respect to the first n* elements, i.e. P_i = const. for i = 1, 2, ... n*. For the remaining parts the body is free from stresses, i.e. $P_i = 0$ for $i = n^* + 1, n^* + 2, \ldots n$.
In this case it would be useful to have $n_{eff} = n^*$. Evaluating Eq. (10) for the specified probability distribution yields exactly the expected result. Having provided a definition of the effective number of elements the effective volume is defined as

$$V_{eff} = n_{eff} \cdot \Delta V \tag{11}$$

A similar definition based on the elemental risk distribution was given in ref. /6/.

It should be pointed out that the left hand side of Eq.(7) is a constant with respect to a variety of load cases, geometries, multi-axial stress states and sizes. Variations in the stress tensors are considered on the element level by the special choice of the quantity k^2, which is fitted to the measured fracture surface. At least one free parameter is necessary for this purpose (see Section 5). Arbitrary changes in the stress distribution which include changes in the load distribution and geometrical boundary conditions are only conceivable if the arithmetic mean of all elemental risks is constant.

This statement can be derived from the presence of the second factor in Eq.(7). Two free parameters are available to fulfill this task, i.e. m and ΔV. Finally, size effects are compensated by the first factor in Eq.(7) which involves additional parameters. In fact, the use of Eq.(7) can be regarded as an attempt to describe the fracture properties on a purely phenomenological basis. For each brittle material the parameters have to be chosen so as to ensure constancy on the right hand side of Eq.(7).

A procedure to obtain the material constants is demonstrated in ref. /7/.
Assuming that the fracture surface of the material has been established experimentally in the usual manner and assuming that the mathematical formulation given in Section 5 provides a satisfactory description of the surface three test specimens of markedly different shape and stress distribution have to be chosen for determining the characteristic set of constants

$$R_c,\ m \text{ and } \Delta V \qquad (12)$$

One of the chosen specimens is preferably the uniaxial tensile test specimen with reference volume, $V_o \approx \Delta V$, as R_c is directly related to the uniaxial tensile strength, $R_c = \sigma_{ut}^m$. Because the tensile test specimen provides a homogeneous stress distribution,

another specimen should be chosen to include a steep gradient of stress distribution. Notched specimens as frequently used in fracture mechanics meet the requirements. It should be pointed out that the Weibull statistical theory /1/ using infinitesimally small elements of volume cannot be employed to obtain finite values of the risk of rupture at a crack tip. The finite element formulation of the risk of rupture presented in this paper, is suited for the derivation of values of risks even at crack tips. This is a considerable advantage because the infinitely high risk evaluated at a crack tip using Weibull's concept /1/ indicates a deficiency of that theory for steep stress gradient in general.

In order to determine the set of material constants (12) one more test specimen has to be chosen to provide a reference to a medium sized stress gradient. This may be a bend test specimen. The effective volumes V_{eff} of all three specimens should be approximately the same as the reference volume V_o chosen for the uniaxial tensile test specimen. Then stress calculations are required, preferably on a finite element basis, including a subsequent averaging procedure to evaluate the risk R according to Eq.(7). In an iterative process the averaging procedure has to be repeated with varying entries for m and ΔV until for both, the notched specimen and the bend specimen, Eq.(7) yields the critical risk $R_c = k_c^m = \sigma_{ut}^m$.

By the special choice of m and ΔV the constancy of the right hand side of Eq.(7) can definitely be obtained as long as three test specimens are involved. Constancy with respect to all other test specimens and components cannot be expected upon the theory but has to be proven by a greater number of experimental tests (Section 7). In Weibull's approach /1/ constancy can only be assured with respect to two specimens which do not have excessively steep stress gradients. In ref. /1/ a bend test and a uniaxial tensile test were chosen for comparison and to establish values for the two free parameters m and R_c.

The procedure for measurement of the set of constants (12) contains another aspect. Eq.(7) is essentially a means to transform any three different values of strength into values for the set of parameters (12). A stress distribution around a sharp crack or a notch is usually not characterized by a strength but by a critical stress intensity factor K_{Ic}. Therefore, we suggest in fact a transformation of the set of constants

$$\sigma_{ut} \qquad \sigma_{b} \qquad K_{Ic} \tag{13}$$

into the set of constants (12). In this way the constants (12) are defined for one material. The definition is independent of the geometry of the test specimens provided that it is proven experimentally that the set of constants (12) can be obtained from any three types of specimens or provided that Eq.(7) can be applied to a great number of test specimens for one set of material constants (12). The set (12) can be regarded as a complete set of material constants. For volumes other than V_o the empirical function f(V) has to be determined according to Eq.(8) causing that R_c, m and ΔV are not depending on size.

5. Multi-Axial Strength

5.1. Introduction to Problems of Multi-Axial Strength

A number of theories concerning biaxial as well as triaxial strengths have been developed /8, 9/. All theoretical approaches suffer from the lack of comprehensive experimental data and from the large scatter of those which are available. In most of the experimental work, variability in mechanical properties between presumeably identical samples has not been considered. This effect alone may be greater than the difference between the predictions of the various theories. Few materials have been examined under complex stress states and it is not known whether different failure theories are required for different types of brittle materials /8/. For engineering design it is not necessary to make a decision on the best theoretical account. Therefore, our objective is to provide a mathematical description of the available data. This formulation necessarily contains some degrees of freedom in order to make it adaptable for realistic conditions. For this purpose we follow a well established line of argument.

It has been suggested at a very early stage of development to consider the strain energy in a unit volume as a quantity relevant to fracture.
Neglecting a constant factor, i.e. neglecting the inverse of twice the Young's modulus, this quantity should be

$$k_{se}^2 = \sigma_1^2 + \sigma_2^2 + \sigma_3^2 - 2\nu(\sigma_1\sigma_2 + \sigma_2\sigma_3 + \sigma_3\sigma_1) \qquad (14)$$

where σ_1, σ_2 and σ_3 are the three principal stresses and ν is the Poisson's ratio. However, due to a completely different behaviour of the material at compression and at tension, corrections have to be applied. Since at hydrostatic pressure large

amounts of strain energy may be stored without causing fracture the elastic energy of an average stress $(\sigma_1 + \sigma_2 + \sigma_3)/3$ in each of the principal directions is usually substracted from the strain energy Eq.(14). The described procedure yields the maximum distortion energy.

$$2\, k_{md}^2 = (\sigma_1 - \sigma_2)^2 + (\sigma_2 - \sigma_3)^2 + (\sigma_3 - \sigma_1)^2 \qquad (15)$$

$$k_{md}^2 = \sigma_1^2 + \sigma_2^2 + \sigma_3^2 - (\sigma_1\sigma_2 + \sigma_2\sigma_3 + \sigma_3\sigma_1) \qquad (15a)$$

The maximum distortion energy concept is widely used for ductile materials. In this field it is known as von Mises' yield criterion or the concept of octahedral shearing stress. For the present purpose we would like to note that Eq.(15a) can formally be derived from Eq.(14) by insertion of a value $\nu = 0.5$ and that in essence the correction was made to have $k_{md}^2 = 0$ for hydrostatic or equi-triaxial pressure i.e. $\sigma_1 = \sigma_2 = \sigma_3$. The value zero for the distortion energy at the point of equi-triaxial pressure indicates that no fracture is expected under such load conditions. Another correction to the strain energy concept was introduced by Ely /12/. Any mathematical description of the fracture surface is required to cover the difference of the breaking strength in tension σ_{ut} and in compression σ_{uc} which can be determined by experiments. Therefore Ely /12/ suggested scale factores S_1, S_2 and S_3 applied to the principal stresses σ_1, σ_2 and σ_3 to ensure that the quantity k^2 assumes the correct measured values for the uniaxial strengths expected if the stress distribution is of uniaxial type.

The following formulation is Ely's /12/ modified strain energy expression:

$$k^2=(S_1\sigma_1)^2+(S_2\sigma_2)^2+(S_3\sigma_3)^2-2\nu(S_1\sigma_1S_2\sigma_2+S_2\sigma_2S_3\sigma_3+S_3\sigma_3S_1\sigma_1) \quad (16)$$

where

$$S_i = \begin{cases} 1 & \text{for } \sigma_i \geq 0 \\ \sigma_{ut}/\sigma_{uc} & \text{for } \sigma_i < 0 \end{cases} \qquad i = 1, 2, 3$$

Eq.(16) was applied to biaxial data and yielded a good description of much of the experimental data in the quadrant where both principal stresses are tensile and in the quadrant where one principal stress is tensile while the other is compressive. It possibly gives a good representation in the quadrant where both stresses are compressive /9/. We would like to point out that the fracture surface where Ely's /12/ modified strain energy was demonstrated is different from the area where hydrostatic pressure becomes dominant. Also, the property of $k^2 = 0$ for equal triaxial compressive stresses, i.e. $\sigma_1 = \sigma_2 = \sigma_3$ can still be attained by using $\nu = 0.5$ in Eq.(16). Thus Ely's modified strain energy can be further modified to provide a maximum distortion energy. For materials including large pores it may be desirable not to have an infinite strength in the hydrostatic pressure case. If pore collapse by localized fracturing is expected at very high compressive stresses Poisson's ratio ν in Eq.(16) may be chosen to be only a little less than 0.5 to obtain a non-zero value in k^2, i.e. $k_c^2 \geq 0$ for critical conditions.

5.2. Symmetries for Triaxial Strength in Isotropic Material

Besides the two regions which have already been discussed there is a third region of the fracture surface which requires particular attention. The classification of multi-axial stresses in terms of quadrants in a rectangular coordinate system is typical for biaxial stresses but is not useful for triaxial stresses. Before discussing the third area of the fracture surface it is advisable to provide a proper reference system. Similar to the two-dimensional case, the basis for the reference system is the cartesian coordinate system given by the directions of the three principal stresses. Within this rectangular special system, the principal diagonal plays an important role. A certain degree of rotational symmetry is expected about this diagonal. For instance, considering an isotropic material, at least a three-fold rotational symmetry is likely. A plane which contains the principal diagonal and one of the coordinate axes can be rotated about the diagonal. At each 120° it contains another coordinate axis with the identical values for the uniaxial, tensile strengths. Therefore it is useful to discuss the fracture surface with reference to a system of spherical coordinates (r, θ, φ). The two values $\theta = \pm 90°$ point along the principal diagonal of the cartesian system away from the origin, towards the polar regions of the sphere, r = const.

The azimuthal angle φ can be defined to be zero at the lateral plane containing both the diagonal and the first axis of the cartesian reference frame, σ_1. For a three-fold symmetry it is only necessary to explore the fracture surface for the first 120° for φ. Furthermore, since the lateral plane at $\varphi = 240°$ also shows the negative part of the axis σ_3 in the lateral plane $\varphi = 60°$ it is only necessary to explore the fracture surface for the first 60° for φ. The region of the fracture surface between $\varphi = 60°$ and $\varphi = 120°$ can be obtained by reflection at

the plane $\varphi = 60°$. It should be repeated that the expectations for the symmetry properties are based on 6 points at the fracture surface, i.e. the 3 uniaxial tensile strengths which are repetitive with $\Delta\varphi = 120°$ and the 3 uniaxial compressive strengths which are also repetitive with $\Delta\varphi = 120°$ but are out of phase with regard to the uniaxial tensile strengths by 60°. Also, they correspond to different values in θ, i.e. $\theta = \pm 35.26°$.

The polar region with its central point at $\theta = -90°$ ("south polar region") is the region where hydraulic pressure predominates and the application of the modified strain energy approach is recommended (Eq.(16) with $\nu = 0.5$). The region of the fracture surface with nearly equitriaxial tension is the polar region surrounding the point $\theta = +90°$ ("north polar region"). The intermediate, equatorial region contains the biaxial quadrants for which the modified strain energy approach, i.e. Eq.(16), was found satisfactory.

5.3. The Predominantely Tensile Region of the Fracture Surface

Complying with the possibilities offered by the modified strain energy approach (Eq.(16)), it is considered to be a conservative choice if ν is given the value zero in the north polar region. For $\nu = 0$ the fracture surface is spherical.

In comparison with existing theories on fracture under multiaxial stresses Weibull's approach /1/ provides a good description

of the fracture surface with respect to the north polar region. The flexibility of the approach with regard to a phenomenological description can be tested by listing the equibiaxial and equi-triaxial strength ratios σ_{bt}/σ_{ut} and σ_{tt}/σ_{ut} as a function of m. This test is performed in Table I. For an independent m ranging between 1 and 32 it would be possible to account for experimental values of strength ratios between 50 % and 93 % for the equi-biaxial strength ratio and between 33 % and 88 % for the equi-triaxial strength ratio. Additionally Table I also contains a column for Poissons ratios ν which by use of Eq.(16) provide the same values for equi-biaxial or equi-triaxial strength ratios as obtained from the Weibull theory for a corresponding value in m. The full range in ν i.e. for values between 0.0 and 0.5 Eq.(16) would account for experimental values in strength ratios between 72 % and 100 % for σ_{bt}/σ_{ut} and between 58 % and 100 % for σ_{tt}/σ_{ut}. The free choice of ν in Eq.(16) is a flexible tool for the description of experimental results similar to Weibull's formula employing a free choice of the parameter m.
The ratio of biaxial-tensile strength σ_{bt} and uniaxial tensile strength σ_{ut} and the corresponding ratio for triaxial-tensile strength σ_{tt} in Table I were evaluated according to Eq.(17) from ref. /1/.

$$\frac{\sigma_{bt}}{\sigma_{ut}} = \left[(2m + 1) \prod_{\mu = 1}^{m} \frac{2\mu}{2\mu + 1} \right]^{-\frac{1}{m}} \qquad (17a)$$

$$\frac{\sigma_{tt}}{\sigma_{ut}} = (2\,m + 1)^{-\frac{1}{m}} \qquad (17b)$$

m	Equi-Biaxial		Equi-Triaxial	
	Strength Ratio σ_{bt}/σ_{ut} in %	Possion's Ratio ν	Strength Ratio σ_{tt}/σ_{ut} in %	Poisson's Ratio ν
1	50	- 1.00	33	- 1.00
3	68	- 0.09	52	- 0.11
4	72	0.04	58	0.00
7	80	0.22	68	0.14
10	84	0.29	74	0.19
13	87	0.33	78	0.22
16	88	0.36	80	0.24
32	93	0.42	88	0.28
∞	100	0.50	100	0.33

Table I: **Equi-Biaxial and Equi-Triaxial Strength as a Function of Weibull's Parameter m**

The disadvantages of Weibull's suggestion are, firstly, that m is not available as a free parameter and, secondly, there is no satisfactory description of the fracture surface in the more compressive regions.

5.4. Discussion of a Global Solution

Ely's modified strain energy approach is well suited for an overall description of the fracture surface if Poisson's ratio is allowed to vary as a function of the polar angle θ. This is necessary for compensating the different behaviour of the material in compression and in tension. Varying Poisson's ratio between 0.0 and 0.5 the fracture surface can be closed like a sphere or opened like a cylinder. The situation is illustrated in Figs. 1a, 1b. It shows a part of the fracture surface defined

by an intersection of the lateral planes $\varphi = 0°$ (Fig. 1 a) or $\varphi = 60°$ (Fig. 1 b). The lateral plane $\varphi = 0°$ contains the principal diagonal, $\sigma_1 = \sigma_2 = \sigma_3$, with the equi-triaxial points, the σ_1 - axis with the uniaxial tensile state and the diagonal of the compression-compression sector, $\sigma_2 = \sigma_3$, with the equi-biaxial point for compression.

The lateral plane $\varphi = 60°$ shows the state of uniaxial compression and the line of equi-biaxial tension of the tension-tension section. For $\nu = 0.5$ Figs. 1a, 1b indicate that the fracture surface is a cylinder with radius $k_c \cdot \sqrt{2/3}$. Due to Ely's modification /12/ the cylinder is inflated in the equatorial zone to a radius $(k_c/S) \cdot \sqrt{2/3}$. The values for $S^{-1} = \sigma_{uc}/\sigma_{ut}$ (here = 3.3) as used in Figs. 1a, 1b apply to graphite. The uniaxial tensile strength k_c was chosen to be 1. For $\nu = 0$ the polar regions are covered by sections of spheres of radii k_c and k_c/S with Ely's modification providing a smooth transition when approaching the equatorial zone. As a possible, practicable solution the lines of the fracture surface with varying Poisson's ratio are also shown in the Figures. In this case ν was interpolated linearly between $\nu = 0$ for $\theta = -90°$ and $\nu = 0.5$ for $\theta = +90°$. As expected the fracture surface for such a choice of ν is closed for hydraulic tension and open for hydraulic compression. This reflects the more real situation characterized by a finite strength in tension and an infinite strength in equi-triaxial compression.

The linear interpolation of Poisson's ratio provides values of stress which are slightly in conflict with the maximum normal stress theory. This theory is the simplest approach towards the problem of multiaxial stresses. It is widely accepted for designing and requires that all principal stresses shall be smaller than the uniaxial stresses thus enclosing the fracture surface in a box of the lengths determined by σ_{ut} and σ_{uc}. The fracture surface as

defined by Eq.(16) is arranged in the all tensile region partly outside the box. For instance the line defined by $\sigma_1 = \sigma_{ut}$ and $\sigma_2 = \sigma_3$ (see Fig. 1 a) intersects the surface twice at $\sigma_2 = 0$ and $\sigma_2 = 2\nu/(1 - \nu)$. The second intersection can be avoided only if Poisson's ratio is chosen to be zero. Then the fore-mentioned line representing part of the box wall is a tangent to the fracture surface. Although the excursion beyond the boundaries set by the maximum normal stress theory is small for the linearly interpolated Poisson's ratio it is sometimes used as an argument against the strain-energy concept. Therefore, in order to be conservative in the north polar region, to be as close as possible to the experimental data in the equatorial region, and to have infinitely high strength for equi-triaxial compression, we propose the use of three different, values for the three different regions, i.e. $\nu = 0$ and 0.5 for the two polar regions and the physically significant Poisson's ratio for the equatorial zone. Such discontinuities in Poisson's ratio do not cause discontinuities in the fracture surface provided that the three different regions are bounded by two circumferential lines which are the simultaneous solutions of Eq.(16) and the Eq. originating from the requirement that the mixed term in Eq.(16) equals zero. According to this definition the boundary lines of the polar regions pass through the uniaxial points

$$(\theta = 35.36°,\ \varphi = 0,\ 120,\ 240°,\ \theta = -35.36°,\ \varphi = 60,\ 180,\ 300°)$$

In the case of the non-modified strain-energy expression, the lines are found on the cones $\theta = \pm 35.36°$. The modified strain energy according to Eq.(16) provides sinusoidal zero-lines. Depending on the ratio σ_{uc}/σ_{ut} the zeros in the lateral planes $\varphi = 60$, 180 and 300° are found between $\theta = +35.26°$ and $\theta = 35{,}26°$ with respect to the north polar region. The boundary

line for the south polar region in the lateral planes $\varphi = 0$, 120 and 240° are found between the polar angles $\theta = -35.26°$ and $\theta = -54.74°$. For graphite the zeros are shown in Figs. 1, 2 and 4.

The fracture surface as seen from a distant point on the positive part of the principal diagonal is shown in Fig. 2. A set of closed lines each representing the intersection of the fracture surface with a cone, θ = const., is also shown in Fig. 2. The two lines marked zero 1 and zero 2 separate the three spherical regions for which different Poisson's ratios were defined. For angles $\theta \leq 60°$ the fracture surface has cylindrical shape. The symmetry properties of the surface with a symmetry sector of $\Delta\varphi = 60°$ are clearly expressed in Fig. 2. Fig. 3 shows the fracture surface as seen from the projected parallel to a direction close to that of $-\sigma_3$. The lower part of the surface which extends cylindrically to infinity was cut at the intersection with the cone $\theta = -60°$.

Fig. 4 is a simultaneous representation of the modified strain energy k^2 and the risk of rupture k^m. The quantity k from Eq.(16) was evaluated for all σ_1, σ_2 and σ_3 obeying the equation

$$\sigma_1^2 + \sigma_2^2 + \sigma_3^2 = \sigma_{ut}^2 = 1 \qquad (18)$$

k was used as the radial component in the polar coordinate system (r, θ, φ). The three-dimensional body was projected

parallel to the direction $\vartheta = -30°$, $\varphi = +30°$. The use of Poisson's ratio, $\nu = 0$, in the north polar region means in essence eliminating the influence of the relief work done by the lateral contraction when tensile stresses are applied. Together with the normalization condition $\sigma_{ut} = 1$ Eq.(16) is identical with Eq.(18). The result is a constant value $k = 1$ which means that in the north polar region the depicted geometrical shape is a sphere of radius $k = 1$. The strain energy, which is proportional to k^2, and the risk of rupture k^m correspondingly are also spheres of radius 1 in the normalized representation of Fig. 4. Strictly speaking the spherical shape extends only within the octant σ_1, σ_2, $\sigma_3 > 0$. Outside that region it is distorted by Ely's modification /12/.

In the equatorial region the lateral forces were taken into account and due to Ely's modification /12/ all compressive stresses were reduced by the factor S given in Eq.(16). Both operations cause a contraction of the closed surface (Fig. 4) towards the origin. The surfaces for the modified strain energy ($\sim k^2 < 1$) and the risk of rupture ($\sim k^m << 1$) are contracted more than the closed surface in Fig. 4 which was evaluated for $k < 1$.

There is further contraction in the south polar region, because the relief work from lateral forces is increased as $\nu = 0.5$, was used and this is also the octant where all stress components are reduced by the factor S. The risk of rupture decreases more rapidly than the energy density when the polar angle ϑ approaches the value $\vartheta = -90°$.

With respect to applications of this concept it has to be noted that the elemental risk of rupture $(\overline{k^2})^{m/2}$ used in Eq.(4) is not negative. This implies that a risk is defined for all elements of the stressed body regardless of the fact that some parts are under compression. These parts will have comparatively low values of risk, and in consequence the sum given in Eq.(4) can be extended over the whole body. In Weibull's formulation /1/ compressive regions are always excluded from the integration by artifically defining a value zero for the risk of rupture. Instead, in the present formulation the transition from the tensile region to the compressive region is performed smoothly. This is achieved by applying a factor $S < 1$ to the principal stresses when passing through zero, and also by increasing Poisson's ratio discontinuously.

Fig. 1 shows a few experimental points which were taken from ref. /16/ and which are found outside the fracture surface. Obviously, the fracture surface with the highest value in V is still conservative with respect to the data when considering the south polar region.

6. Influence of Size

6.1. The Strength-Density Correlation

It was stated in section 4 that the proposed fracture criterion can only work satisfactorily if the right hand side of Eq.(7) remains constant with varying geometries. This statement requires experimental verification. The function $f(V_{eff})$ especially ensures independence with respect to the size of the stressed body. The definition of the effective volume, V_{eff}, used as an entry to the volume function was designed to meet the special conditions induced by non-uniform stress distributions. For simplicity we limit our experimental studies on the size influence to the uniaxial tensile test specimen. In this case the effective volume V_{eff} and the geometrical volume V are identical (viz section 4).

In many experiments it was confirmed that Weibull's theoretical approach i.e. $f(V) = n$ provides a satisfactory description of medium sized specimens. Brocklehurst /11/ gives a review on the work performed on graphite. With bend specimens it was not difficult to show that the expected dependency of strength on volume exists for specimen sizes greater than 1 cm^3. Specimens with volumes smaller than 1 cm^3 showed an increase in strength for increasing volume while larger tests specimens provided good agreement with Weibull's theory /1/ using m = 16. However, tensile test specimens were found to be at variance with the described dependency. The tensile data showed an increasing strength with increasing volume, tending to saturate at a maximum value for volumes greater than 8 cm^3.
Additionally, in an attempt to apply Weibull's statistical theory /1/ to test specimens of various kinds and sizes, Price and Cobb /13/ reported that there was reasonable agreement with the observations for all series of tests if the dependence of strength on volume was neglected. In effect this statement is in support of the fore-mentioned saturating curve.

The situation became clearer when Lanza und Burg /14/ pointed out that frequently sets of samples from the same grade but with different volumes exhibit different mean densities. As there exists a strong correlation between bulk density and strength, in consequence a density effect is superimposed upon the volume effect and tends to cover it. With samples having the same-bulk density it was shown that the expected volume dependency can be reproduced in tension as well as in compression. This above statement can be fully supported by our own experiments which were performed in tension only /15/.

Lanza und Burg /14/ further studied grain size effects. They defined a critical volume which separates the region of volume where Weibull's theory is applicable from the low volume region in which the strength increases with volume. The critical volume was found to be larger for graphite grades with larger grain sizes. We would like to point out that the critical volume and the element of volume ΔV discussed in section 2 of the present work have two features in common.

- Firstly, the element of volume ΔV is the lower limit for all volumes of specimens and components that are amenable to a statistical analysis.

- Secondly, the element of volume is expected to be larger for larger grain sizes because it must be large enough to include the spectrum of grain sizes.

Although according to the work of Lanza and Burg /14/, the characteristics of the volume dependency of graphite were proven to be dependent on bulk density, the fact represents a serious problem with respect to the applicability of the statistical theory. The fluctuations in density are obviously large scale fluctuations because in our experiments a large number of specimens (238) with a total volume

of 309 cm^3 was not sufficient to determine an average bulk density. The average density of that set was 1.780 g/cm^3 while another set of 240 specimens with a total volume of 7536 cm^3 had an average density of 1.804 g/cm^3. As mentioned earlier it is required that all bulk properties, including the density, should be obtainable from the element of volume ΔV. The size of 1 cm^3 also mentioned earlier is already a large size as compared with the dimensions of the components used for instance in the core of a nuclear reactor. Larger sizes of ΔV are not suited to resolve the complexity of the stress distributions within the component.

To proceed with a statistical analysis there are two possibilities available; either the density effect is included in the analysis in a deterministic manner or it is completely ignored. The penalty for ignoring the density effect is a larger uncertainty. In consequence the material constants (12) are also more uncertain. In practice it means that there is a larger probability for failure at low stress levels.

6.2. Uniaxial Tensile Strength as a Function of Volume

The uniaxial tensile strength measured as a function of volume and density is shown in Figs. 5-8 for four different graphite grades. In order to evaluate the dependence on volume (Eq.(7)) $\sigma_{ut}(V)$ has to be described mathematically. Weibull's approach, $\sigma_{ut} \sim V^{-1/m}$, can be verified experimentally for parts of the measured curves. Therefore, this approach has been chosen as the basis for a more comprehensive formulation of the functional dependence.

Firstly, we suggest the enlargement of the formula by an additive constant such that $\sigma_{ut} \sim V^{-1/m}$ + const. The additional constant ensures that there is a residual strength for large volumes. The formulation without the residual strength is based on the idea that an increment in volume may always contain a flaw larger in size than the flaws already present in the volume. The statement tacitly assumes the existence of infinitely large flaws. The assumption of a spectrum of flaw sizes with an upper limit leads to a residual strength for very large volumes which justifies the additional constant.

Secondly, it was observed in many experiments that Weibull's approach /1/ is not applicable to small volumes. This property of the strength function cannot be accounted for by the ($V^{-1/m}$ + const.) law. The reason for the initial low values is the granular texture of the material. In an extreme case, it can be assumed that a very small test volume merely contains one flaw the strength of which is zero. Therefore, we suggest a functional dependence capabable of sharply reducing the strength to zero at a given critical volume. This task can be achieved by Eq.(19).

$$\sigma_{ut}(V,\rho) = \exp\left[-\frac{1}{s(V)} + 1\right] \cdot (V^{-\frac{1}{m}} + a)\cdot(b\,p + c) \quad (19)$$

with

$$s(V) = 0{,}5 \times \left[1 + \tanh\left(\frac{\alpha}{V} + \beta + \gamma \cdot V\right)\right] \quad (19\,a)$$

and with the constants a, b, c, d, α, β, γ, and the variables for density and V for volume.

To explain Eq.(19) we consider the three factors of which ($V^{-1/m}$ + a) was already discussed. It would provide infinitely

high values of strength for diminishing volumes. In order to compensate this development the exponential factor is introduced. The factor operates like a switch function. When increasing the volume V there is a certain volume at which the function s(V) rapidly changes its value from zero to two. Simultaneously the exponential function changes its value from zero to one raising its value abruptly. As a result there are two regions of volume.

- one region in which the strength is conservatively low and
- another region in which the strength follows the function $(V^{-1/m} + a)$

It is obvious that the size of the characteristic volume ΔV cannot be chosen from the region having reduced strength.

The uniaxial tensile strength as derived from Eq.(19) also depends on the bulk density ρ. This factor was not used to calculate probabilities for fracture because for such a purpose the density ρ of each of the specimens has to be measured as a function of space coordinates. As a simple approach the same average bulk density was applied for all specimens.

7. Experiments Proving Geometrical Independence of the Fracture Criterion

7.1. Geometries and Graphite Grades

Each of the Figs. 9-11 shows the 16 different types of specimens used for experimental investigations. One of the 16 specimens labelled Ia is a CT-specimen. The other 15 specimens (labelled I b - d, II a - d, III a - d and IV a - d) are modifications derived from the CT-specimen in the following manner:

- The two holes into which the load is introduced are shifted towards the left hand side in four steps, I to IV
- The crack tip is blunted by introducing an extra bore the diameter of which is increased in steps, a to d

The combined steps yield a matrix of 4 x 4 specimens as shown in the figures. At the extreme the specimens are closer to

- a tensile test specimen (IV a), and
- a bending beam type of specimen (I d).

The specimens are plane sheets with 20 mm thickness, 150 mm length and 130 mm breadth as far as the ones from Figs. 10 and 11 are concerned. The specimens shown in Fig. 9 are scaled down to 135 x 117 mm^2 but leaving the diameter of the load bores unchanged. In the regular cases the diameter of the holes amounts to 15 mm, the holes for blunting measured 10, 20 and 30 mm in diameter. Additional measures are shown in the Figs. 12 - 13.

The experiments were done using three graphite grades,

- a fine grained graphite grade, V 483 T, maximum grain size 0.1 mm, Fig. 9
- a graphite grade with medium grain size, AS 2-F-500 maximum grain size 1mm, Fig. 10
- a coarse grained graphite grade, M 2190, maximum grain size 6 mm, Fig. 11.

7.2. Experimental Results

At least twenty specimens of each specimen type were tested. 24 specimens were tested in the case of the coarse grain graphite. The average loads at fracture and their mean square deviations are noted in the Figs. 9-11. The figures also provide information on the fracture pattern and the relative abundances of crack paths, which are subject to a comparison between experimental and theoretical analysis although the analysis at the best can only predict the origin of a crack path. The denomination 18/20 (for example Fig. 9, specimen Ia) expresses the fact that 18 out of 20 crack paths took the indicated (dashed line) direction.

7.3. Fracture Analysis

The fracture criterion described in the preceding sections was applied to the experiments. The first step of the analysis was a linear elastic finite-element calculation using a finite-element mesh with finer grading than that expected for the partitioning of the body into statistical cells of size ΔV. The stresses were evaluated using the average loads of fracture shown in Fig. 9 - 11.

Subsequent to the elastic calculation surface elements of area $\Delta F = \Delta V^{2/3}$ were formed. They were obtained by joining the elements of the finite element calculation to a size $\Delta F_i \simeq \Delta F$ employing the extra condition that the surface element ΔF_i should be as compact as possible.
Average values $\overline{k^2}$ and the probabilities for fracture for each element were evaluated and arranged in a set of numbers with descending values (Eqs.(2), (9), (10)). The results were used to determine the effective number of elements and the effective volume (Eqs.(10), (11)), which were subsequently employed in the volume correction as given by Eqs.(8) and (19).

In a first set of calculations comprising the statistical calculations for all types of specimens initial values for the material parameters ΔV and m are required, i.e. the size of the statistical cell and Weibull's parameter m. The values for uniaxial tensile stresses also necessary for the calculations were derived via Eq.(19) with the constants a, b, c, α, β and γ given in the Figs.5-7. Improved values for m and ΔV were attained by repeating the set of calculations with the objective to approach the value P = 1/2 in Eq.(3) for all specimen types.

7.4. Results of the Fracture Analysis

The iteration process on the parameters m and ΔV resulted in values which are shown in Table II. The Table also contains values for other correlated quantities.

Graphite Grade	Max.Grain size mm	Uniaxial Tensile Strengh N/mm^2	Size of Statistical Cell ΔV mm^3	Weibull Parameter m
V 483 T	0.1	20.2	125	6
AS2-F-500	1	11.5	1154	5
M 2190	6	2.7	2619	3

Table II: **Material Characteristics**

Figs. 14-61 provide detailed information of the combined finite-element, statistical analysis. The Figs. show the partioning of the geometry into statistical cells. Each cell is marked by an integer number according to decreasing probability of fracture. The decimal fractions express the probability of fracture for each individual cell. Values lower than $0.5 \cdot 10^{-3}$ are not printed.

The Figs. 14-61 have been compared with the experimental results shown in Figs. 9-11. For each specimen type the observed cracks were counted and sorted into categories distinguished by their apparent points of crack initiation. The number of crack paths in the different categories were then counted and related to their total number. The relative abundancies of crack paths obtained in such a manner are found to be in fairly good agreement with the calculated probabilities of crack initiation. Exceptions are discussed below.

Comparing the specimens in the successive columns I to IV as labelled in the Figs. 9-11 it is noted that the crack paths increasingly include the holes for load insertion. This characteristic behaviour can also be recognized in Figs. 14-61. However,

predictions are better for the specimens in the rows labelled "d" compared with those for specimens from rows labelled "a". The effect is believed to be caused by numerical difficulties in evaluating the correct elastic stress distribution in the near neighbourhood of the crack tip. The difficulty become most prominent in case of the fine grain grade V 483 T in which case the statistical cell was so small that there were only a few finite elements for each statistical cell. It is expected that the analysis probably would provide better results if the singularities in stress distributions are treated with special singular elements.

Integral values for probability of failure for each specimen type and each graphite grade can be depicted from Figs. 62-64. The calculated probabilities are contained in a diagram with probability of failure plotted versus the average value of critical load as given by the corresponding experiment. The diagrams are read in the following manner. If the theoretical approach was fully successful and, furthermore, if there was no statistical scatter of the average load values then all predictions should result in one value i.e. 50 % failure. Since the predictions are not located on the 50 %-line but deviate from it, the predictions are not fully reliable. With three exceptions the diagrams show that the predicted values are found within one standard deviation from 50 % although the experiments provided the load values for 50 % failure. Vice versa the following statement can be made. A predicted 50 % failure may turn out to be a 16 % or 84 % failure.

The three exceptions from the above statements concern the specimen types I a, II a and III a in the case of the graphite grade V 483 T. It is believed that the finite element mesh was not sufficiently fine to reproduce the correct values of stress at the crack tips and subsequently the probabilities for failure were calculated too small.

It is noted that the calculated probabilities are not distributed evenly around the 50 % line. The deviations show a systematic trend. In all experiments in which failure predominantly occurred at sharp crack tips the calculated probabilities appear to be lowest. This again indicates that it is essential for this method to reproduce the correct elastic stress at the crack tips although in the next step high values of stress are eliminated by averaging.

There is also a trend for higher loads to be related to higher probabilities of failure. This may be caused by the fact that critical loads experimentally are not well defined. The effect is most obvious in Fig. 64 showing the results for coarse grain graphite grade M 2190. The specimen types loaded with bending moments are on the lower end of the scale for critical loads while those specimens which are stressed more uniformly are found at the upper end of the scale.

In conclusion, it has been proved to be possible that failure probabilities can be calculated although if tested, a predicted 50 % failure rate may turn out to be either 16 % or 84 % at the extremes.

8. Summary and Conclusions

8.1. Introduction of a Statistical Cell

An additional parameter had to be introduced into the Weibull statistical theory /1/. The necessity for this operation can be summarized as follows.

Basically all statistical problems are treated in the same manner. A system that responds statistically is subdivided into smaller subsystems with the essential property that the events occurring in the different subsystems are independent of each other. In most of the cases the statistical properties of the subsystems are identical and the statistical properties of the total system may be calculated from those of the subsystems.

More specifically, if the distribution function for failure of one link of a chain has been determined experimentally and described mathematically then it is possible to calculate the distribution function for failure of the whole chain. This assumes that all links were fabricated according to the same specification and all links break independently.

In the case of a continuum extending in three dimensions the subsystem is characterized as a piece of material contained in a small part of volume. It is of importance to realize that in practice the statistical properties of such a part of volume are almost exclusively studied with cylindrical test specimen under uniaxial load. This implies that only a finite part in volume of the size of a cylindrical test specimen is available for the statistical analysis of a larger body. Naturally, it is desireable to improve the geometrical resolution by studying the properties of test specimens which are smaller in size. But there is a limit given by the grain size.

Parts of the material which are smaller than the grain are not easy to handle and often break accidentally. That is a typical feature of any statistical subsystem. If it is chosen too small the relevant statistical properties are lost. It is therefore necessary to perform experimental studies on samples of finite size and then the results in a statistical analysis of fracture for large components.

8.2. Definition of the Statistical Properties as Related to the Statistical Cell

Having introduced a finite volume ΔV which enters the Weibull statistical theory /1/ as an additional parameter there are secondary problems to be solved. A complete knowledge about the mechanical and statistical response of a small piece of material is required. It is not sufficient to provide data for uniaxial, evenly distributed loads in tension or compression, the requirements are more comprehensive.
If the basic element in volume responds differently in fracture whether it is loaded in

- uniaxial tension or
- torsion or
- bending or if it is loaded with
- multiaxial stresses or contains
- singular stresses at crack tips or ... etc.

then this behaviour has to be specified in terms of risk. Further subdividing of the statistical system in terms of volume drastically changes the properties of the subsystem. The problem has been discussed by Brocklehurst /11/ in terms of a weak link concept as opposed to an interacting "grain size effect". The statistical subsystems are related to the pore distribution, fracture of large grains, coincidence alignement of such

grains etc. For each of the additional systems the problem of finding a statistical cell and the problem of providing a mathematical description for its basic properties poses itself anew. An approach has been made recently /17/ /18/ and in a long term development of a fracture criterion for graphite or possibly other brittle materials, this can be an alternative basis for describing the statistical properties of a piece of graphite contained in an element of volume.

As compared with Weibull's approach to the problem in the present paper a more phenomenological approach is favoured.

To be more specific, it is assumed that in the more general case of multiaxial, non-uniform stresses the risk R for one element of volume is evaluated by the proportional relationship

$$R \sim (\overline{k^2})^{\frac{m}{2}} \cdot \Delta V$$

With respect to uniformly and uniaxially loaded types of specimens $\left((\overline{k^2})^{m/2} = \sigma^m\right)$ the definition is identical to that given by Weibull /1/. For uniaxial but not uniform loading (bending) the energy proportional quantity σ^2 is averaged within one element of volume and subsequently used to evaluate risks. Finally, for multiaxial, non-uniform stresses the energy proportional quantity k^2 is averaged prior to evaluation of risks. The quantity k^2 is a function of the three principal stresses characterized by critical values for coordinate points located on the measured fracture surface.

8.3. Volume Correction of the Risk Function

In the present paper attention was also given to the volume dependency of the risk function. According to Weibull the risk for failure increases proportional to the total volume. The statement is not true for parts of the volume smaller than one basic element of volume ΔV. The experimental curve shows a dramatic loss in strength for volumes smaller than ΔV. Also, for materials which have been proof-tested it is expected that there is no infinitely large risk for failure if the volume is infinitely large. Therefore, in the present paper the strength of a uniaxial test specimen was measured as a function of volume, it was described by means of a mathematical function and it was used to correct the risk function. The correction function is entered by an effective volume which is that portion of the volume in which fracture predominantly occurs. The effective volume can be evaluated by employing the probability of failure for each volume element i.e. accumulating only those elements of volume with a relatively high probability for failure.

8.4. Application of the Theory to Experiments - Further Improvements

The theory was applied to a large set of experiments varying the stress distribution and varying the grain size. As a result it can be stated that for the optimal choice of the parameters and a given load of the specimen the probability of failure can be predicted. If 50 % failure rate is expected the experiment may prove that the prediction failed by one standard deviation. The analysis also provides probabilities for crack initiation at various locations within the specimen. The correct evaluation of the crack tip stress distribution seems to be a problem with consequences also to the statistical analysis.

Concerning the future development of the method the authors would like to discuss further the assumption of statistical independence. The assumption is in fact an idealization with the purpose to avoid the calculation of inelastic effects. The actual material response of an element in volume is inelastic yielding by developing subcritical microcracks. If incorporated into a larger body local yielding causes immediate redistribution of stresses within the body such that the particular element in volume which yielded eventually is stress--relaxed. If stress relaxation is accompanied by changes in strain the particular element in volume becomes geometrically incompatible. Therefore the described process reveals interaction of the different statistical elements during fracture.

In order to remove interdependency so in order to obtain more exact values of failure probability it is necessary not to perform a linear elastic analysis as presently done but an inelastic analysis prior to the statistical analysis. The two analyses have to be performed successively for each load increment thus evaluating increments of failure probability. For this purpose it is also necessary to provide a material law.

Involving more microscopic information and including inelastic finite element analysis are the outlines for future improvements of the fracture criterion which in its present state is capable of predicting failure of components within the margins of one standard deviation.

References

1. W. Weibull
   A Statistical Theory of the Strength of Materials, Proc. Ing. Vetenskapsakademiens Nr. 151, Stockholm 1939

2. A. M. Freudenthal
   Statistical Approach to Brittle Fracture, Academic Press 1968, Chapter 6, Vol. II

3. H. Neuber
   Kerbspannungslehre, Springer, Berlin 1958, p. 164

4. G. Kraus, J. Semmler
   Die Charakterisierung des mechanischen Verhaltens von Kohlenstoff- und Graphitmaterialien mit Hilfe der Schallemissionsanalyse, Carbon, 16 (1978) 185

5. M. Rödig, G. Kleist, H. Schiffers, H. Nickel
   Zur Bruchmechanischen Untersuchung von Reaktorgraphit, Kernforschungsanlage Jülich GmbH, JÜL-1275, März 1976

6. H. Cords, A. Djaloeis, G. Kleist, J. Mönch, B. Öfinger, R. Zimmermann
   Ein Beitrag zum Thema Bruchkriterien für Graphit, Kernforschungsanlage Jülich GmbH, JÜL-1355, Okt. 1976

7. H. Cords, G. Kleist, J. Mönch, H. Schuster, R. Zimmermann
   A Contribution to Fracture Criteria for Nuclear Graphite, Transactions of the 4th International Conference on Structural Mechanics in Reactor Technology, San Francisco, Aug. 1977, Contribution D 5/6

8. W. H. Dukes
Handbook of Brittle Material Design Technology, Advisory Group for Aerospace Research and Development, AGARD-AG-152-71, London, Feb. 1971, p. 96

9. J. E. Brocklehurst
Fracture in Polycrystalline Graphite, Chemistry and Physics of Carbon 13 (1977) 175

10. I. B. Mason
Proc. 5th Carbon Conference, Penn. State, 1961, Vol. II, Pergamon Press, Oxford, 1963, p. 597

11. J. E. Brocklehurst
ibidem ref. 9, p. 183 - 193

12. R. E. Ely
Cerm. Bull., 47 /5 (1968) 489

13. R. J. Price, H. R. W. Cobb
Application of the Weibull Statistical Theory to the Strength of Reactor Graphite, Proceedings of the Conference on Continuum Aspects of Graphite Design, Gatlinburg, 1970 (W. L. Greenstreet and G. C. Battle, Jr., Eds.), USAEC Report CINF-701105, Feb. 1972, p. 547

14. F. Lanza, H. Burg
Investigation of the Volume Effect on Mechanical Properties of Various Industrial Graphites, 11th Biennial Conference on Carbon, Gatlinburg 1973, Conference Proceedings, MP 4, p. 223

15. G. Kraus
to be published

16. J. E. Brocklehurst
ibidem ref. 9, p. 178

17. J. D. Buch
Mechanical Behaviour Model for Graphites, Properties Related to Fracture Thoughness, ASTM STP 605 (1976) 124

18. A. P. G. Rose and M. O. Tucker
A Fracture Criterion for Nuclear Graphite, Journal of Nuclear Materials, 110 (1982) 186 - 195

List of Figs

Fig. 1 a Lateral Plane $\varphi = 0°$ with Line Sections of the Fracture Surface for Different Values of Poissons Ratio

Fig. 1 b Lateral Plane $\varphi = 60°$ with Line Sections of the Fracture Surface for Different Values of Poisson's Ratio

Fig. 2 Fracture Surface as Projected Parallel to the Principal Diagonal

Fig. 3 Fracture Surface as Projected Parallel to the Direction $\theta = -30°$, $\varphi = 60°$

Fig. 4 Representation of the Modified Strain Energy and the Risk of Rupture for Triaxial Stresses (m = 2)

Fig. 5 Uniaxial Tensile Strength as a Function of Specimen Size V and Density ρ-Experimental and Theoretical - Graphite Grade V 483 T

Fig. 6 Uniaxial Tensile Strength as a Function of Specimen Size V and Density ρ-Experimental and Theoretical - Graphite Grade AS2-F-500

Fig. 7 Uniaxial Tensile Strength as a Function of Specimen Size V and Density ρ-Experimental and Theoretical - Graphite Grade M 2190

Fig. 8 Uniaxial Tensile Strength as a Function of Specimen Size V and Density ρ-Experimental and Theoretical - Graphite Grade H 451

Fig. 9 Geometry of Tested Specimens, Relative Abundances of Cracks and Critical Loads P with Standard Deviations Graphite Grade V 483 T

Fig. 10 Geometry of Tested Specimens, Relative Abundances of Cracks and Critical Loads P with Standard Deviations Graphite Grade AS2-F-500

Fig. 11 Geometry of Tested Specimens, Relative Abundances of Cracks and Critical Loads P with Standard Deviations Graphite Grade M 2190

Fig. 12 Dimensions of the Test Specimens as Shown in Fig. 9

Fig. 13 Dimensions of the Test Specimens as Shown in Figs. 10-11

Fig. 14 Partitioning into Statistical Cells of Size $\Delta F = 25$ mm² Specimen Type Ia Graphite Grade V 483 T

Fig. 15 Partitioning into Statistical Cells of Size $\Delta F = 25$ mm² Specimen Type Ib Graphite Grade V 483 T

Fig. 16 Partitioning into Statistical Cells of Size $\Delta F = 25$ mm² Specimen Type Ic Graphite Grade V 483 T

Fig. 17 Partitioning into Statistical Cells of Size $\Delta F = 25$ mm² Specimen Type Id Graphite Grade V 483 T

Fig. 18 Partitioning into Statistical Cells of Size $\Delta F = 25$ mm² Specimen Type IIa Graphite Grade V 483 T

Fig. 19 Partitioning into Statistical Cells of Size $\Delta F = 25$ mm² Specimen Type IIb Graphite Grade V 483 T

Fig. 20 Partitioning into Statistical Cells of Size $\Delta F = 25$ mm² Specimen Type IIc Graphite Grade V 483 T

Fig. 21 Partitioning into Statistical Cells of Size $\Delta F = 25$ mm² Specimen Type IId Graphite Grade V 483 T

Fig. 22 Partitioning into Statistical Cells of Size $\Delta F = 25$ mm^2
Specimen Type IIIa Graphite Grade V 483 T

Fig. 23 Partitioning into Statistical Cells of Size $\Delta F = 25$ mm^2
Specimen Type IIIb Graphite Grade V 483 T

Fig. 24 Partitioning into Statistical Cells of Size $\Delta F = 25$ mm^2
Specimen Type IIIc Graphite Grade V 483 T

Fig. 25 Partitioning into Statistical Cells of Size $\Delta F = 25$ mm^2
Specimen Type IIId Graphite Grade V 483 T

Fig. 26 Partitioning into Statistical Cells of Size $\Delta F = 25$ mm^2
Specimen Type IVa Graphite Grade V 483 T

Fig. 27 Partitioning into Statistical Cells of Size $\Delta F = 25$ mm^2
Specimen Type IVb Graphite Grade V 483 T

Fig. 28 Partitioning into Statistical Cells of Size $\Delta F = 25$ mm^2
Specimen Type IVc Graphite Grade V 483 T

Fig. 29 Partitioning into Statistical Cells of Size $\Delta F = 25$ mm^2
Specimen Type IVd Graphite Grade V 483 T

Fig. 30 Partitioning into Statistical Cells of Size $\Delta F = 110$ mm^2
Specimen Type Ia Graphite Grade AS2-F-500

Fig. 31 Partitioning into Statistical Cells of Size $\Delta F = 110$ mm^2
Specimen Type Ib Graphite Grade AS2-F-500

Fig. 32 Partitioning into Statistical Cells of Size $\Delta F = 110$ mm^2
Specimen Type Ic Graphite Grade AS2-F-500

Fig. 33 Partitioning into Statistical Cells of Size $\Delta F = 110$ mm^2
Specimen Type Id Graphite Grade AS2-F-500

Fig. 34 Partitioning into Statistical Cells of Size ΔF = 110 mm²
Specimen Type IIa Graphite Grade AS2-F-500

Fig. 35 Partitioning into Statistical Cells of Size ΔF = 110 mm²
Specimen Type IIb Graphite Grade AS2-F-500

Fig. 36 Partitioning into Statistical Cells of Size ΔF = 110 mm²
Specimen Type IIc Graphite Grade AS2-F-500

Fig. 37 Partitioning into Statistical Cells of Size ΔF = 110 mm²
Specimen Type IId Graphite Grade AS2-F-500

Fig. 38 Partitioning into Statistical Cells of Size ΔF = 110 mm²
Specimen Type IIIa Graphite Grade AS2-F-500

Fig. 39 Partitioning into Statistical Cells of Size ΔF = 110 mm²
Specimen Type IIIb Graphite Grade AS2-F-500

Fig. 40 Partitioning into Statistical Cells of Size ΔF = 110 mm²
Specimen Type IIIc Graphite Grade AS2-F-500

Fig. 41 Partitioning into Statistical Cells of Size ΔF = 110 mm²
Specimen Type IIId Graphite Grade AS2-F-500

Fig. 42 Partitioning into Statistical Cells of Size ΔF = 110 mm²
Specimen Type IVa Graphite Grade AS2-F-500

Fig. 43 Partitioning into Statistical Cells of Size ΔF = 110 mm²
Specimen Type IVb Graphite Grade AS2-F-500

Fig. 44 Partitioning into Statistical Cells of Size ΔF = 110 mm²
Specimen Type IVc Graphite Grade AS2-F-500

Fig. 45 Partitioning into Statistical Cells of Size ΔF = 110 mm²
Specimen Type IVd Graphite Grade AS2-F-500

Fig. 46 Partitioning into Statistical Cells of Size ΔF = 190 mm²
Specimen Type Ia Graphite Grade M 2190

Fig. 47 Partitioning into Statistical Cells of Size ΔF = 190 mm²
Specimen Type Ib Graphite Grade M 2190

Fig. 48 Partitioning into Statistical Cells of Size ΔF = 190 mm²
Specimen Type Ic Graphite Grade M 2190

Fig. 49 Partitioning into Statistical Cells of Size ΔF = 190 mm²
Specimen Type Id Graphite Grade M 2190

Fig. 50 Partitioning into Statistical Cells of Size ΔF = 190 mm²
Specimen Type IIa Graphite Grade M 2190

Fig. 51 Partitioning into Statistical Cells of Size ΔF = 190 mm²
Specimen Type IIb Graphite Grade M 2190

Fig. 52 Partitioning into Statistical Cells of Size ΔF = 190 mm²
Specimen Type IIc Graphite Grade M 2190

Fig. 53 Partitioning into Statistical Cells of Size ΔF = 190 mm²
Specimen Type IId Graphite Grade M 2190

Fig. 54 Partitioning into Statistical Cells of Size ΔF = 190 mm²
Specimen Type IIIa Graphite Grade M 2190

Fig. 55 Partitioning into Statistical Cells of Size ΔF = 190 mm²
Specimen Type IIIb Graphite Grade M 2190

Fig. 56 Partitioning into Statistical Cells of Size ΔF = 190 mm²
Specimen Type IIIc Graphite Grade M 2190

Fig. 57 Partitioning into Statistical Cells of Size ΔF = 190 mm²
Specimen Type IIId Graphite Grade M 2190

Fig. 58 Partitioning into Statistical Cells of Size ΔF = 190 mm^2 Specimen Type IV a Graphite Grade M 2190

Fig. 59 Partitioning into Statistical Cells of Size ΔF = 190 mm^2 Specimen Type IVb Graphite Grade M 2190

Fig. 60 Partitioning into Statistical Cells of Size ΔF = 190 mm^2 Specimen Type IVc Graphite Grade M 2190

Fig. 61 Partitioning into Statistical Cells of Size ΔF = 190 mm^2 Specimen Type IVd Graphite Grade M 2190

Fig. 62 Probabilities of Failure Calculated from Experimentally Found Averaged Critical Loads for Graphite Grade V 483 T

Fig. 63 Probabilities of Failure Calculated from Experimentally Found Averaged Critical Loads for Graphite Grade AS2-F-500

Fig. 64 Probabilities of Failure Calculated from Experimentally Found Averaged Critical Loads for Graphite Grade M 2190

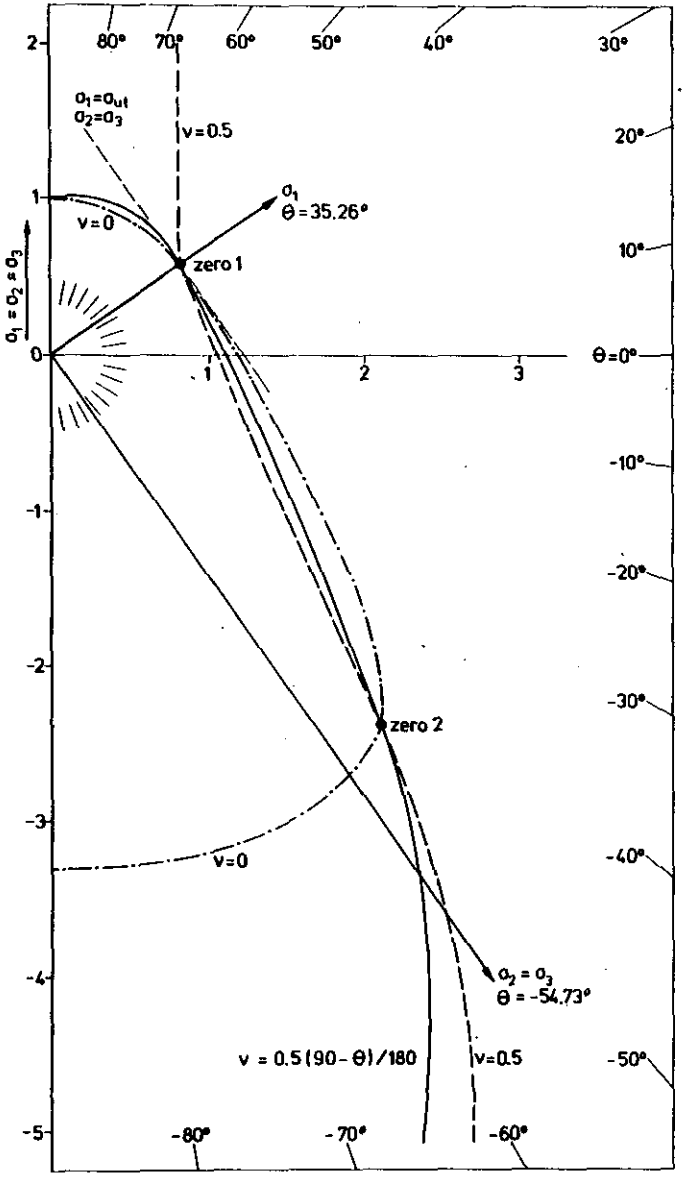

Fig. 1a : Lateral Plane $\varphi = 0°$ with Line Sections of the Fracture Surface for Different Values of Poisson's Ratio

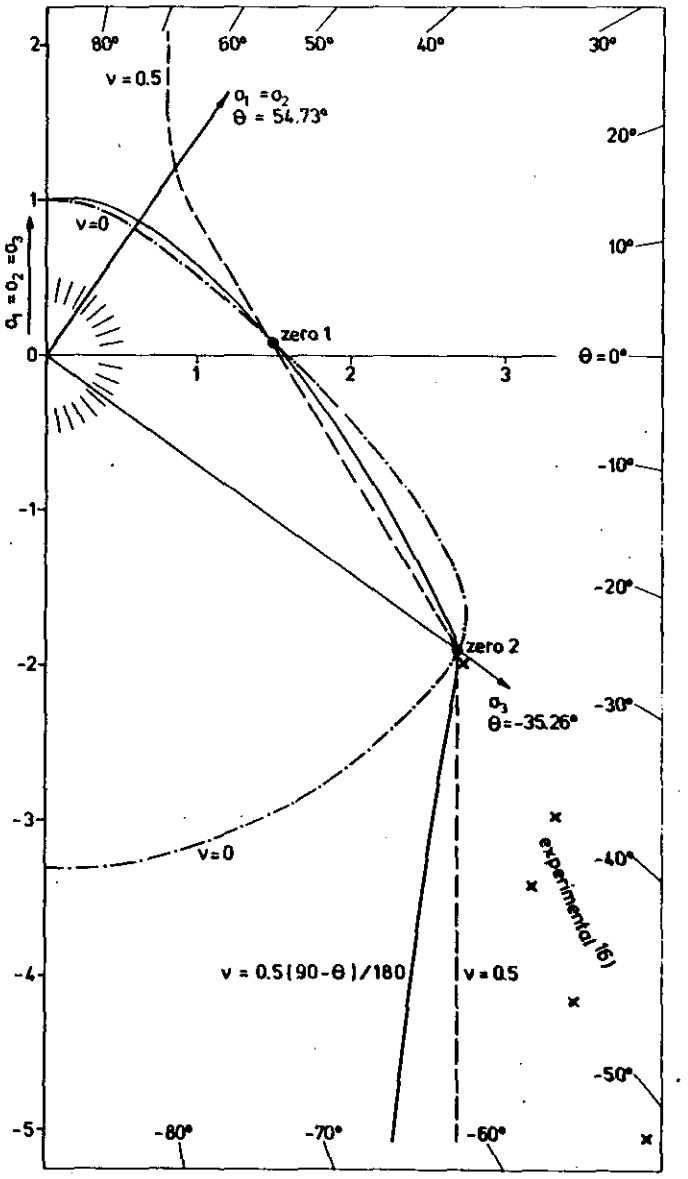

Fig. 1b : Lateral Plane $\varphi = 60°$ with Line Sections of the Fracture Surface for Different Values of Poisson's Ratio

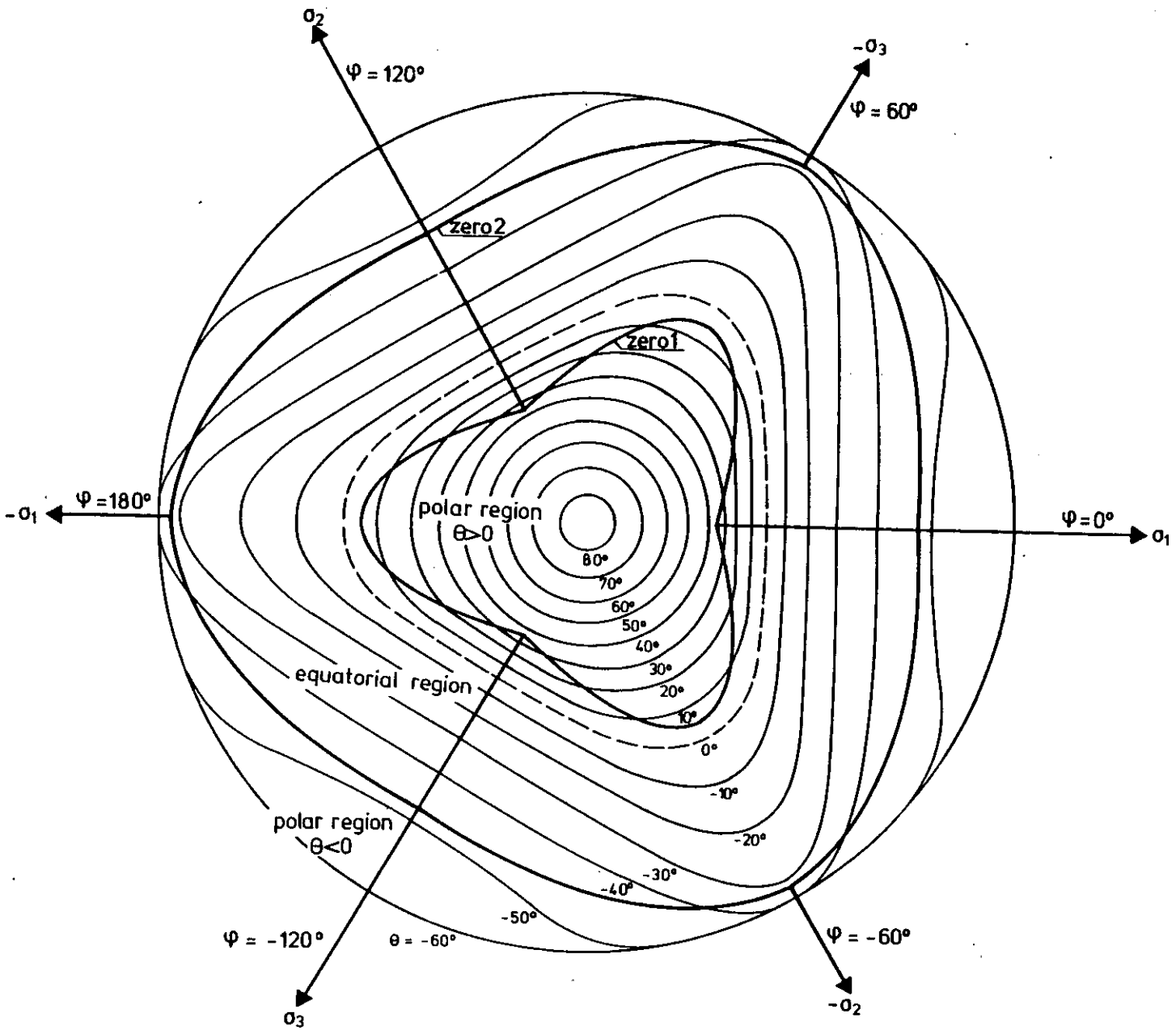

Fig. 2 : Fracture Surface as Projected Parallel to the Principal Diagonal

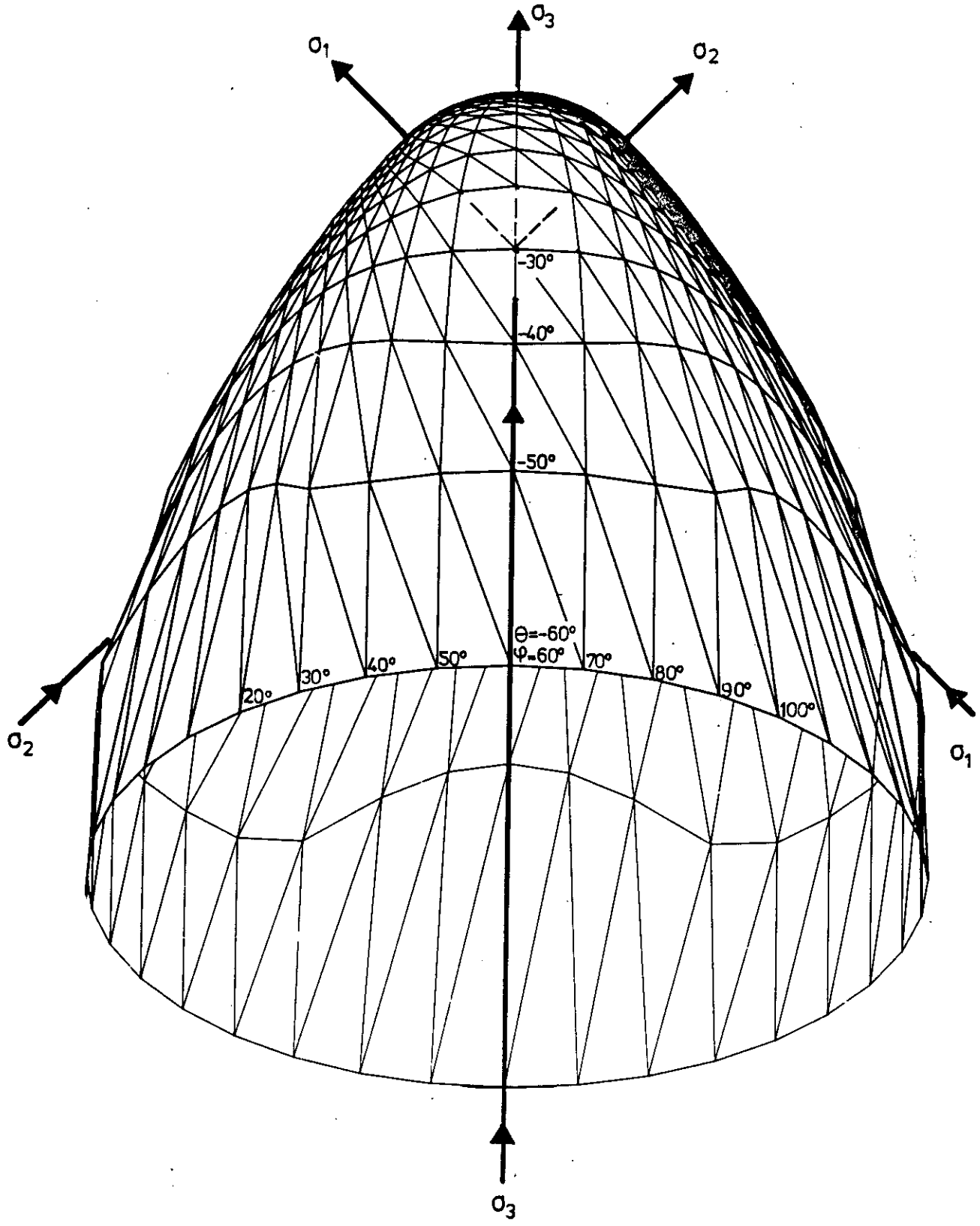

Fig. 3 : Fracture Surface as Projected Parallel to the Direction $\Theta = -30°$, $\varphi = 60°$

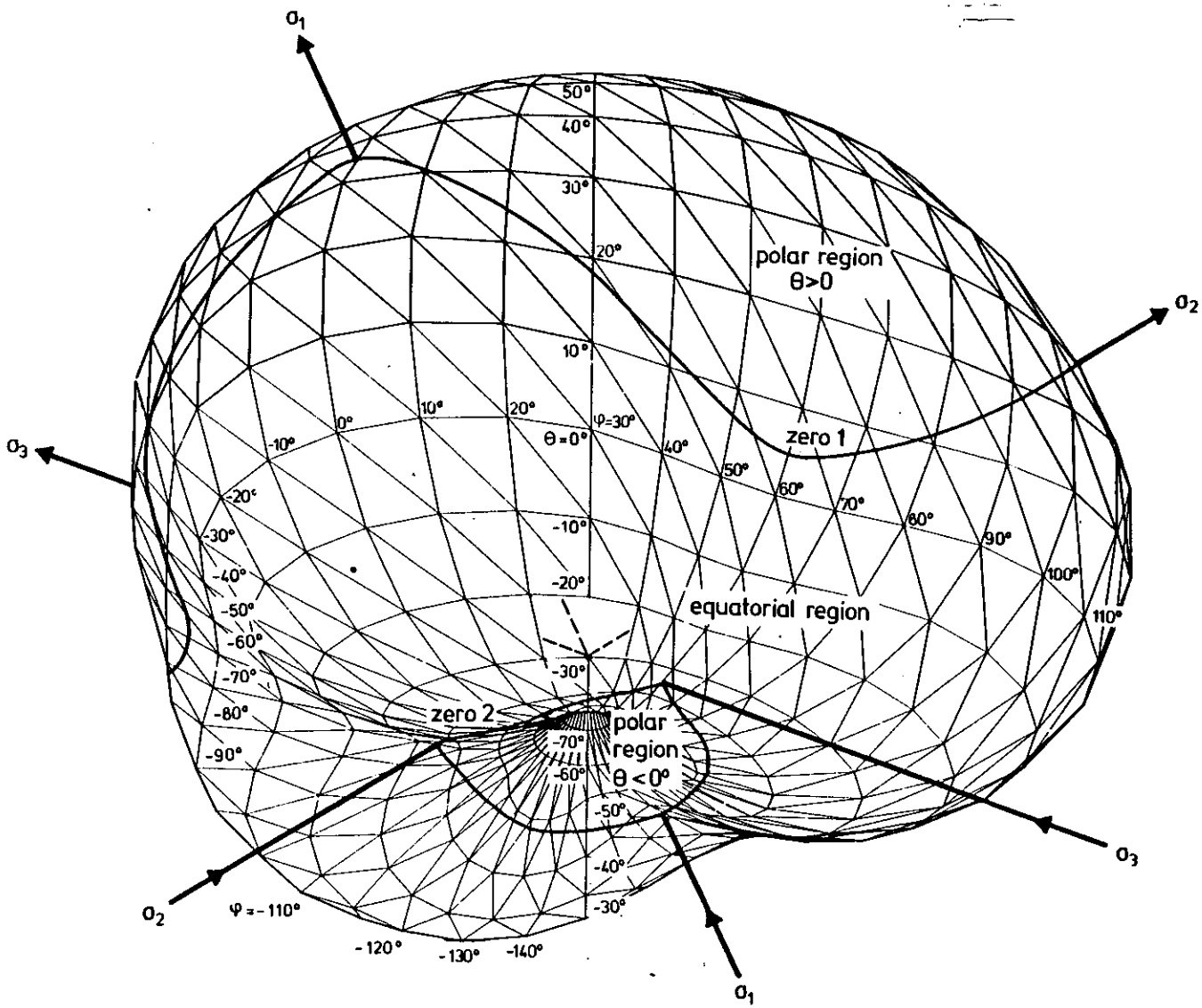

Fig.4 : Representation of the Modified Strain Energy and the Risk of Rupture for Triaxial Stresses (m = 2)

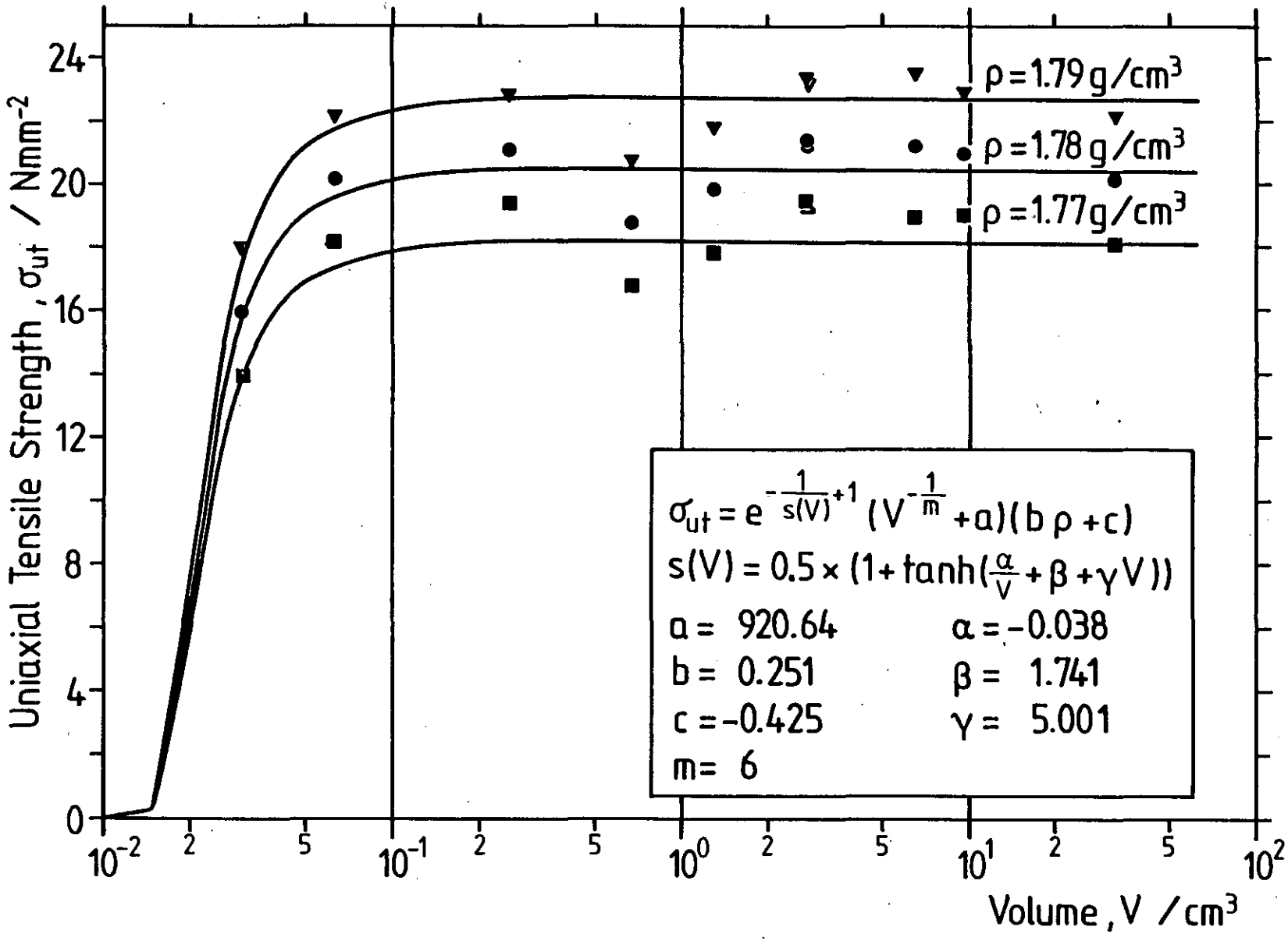

Fig.5 : Uniaxial Tensile Strength as a Function of Specimen Size V and Density ρ - Experimental and Theoretical - Graphite Grade V483T

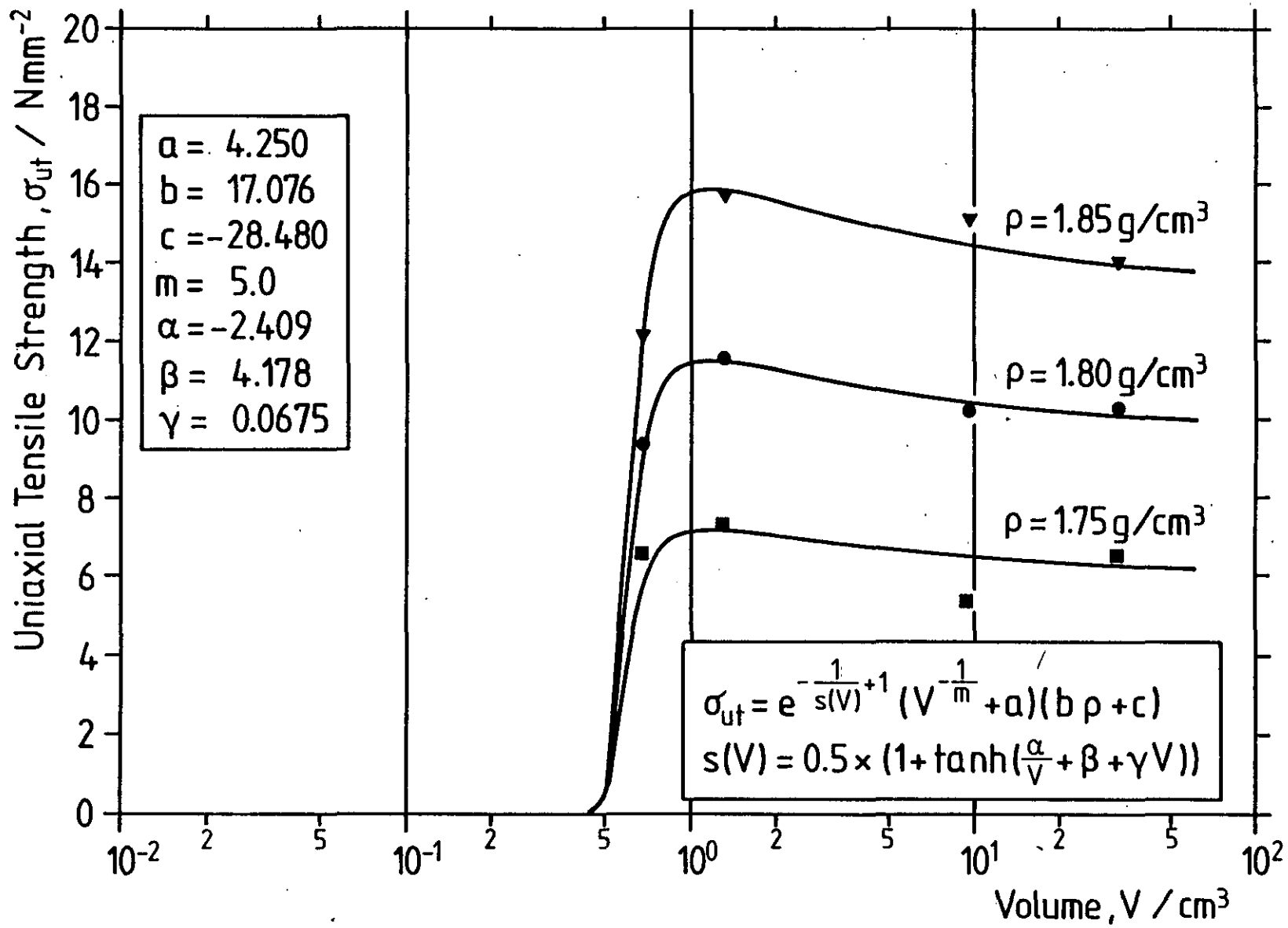

Fig. 6 : Uniaxial Tensile Strength as a Function of Specimen Size V and Density ρ - Experimental and Theoretical - Graphite Grade AS2-F-500

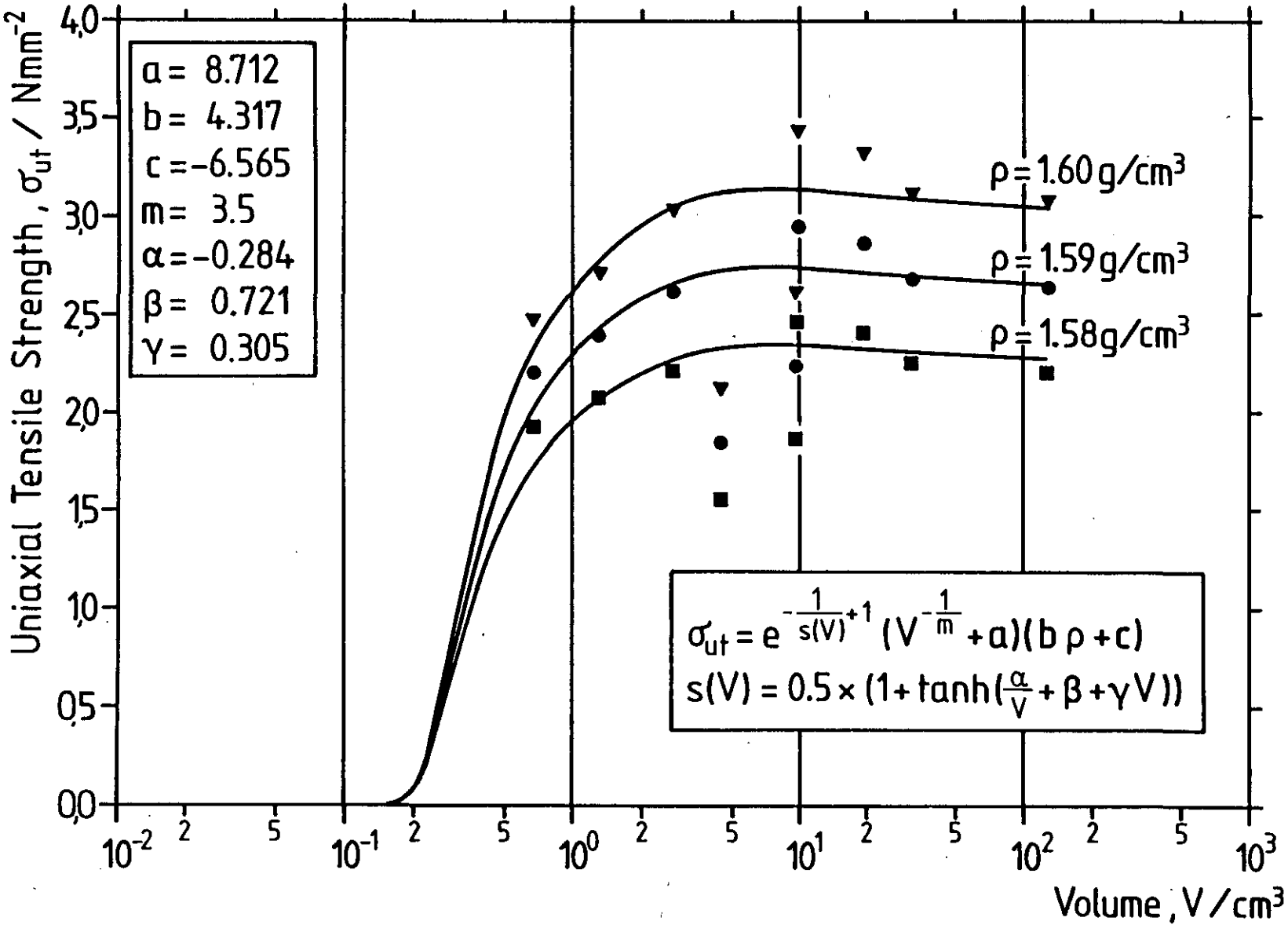

Fig. 7: Uniaxial Tensile Strength as a Function of Specimen Size V and Density ρ – Experimental and Theoretical – Graphite Grade M2190

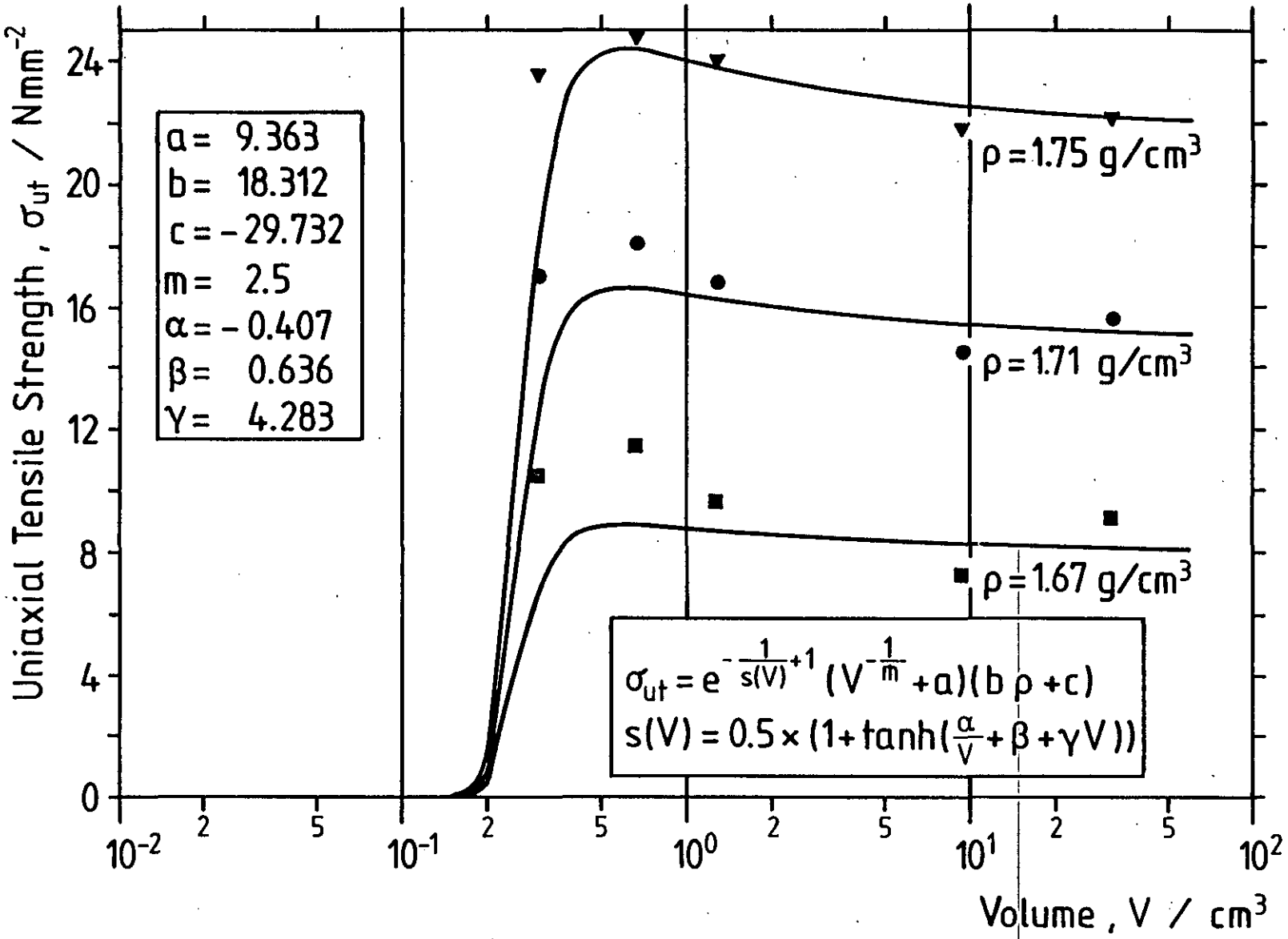

Fig. 8: Uniaxial Tensile Strength as a Function of Specimen Size V and Density ρ -Experimental and Theoretical - Graphite Grade H451

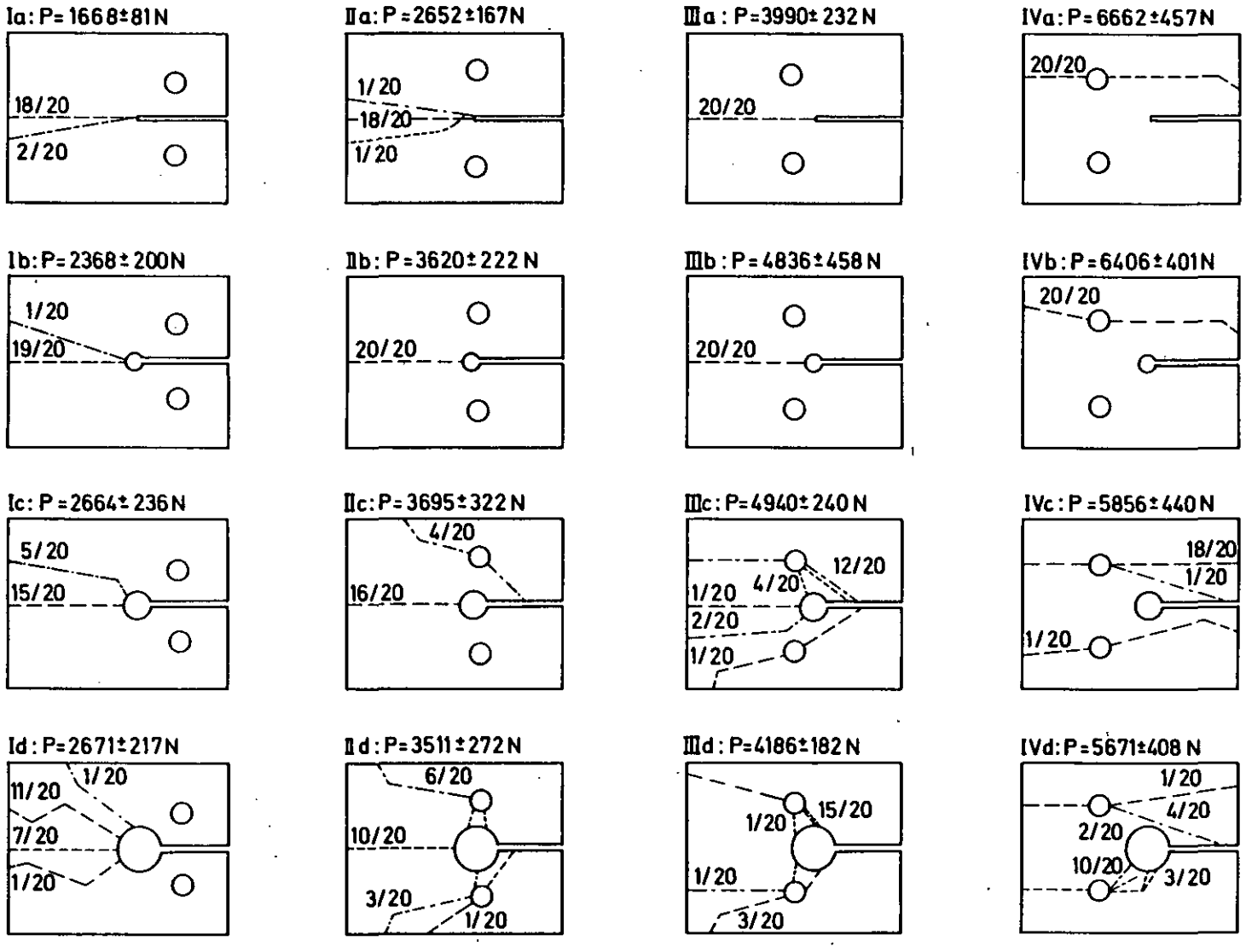

Fig. 9: Geometry of Tested Specimens, Relative Abundance of Cracks and Critical Loads P with Standard Deviations Graphite Grade V483T

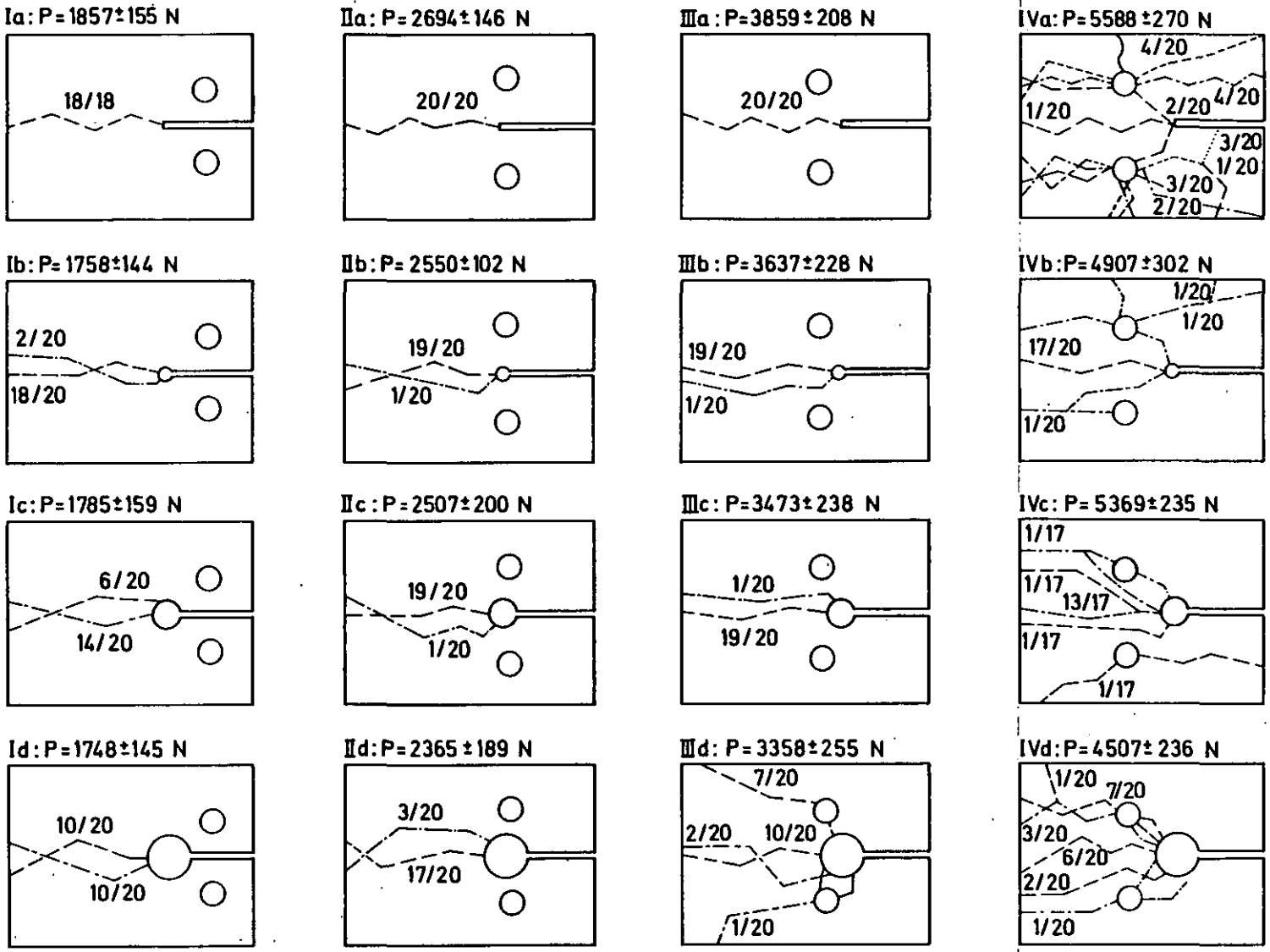

Fig. 10: Geometry of Tested Specimens, Relative Abundance of Cracks and Critical Loads P with Standard Deviations Graphite Grade AS2 -F- 500

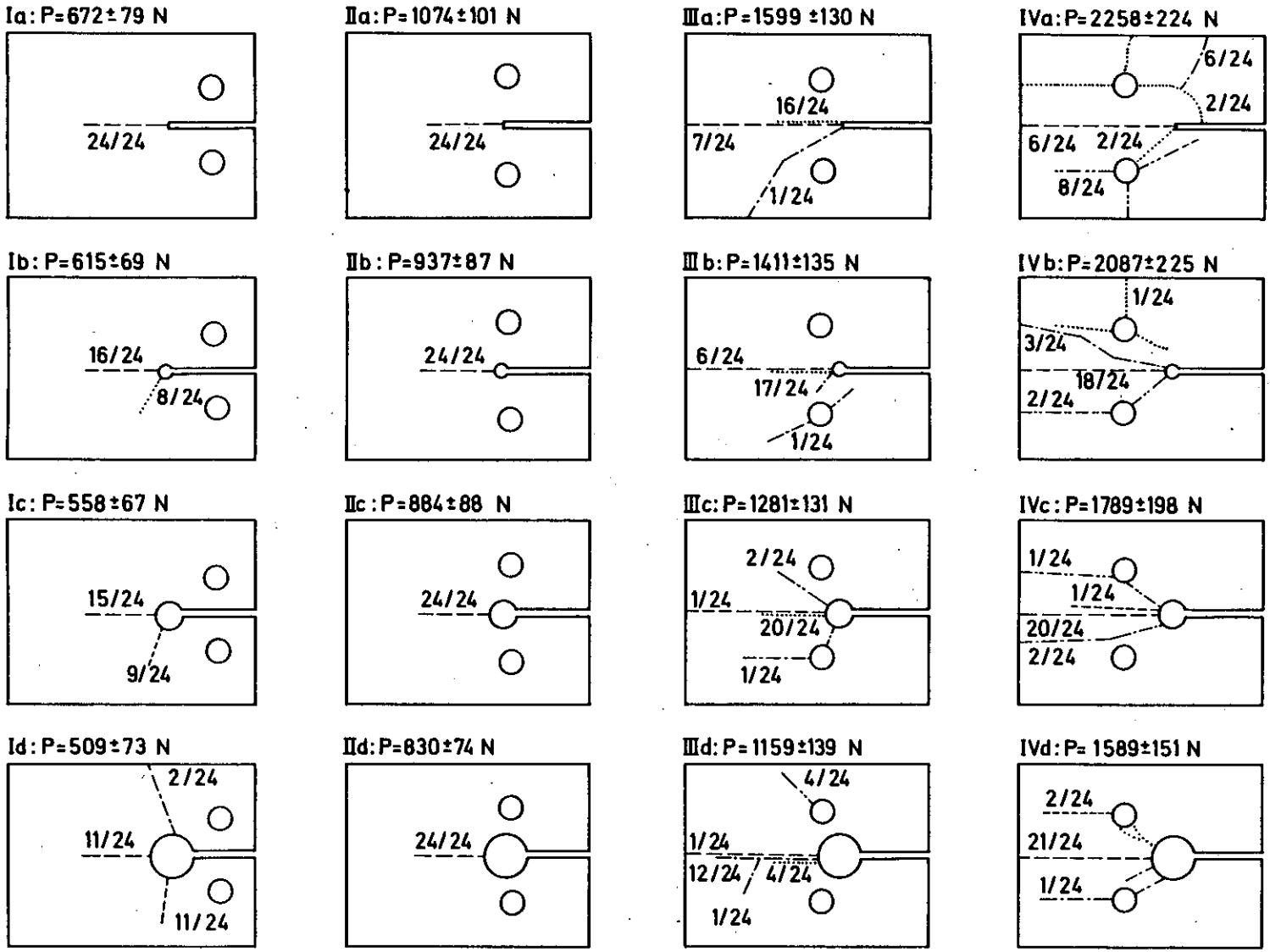

Fig.11: Geometry of Tested Specimens, Relative Abundance of Cracks and Critical Loads P with Standard Deviations Graphite Grade M 2190

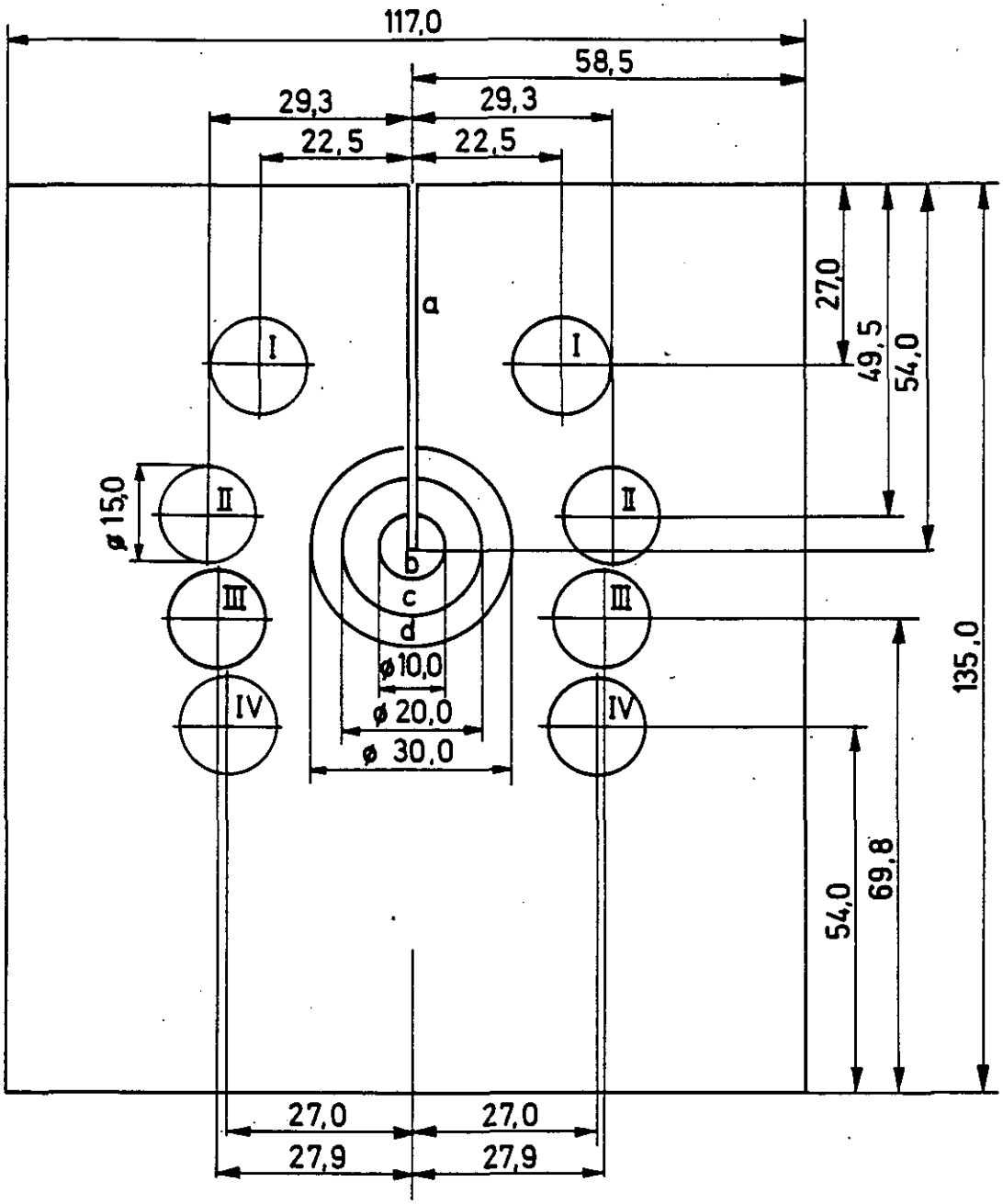

Fig. 12 : Dimensions of the Test Specimens as shown in Fig. 9 Units: mm, Thickness: 20mm

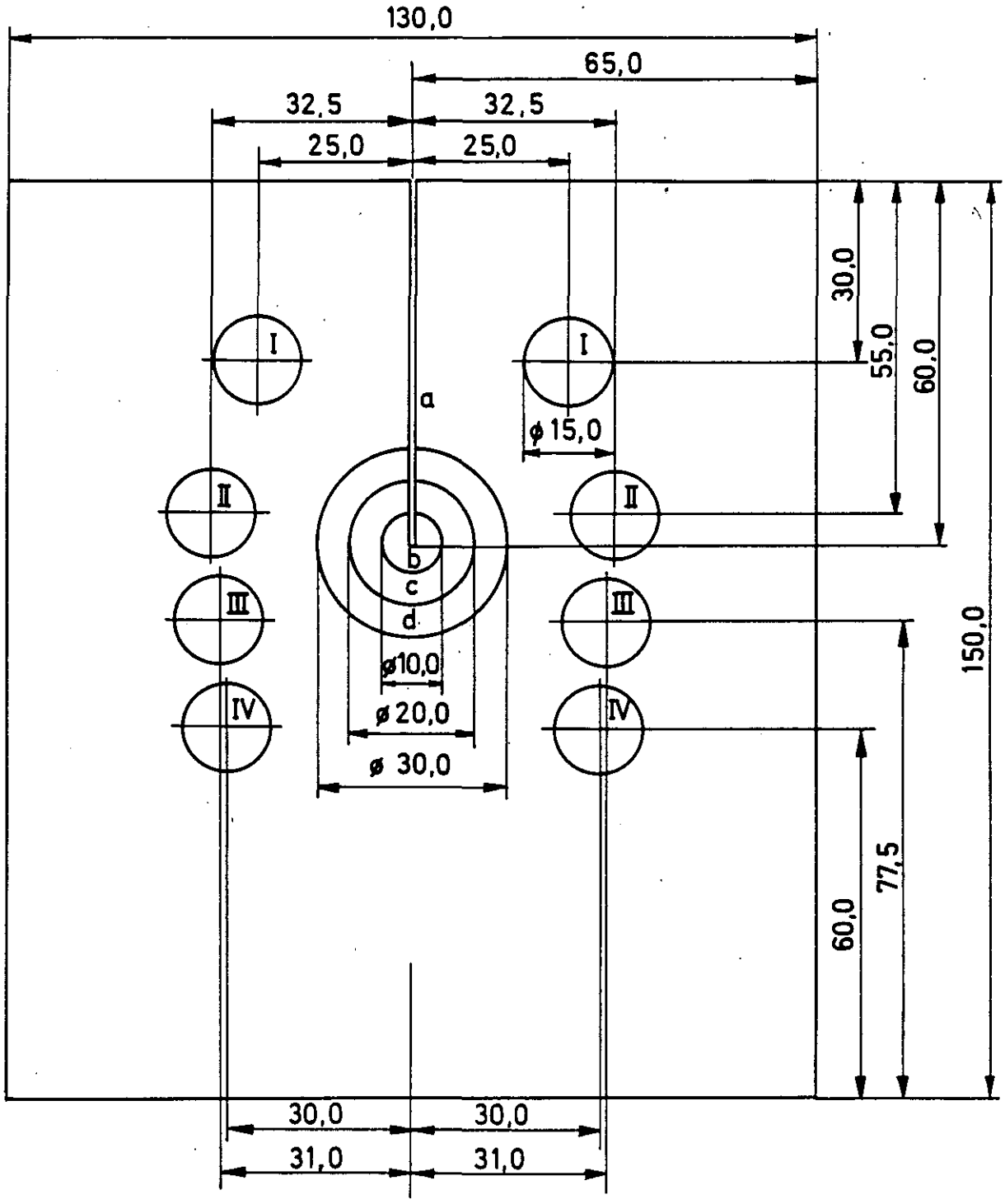

Fig. 13: Dimensions of the Test Specimens as shown in Figs. 10, 11
Units: mm, Thickness: 20mm

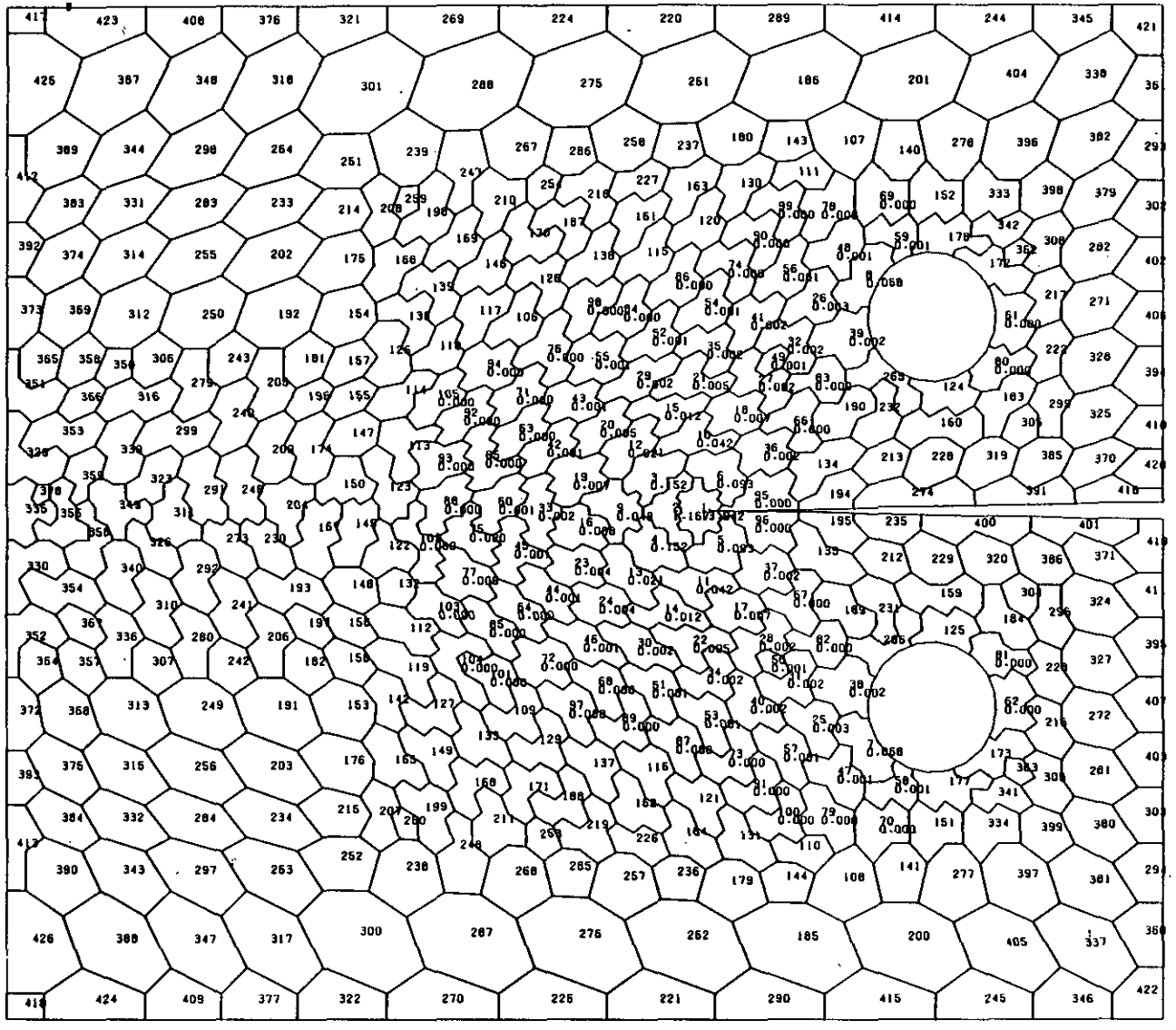

Fig. 14: Partitioning into Statistical Cells of Size $\Delta F = 25 mm^2$
Specimen Type Ia $n_{eff} = 2{,}21$ Graphite Grade V483T

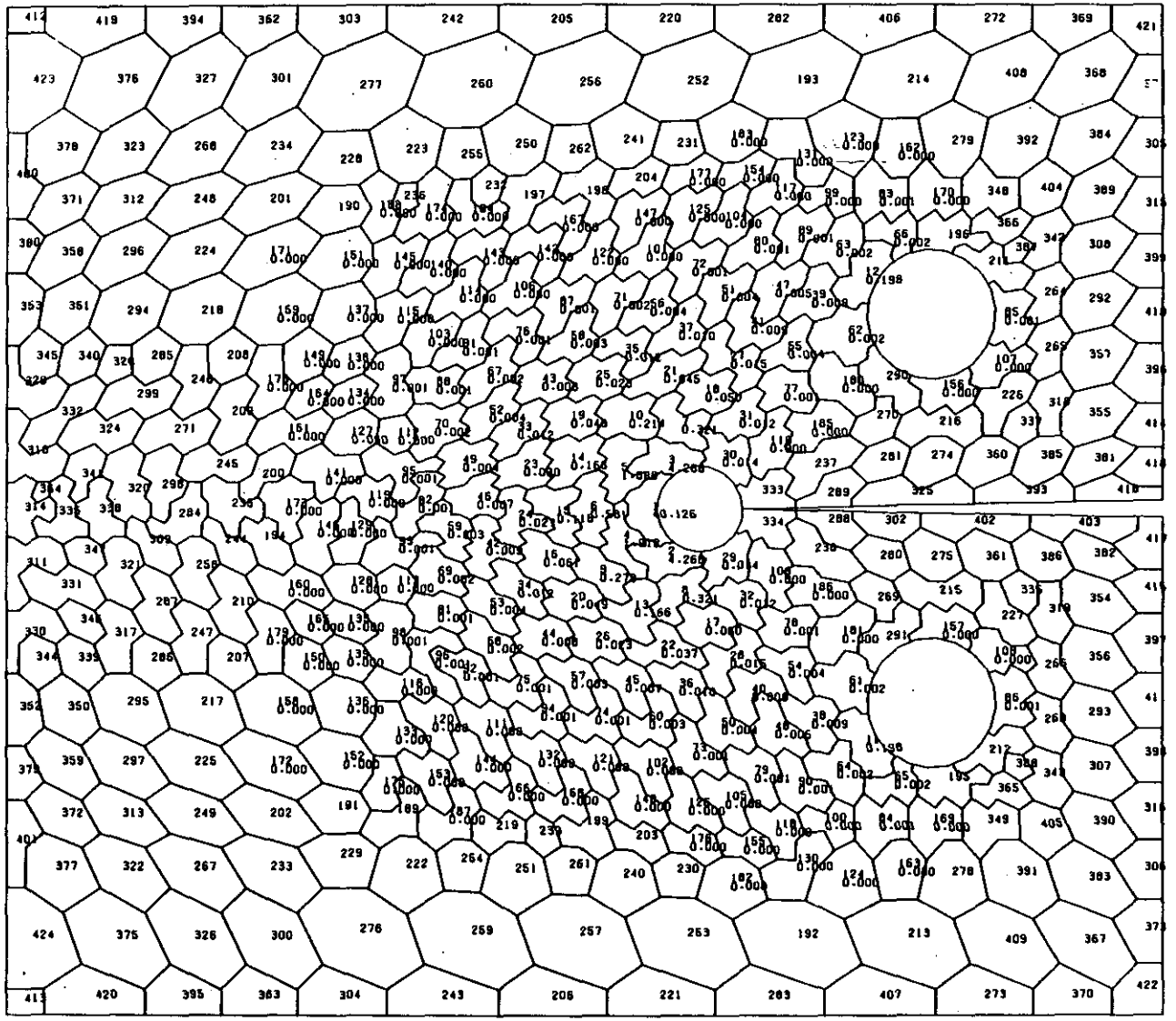

Fig. 15: Partitioning into Statistical Cells of Size $\Delta F = 25\,mm^2$
Specimen Type Ib $n_{eff} = 5{,}47$ Graphite Grade V483T

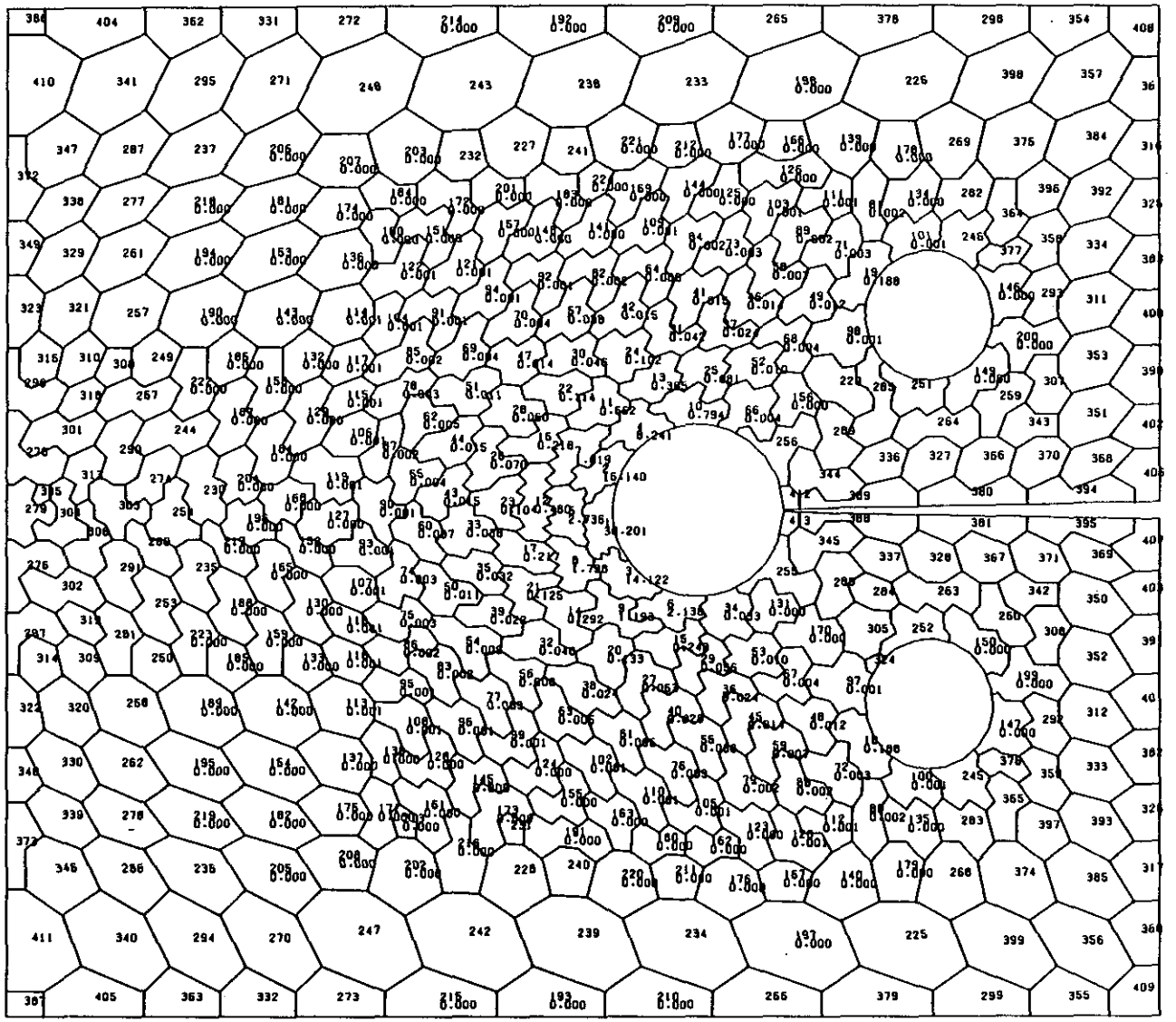

Fig.16: Partitioning into Statistical Cells of Size $\Delta F = 25mm^2$
Specimen Type Ic $n_{eff} = 9{,}30$ Graphite Grade V483 T

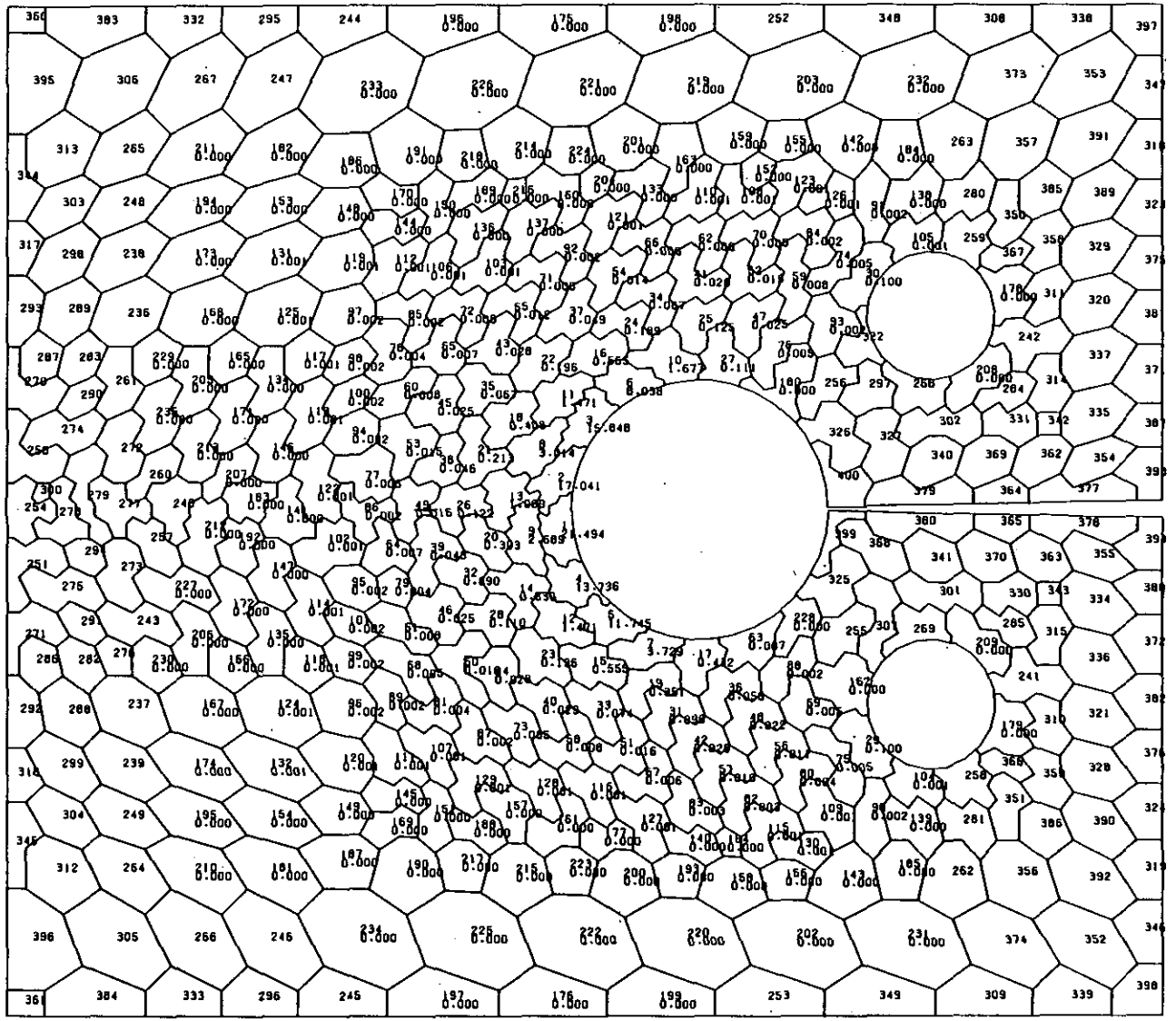

Fig.17 Partitioning into Statistical Cells of Size $\Delta F = 25\,mm^2$
Specimen Type Id $n_{eff} = 12{,}98$ Graphite Grade V483T

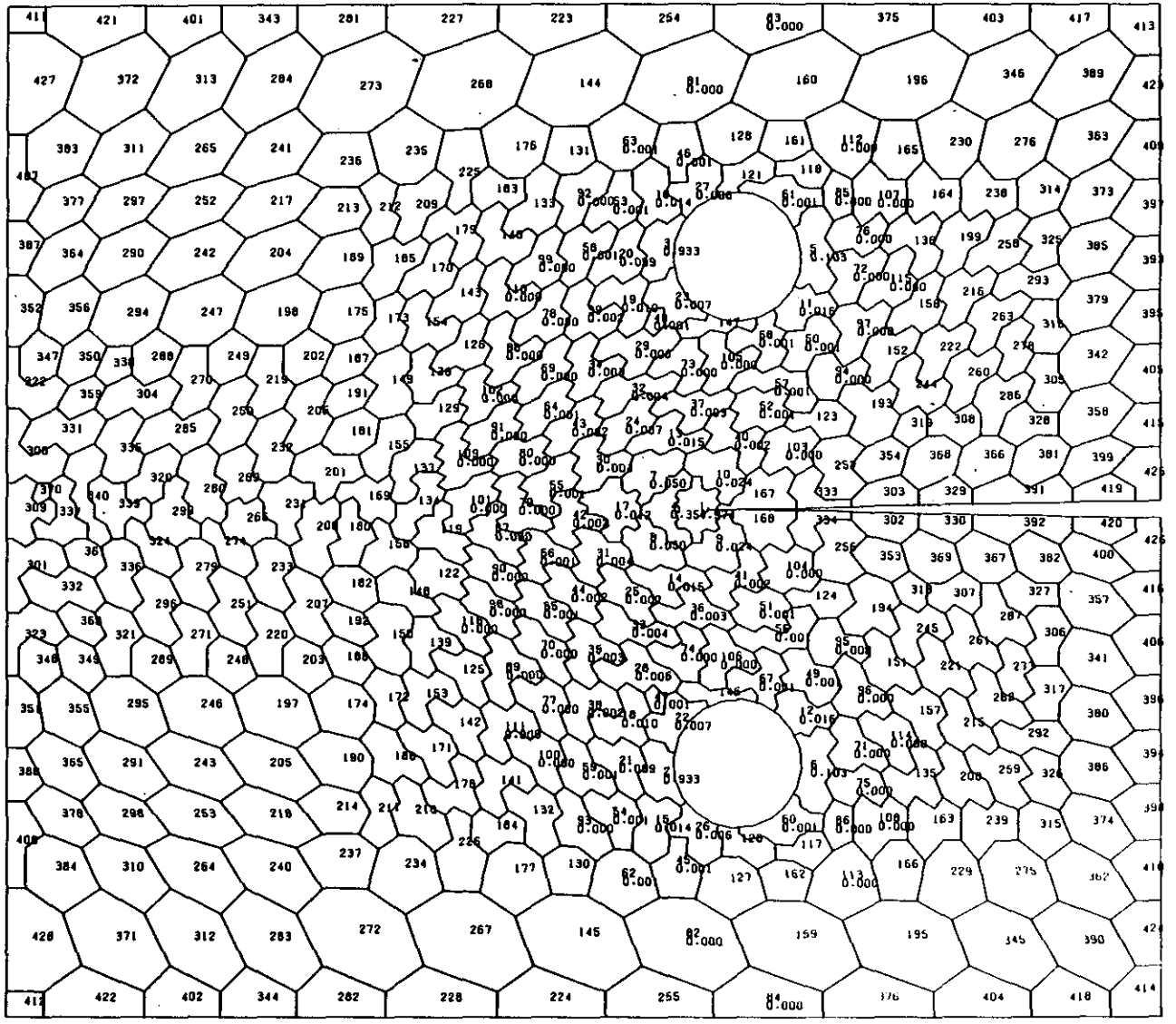

Fig.18 Partitioning into Statistical Cells of Size $\Delta F = 25 mm^2$
Specimen Type IIa $n_{eff} = 4,32$ Graphite Grade V483T

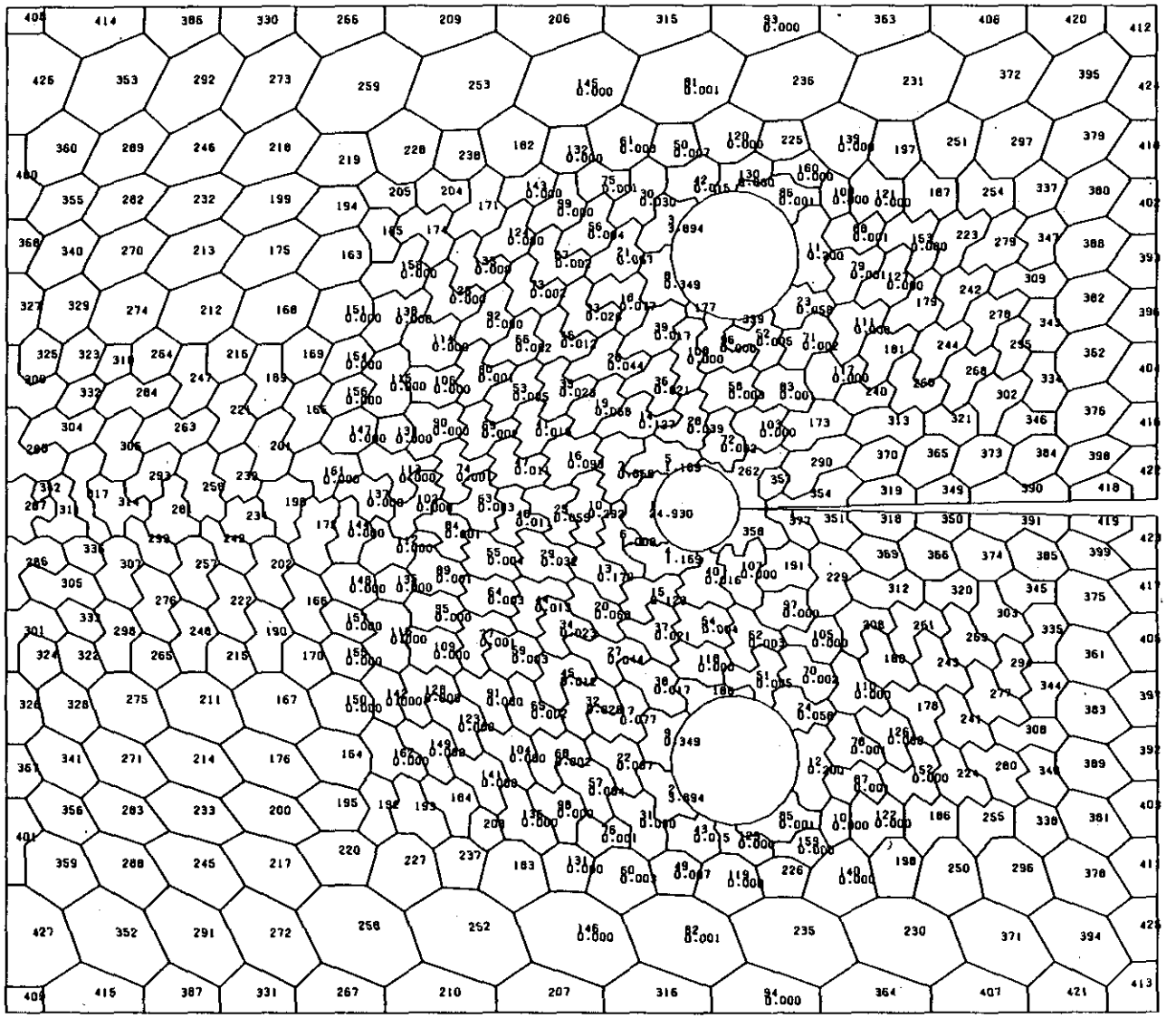

Fig.19: Partitioning into Statistical Cells of Size $\Delta F = 25 mm^2$
Specimen Type IIb $n_{eff} = 7,67$ Graphite Grade V483T

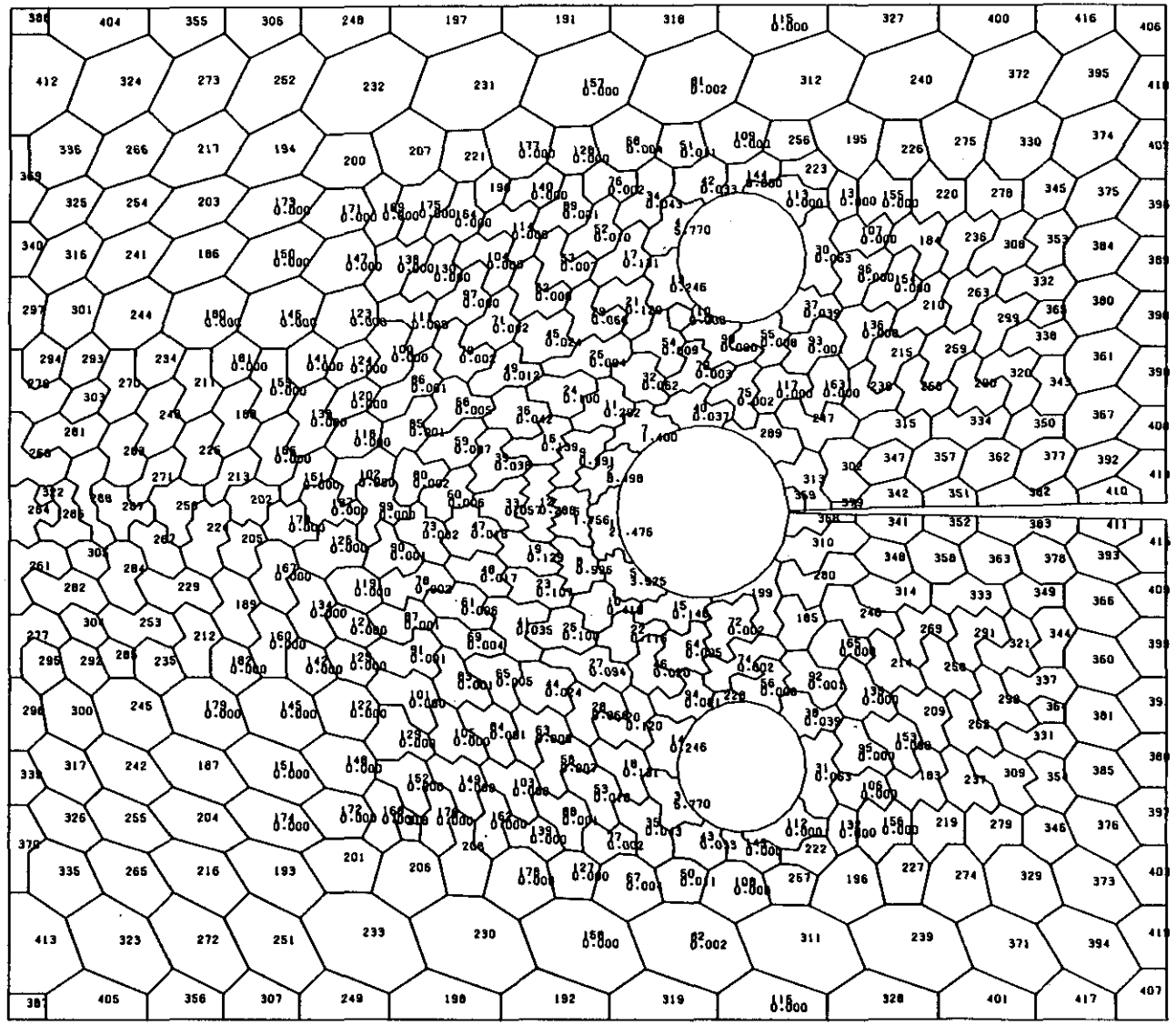

Fig. 20: Partitioning into Statistical Cells of Size $\Delta F = 25\,mm^2$
Specimen Type IIc $n_{eff} = 10{,}06$ Graphite Grade V483T

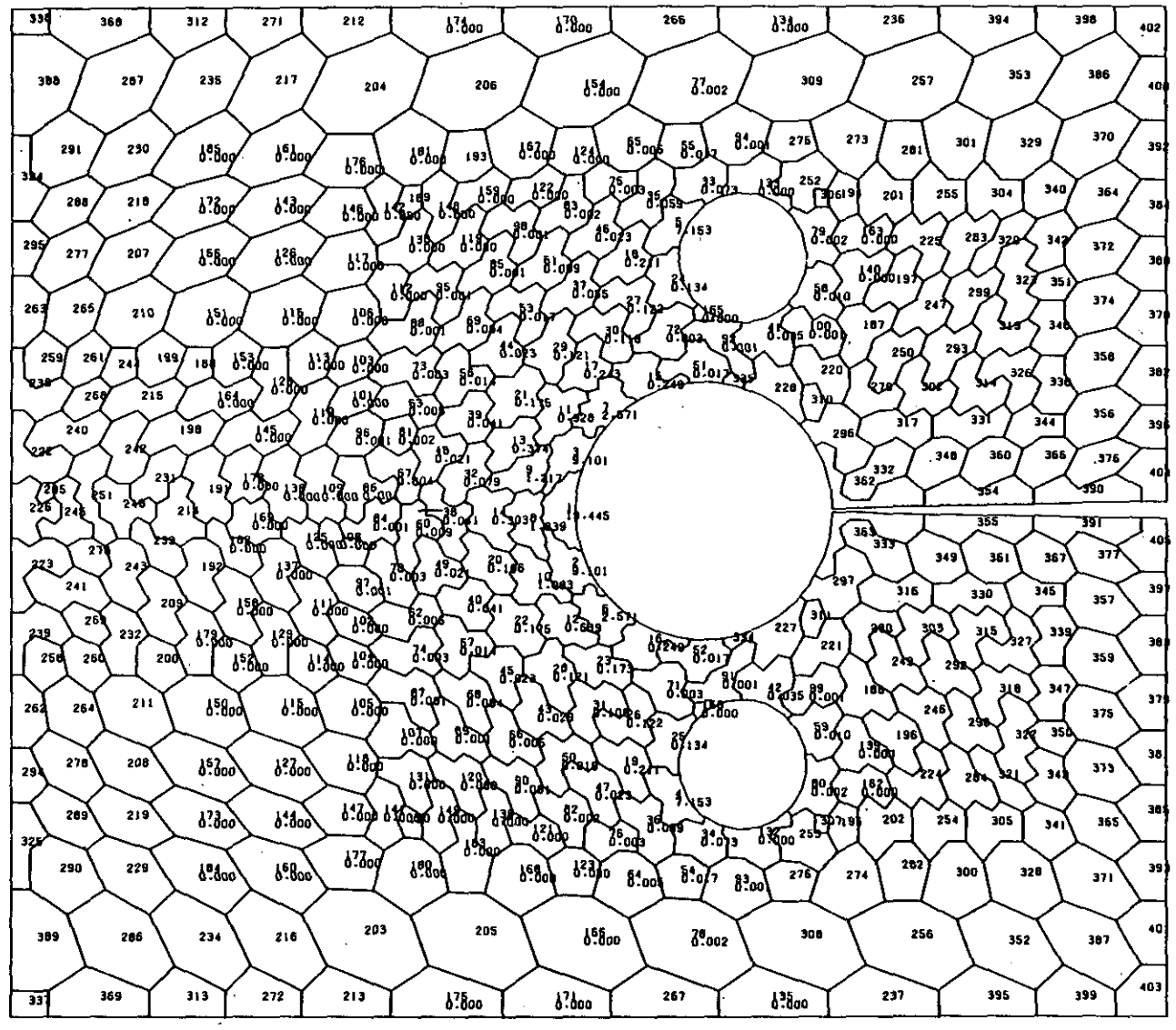

Fig. 21: Partitioning into Statistical Cells of Size $\Delta F = 25\,mm^2$
Specimen Type IId $n_{eff} = 12{,}03$ Graphite Grade V483T

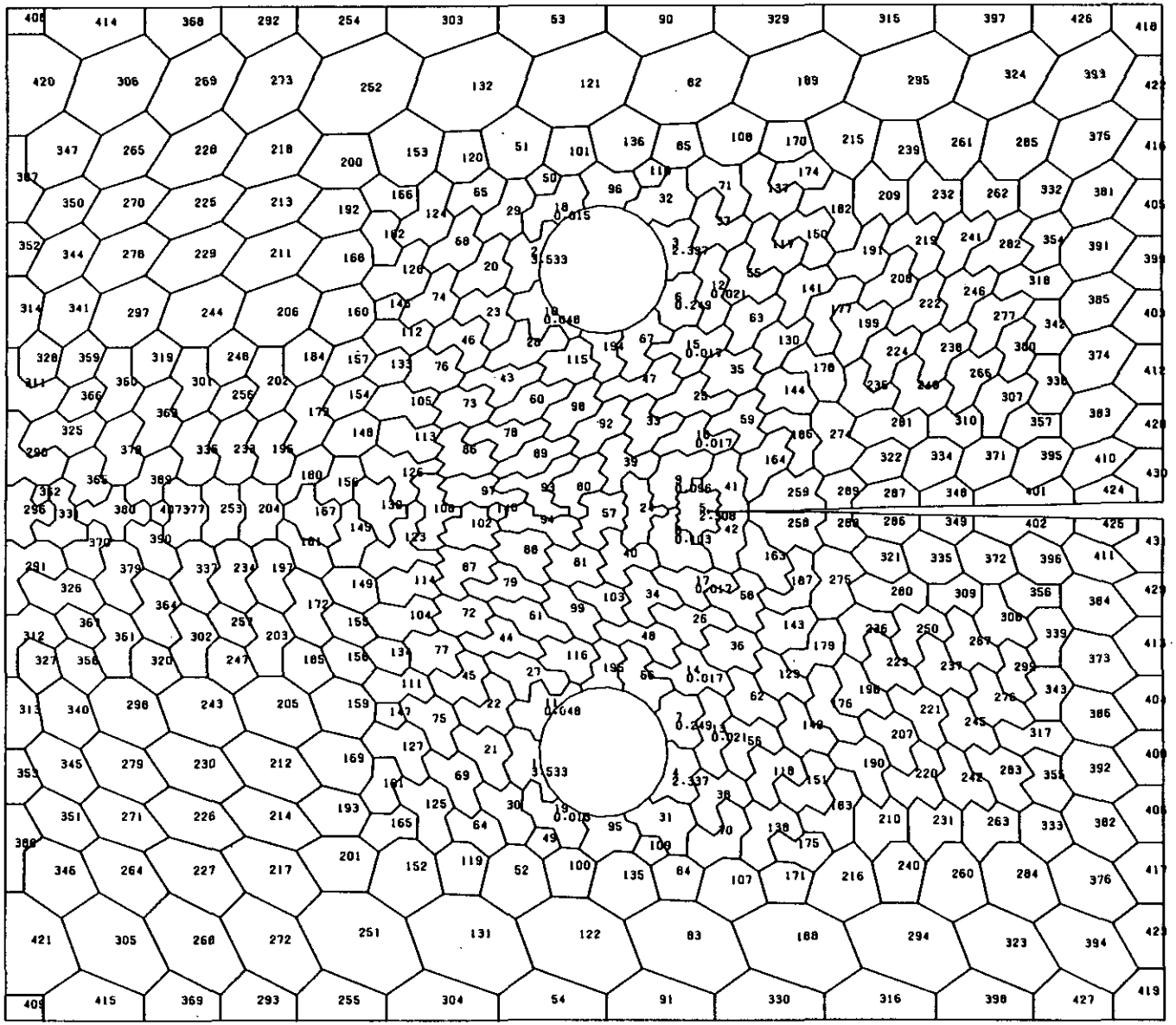

Fig.22: Partitioning into Statistical Cells of Size $\Delta F = 25 mm^2$
Specimen Type IIIa $n_{eff} = 6{,}37$ Graphite Grade V483T

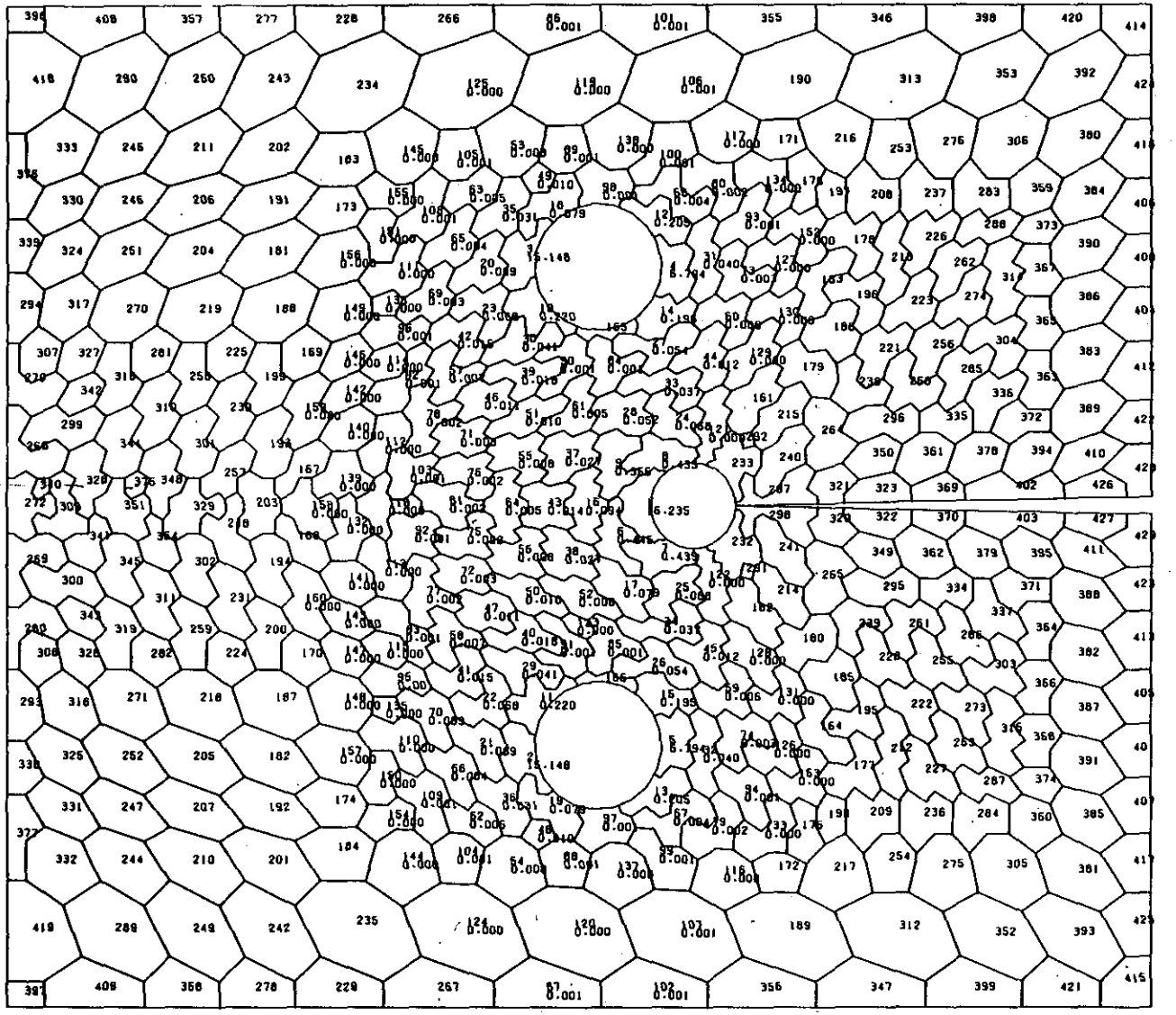

Fig.23: Partitioning into Statistical Cells of Size $\Delta F = 25 mm^2$
Specimen Type IIIb $n_{eff} = 7,47$ Graphite Grade V 483 T

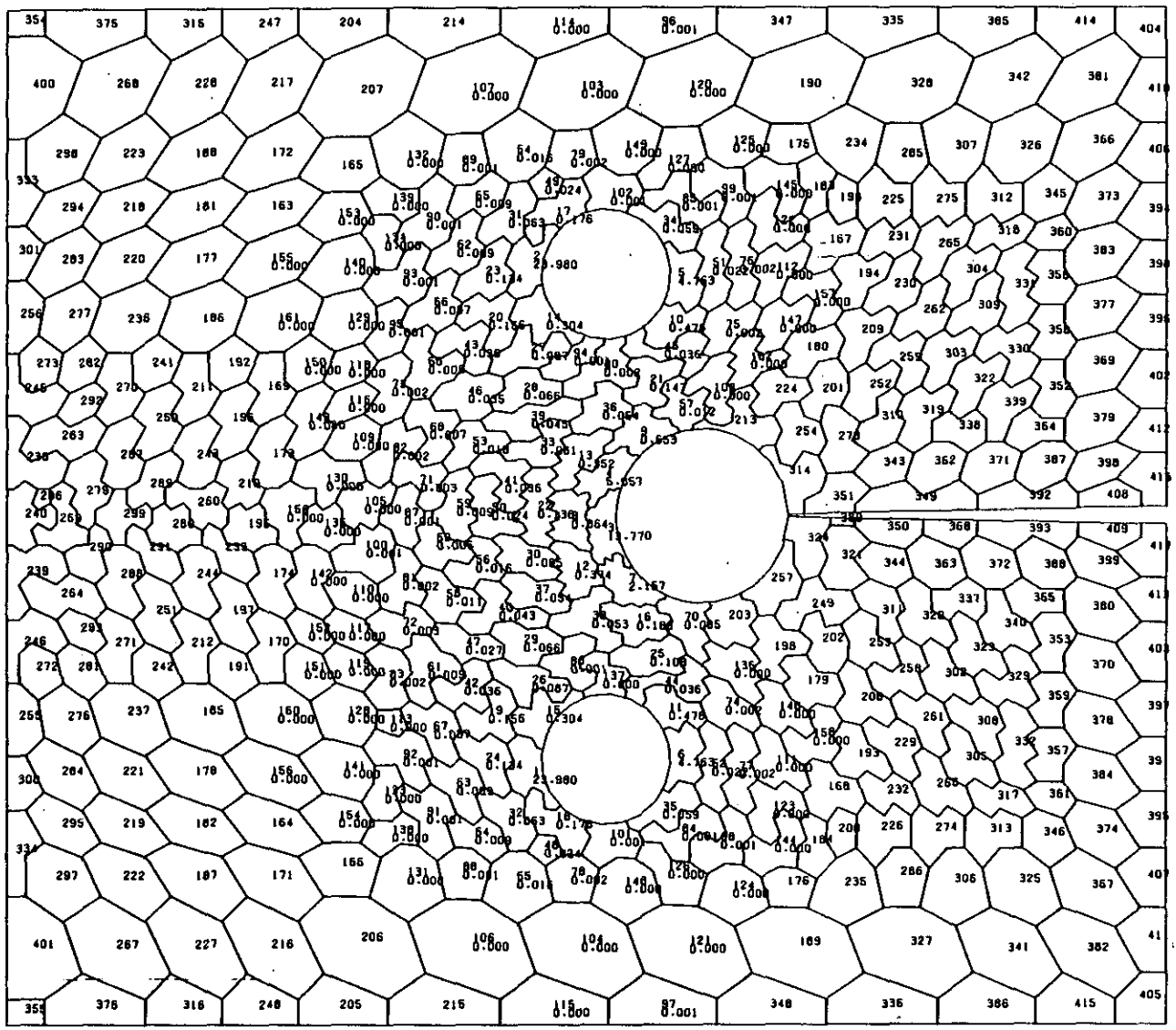

Fig.24: Partitioning into Statistical Cells of Size $\Delta F = 25\,mm^2$
Specimen Type IIIc $n_{eff} = 10,27$ Graphite Grade V483T

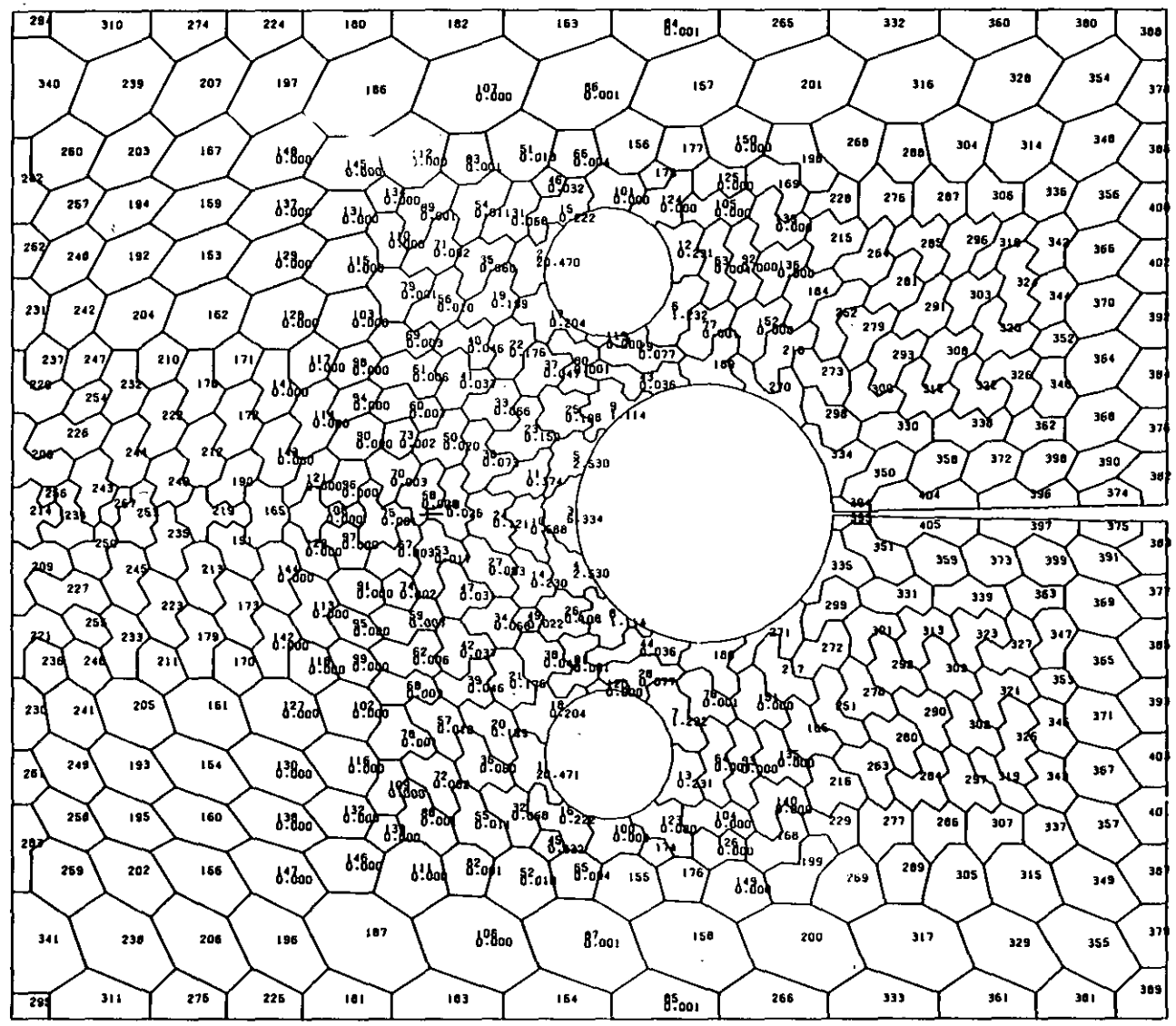

Fig. 25: Partitioning into Statistical Cells of Size $\Delta F = 25\,mm^2$
Specimen Type IIId $n_{eff} = 10{,}95$ Graphite Grade V483T

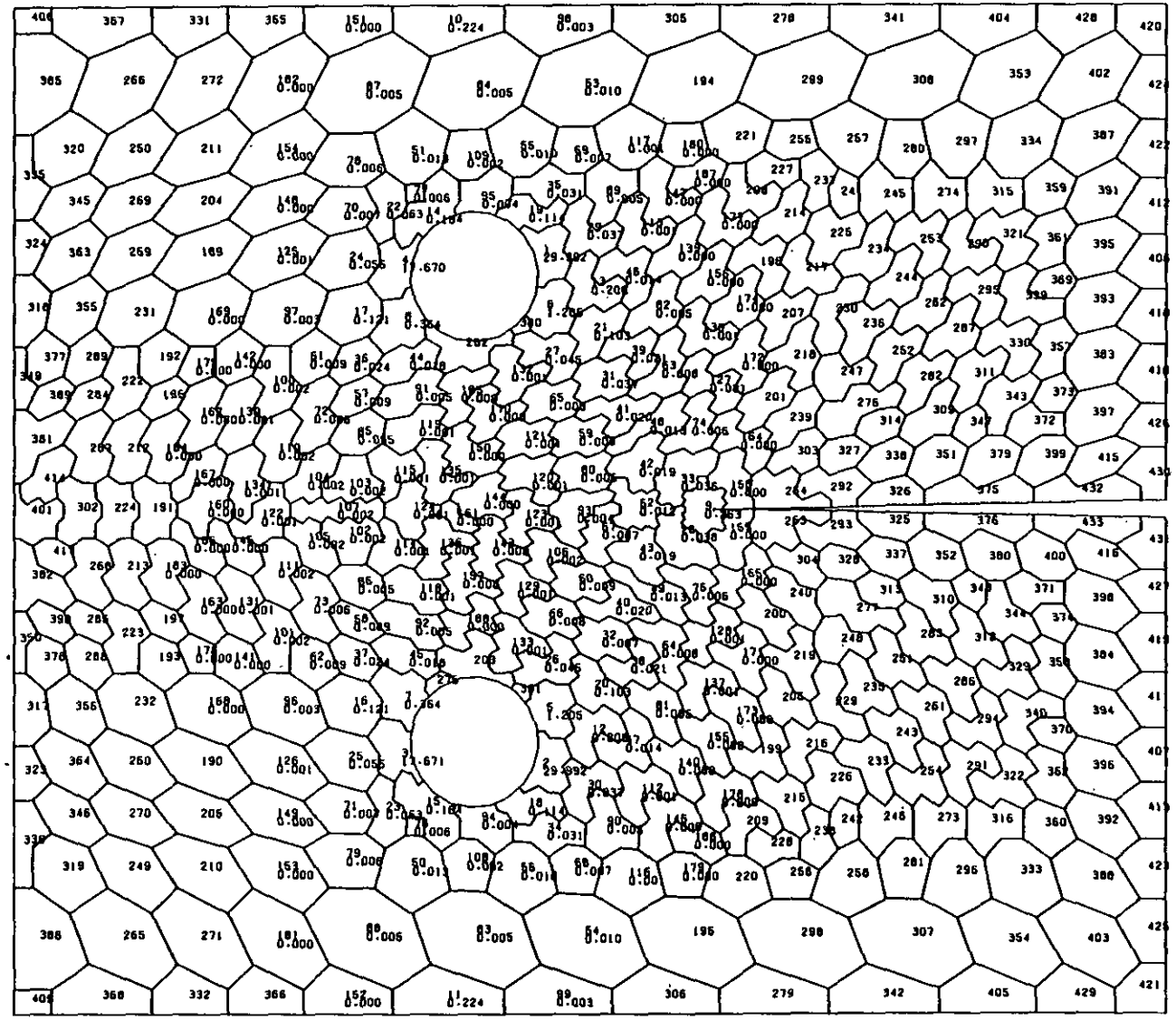

Fig.26: Partitioning into Statistical Cells of Size $\Delta F = 25 mm^2$
Specimen Type IVa $n_{eff} = 7{,}52$ Graphite Grade V483T

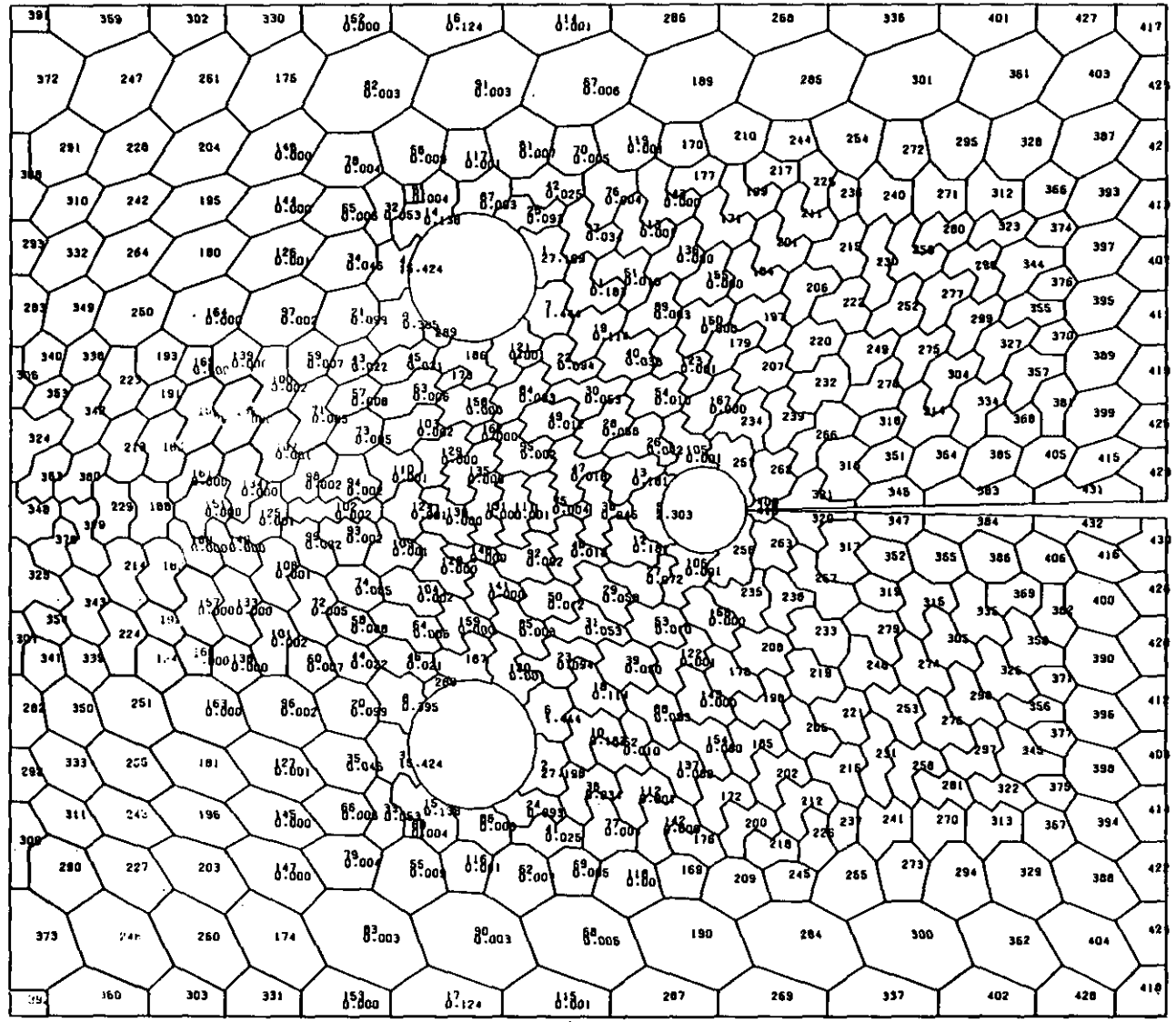

Fig.27: Partitioning into Statistical Cells of Size $\Delta F = 25 mm^2$
Specimen Type IVb $n_{eff} = 8{,}00$ Graphite Grade V483T

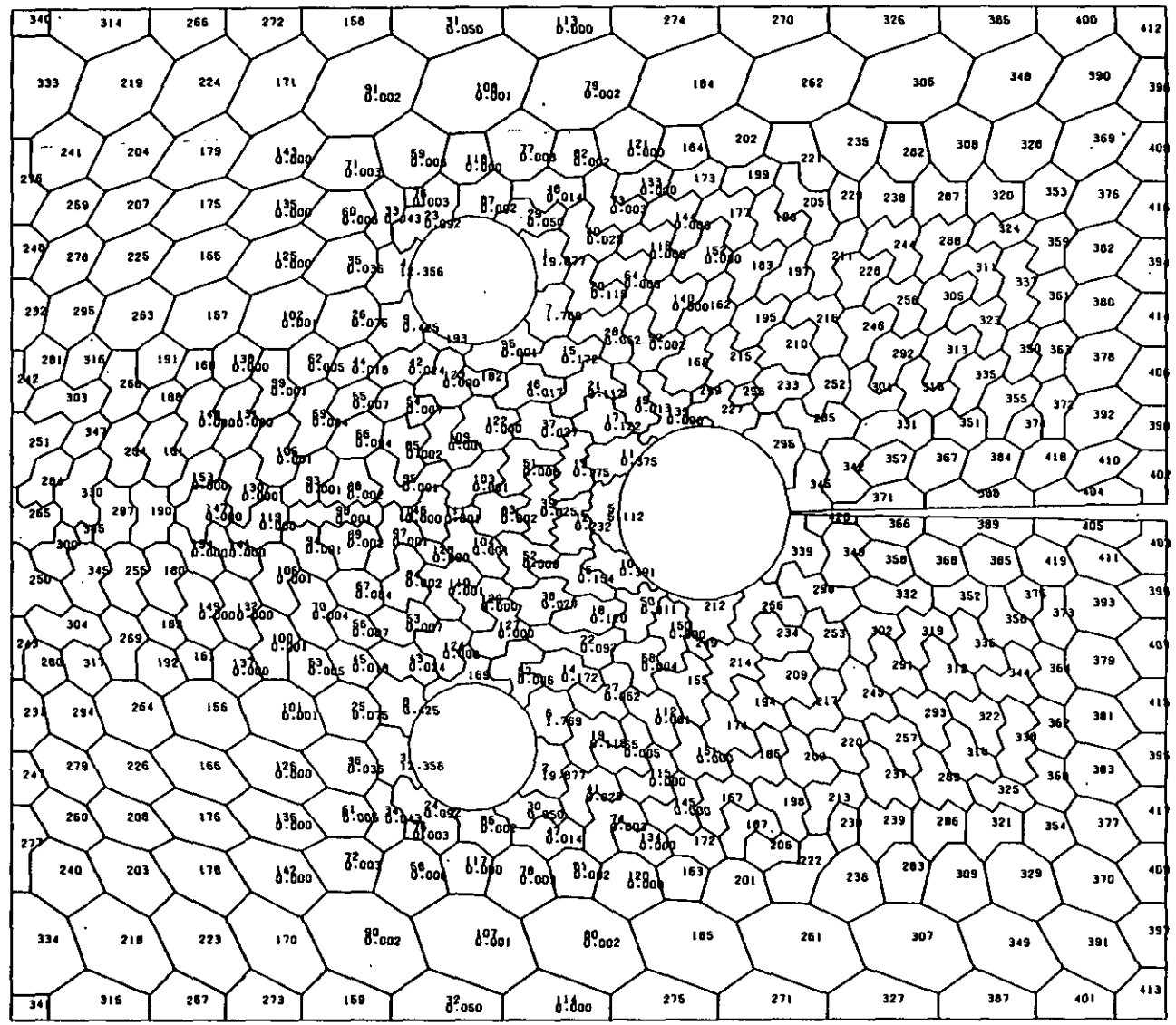

Fig.28: Partitioning into Statistical Cells of Size $\Delta F = 25 mm^2$
Specimen Type IVc $n_{eff} = 8,22$ Graphite Grade V483T

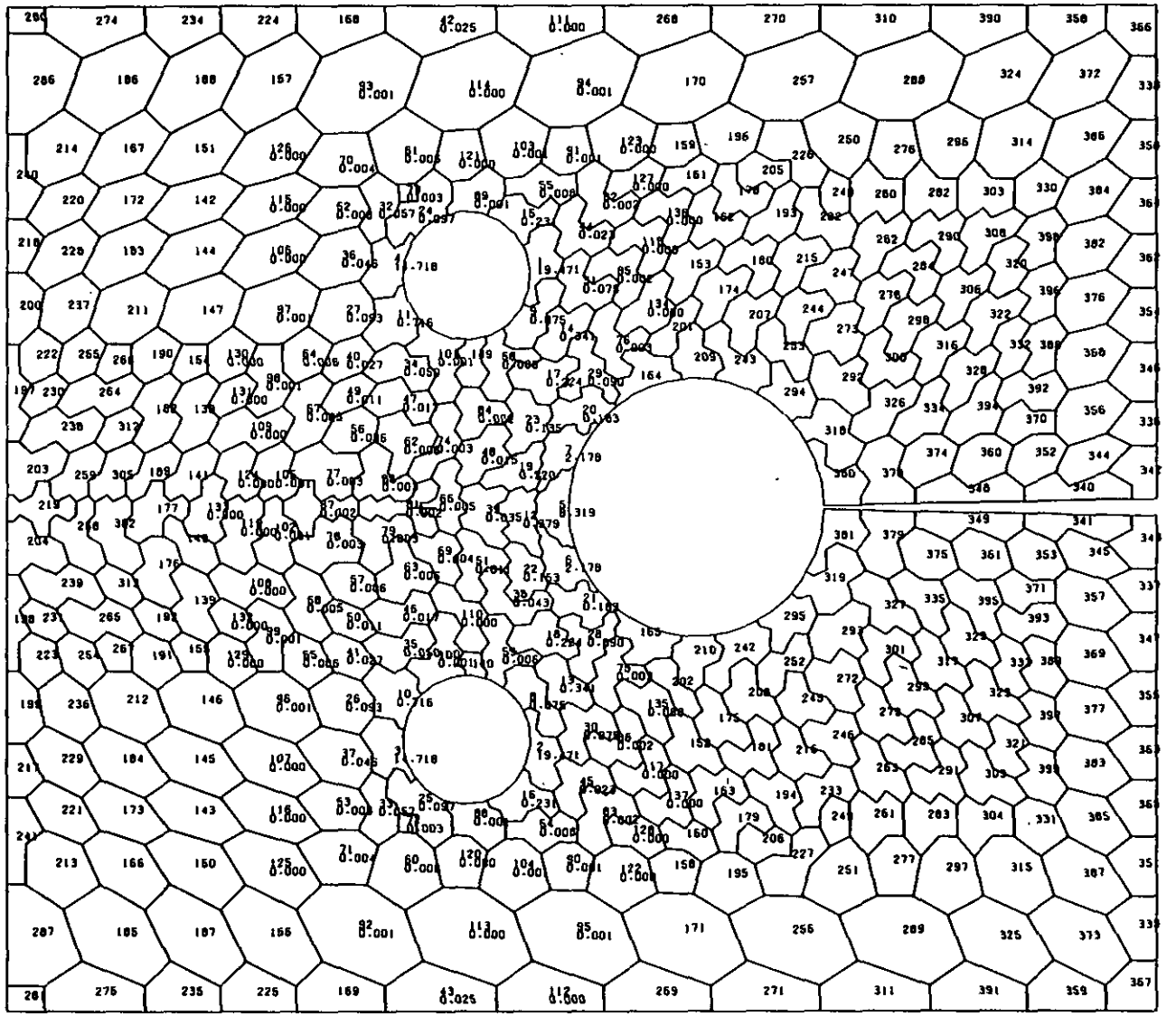

Fig.29: Partitioning into Statistical Cells of Size $\Delta F = 25 mm^2$
Specimen Type IVd neff = 9,73 Graphite Grade V483T

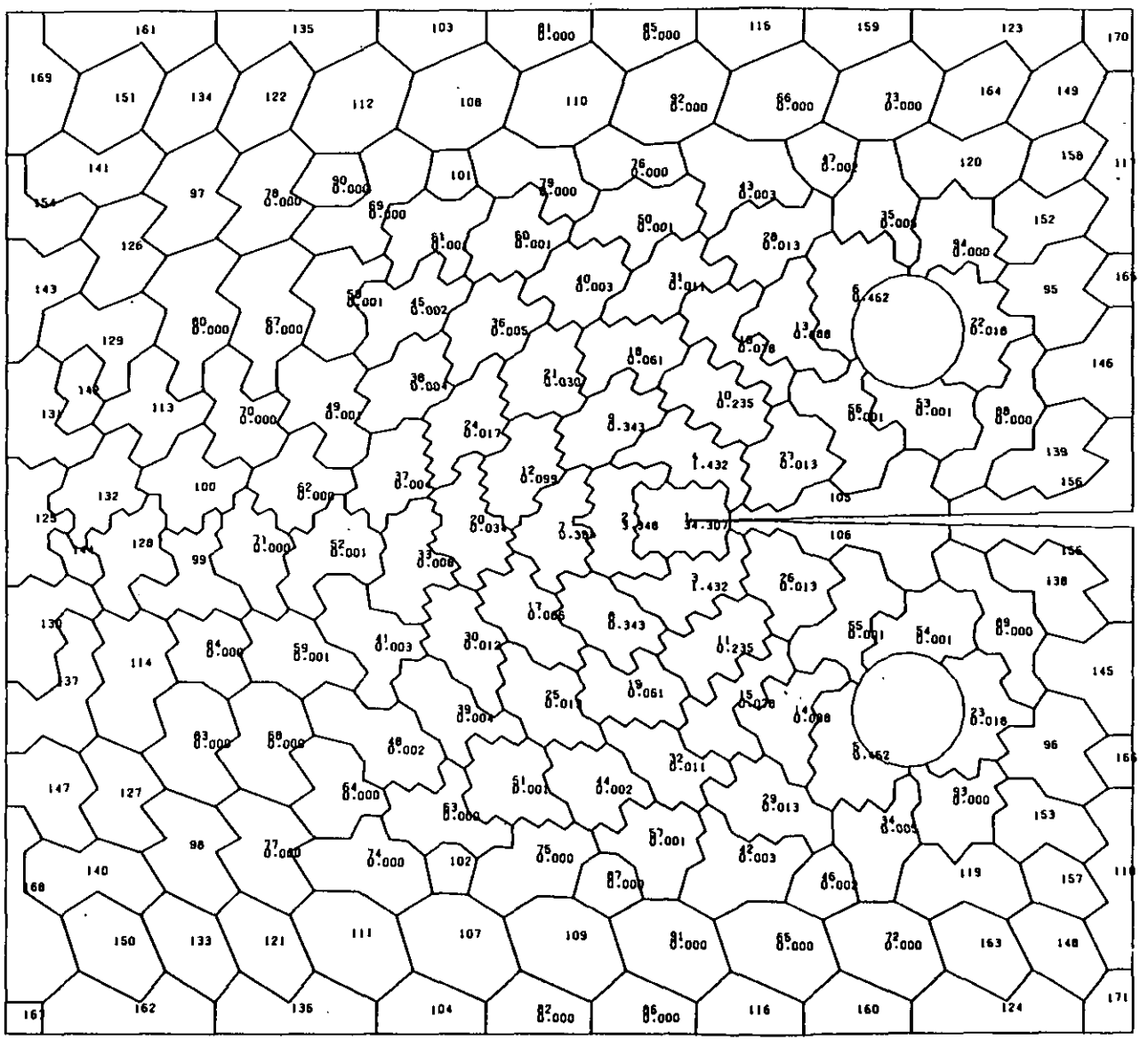

Fig. 30: Partitioning into Statistical Cells of Size $\Delta F = 110\,mm^2$
Specimen Type Ia $n_{eff} = 3{,}47$ Graphite Grade AS2 -F-500

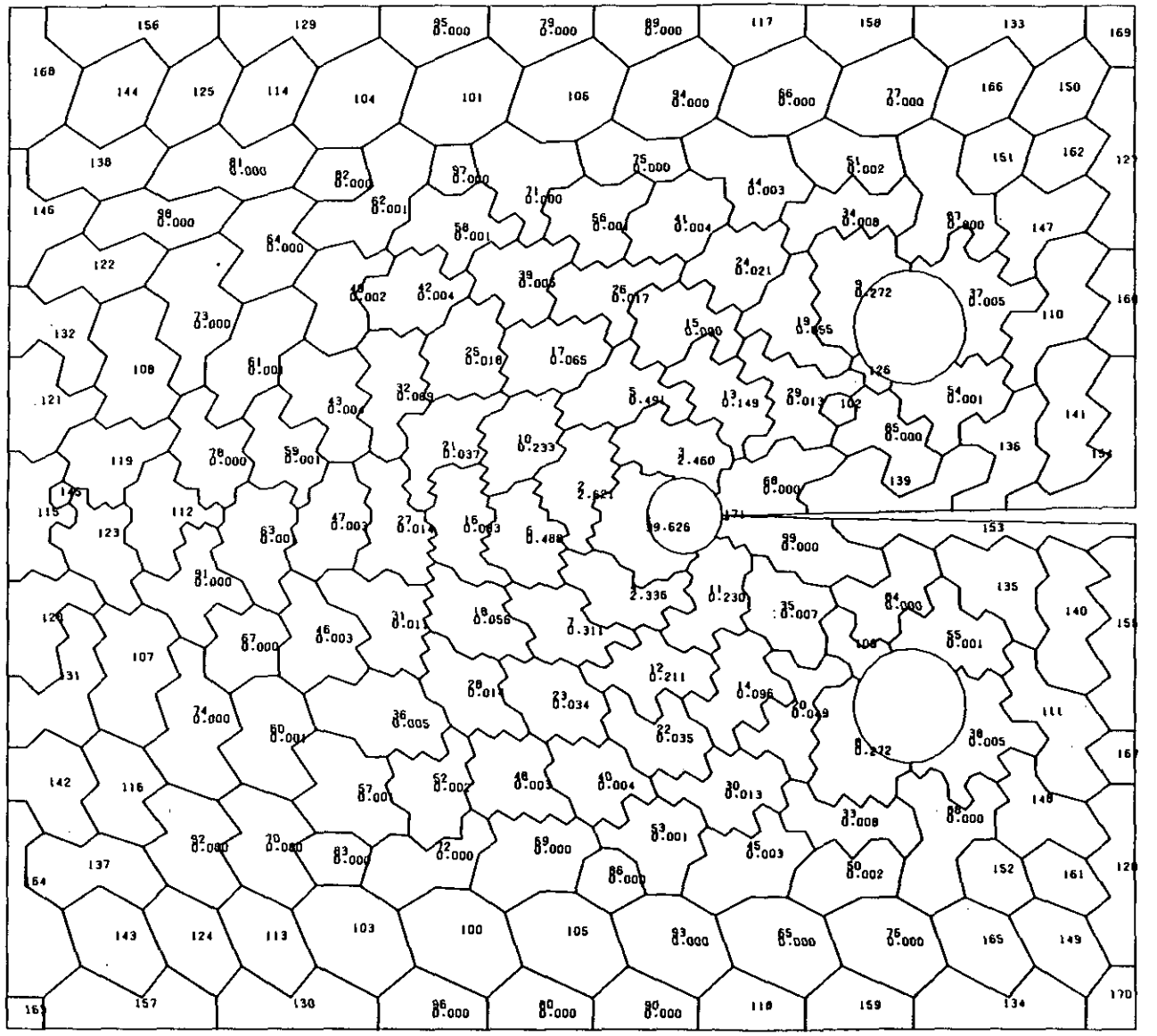

Fig.31: Partitioning into Statistical Cells of Size $\Delta F = 110\,mm^2$
Specimen Type 1b $n_{eff} = 3,64$ Graphite Grade AS2-F-500

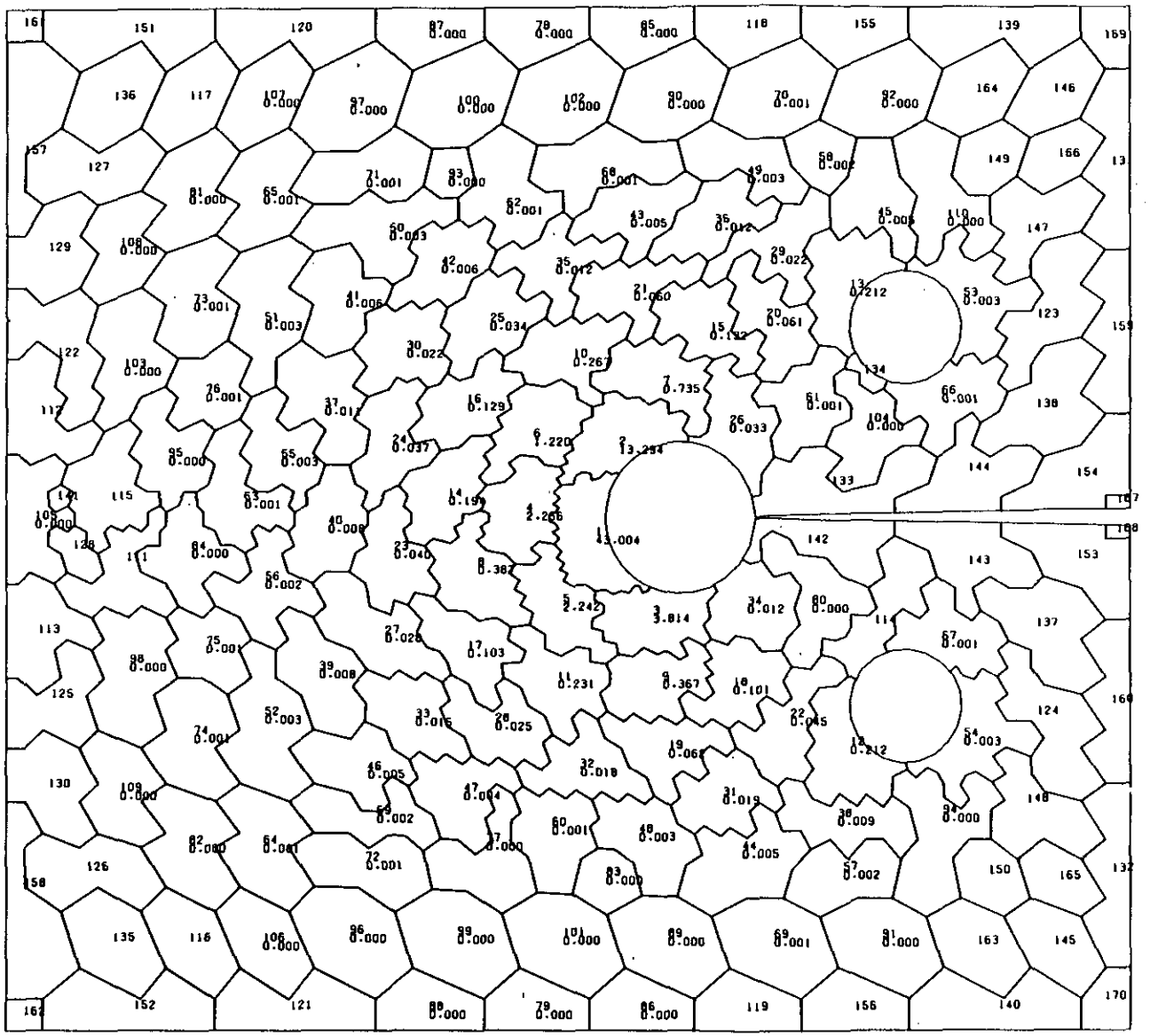

Fig.32: Partitioning into Statistical Cells of Size $\Delta F = 110\,mm^2$
Specimen Type Ic $n_{eff} = 4{,}47$ Graphite Grade AS2-F-500

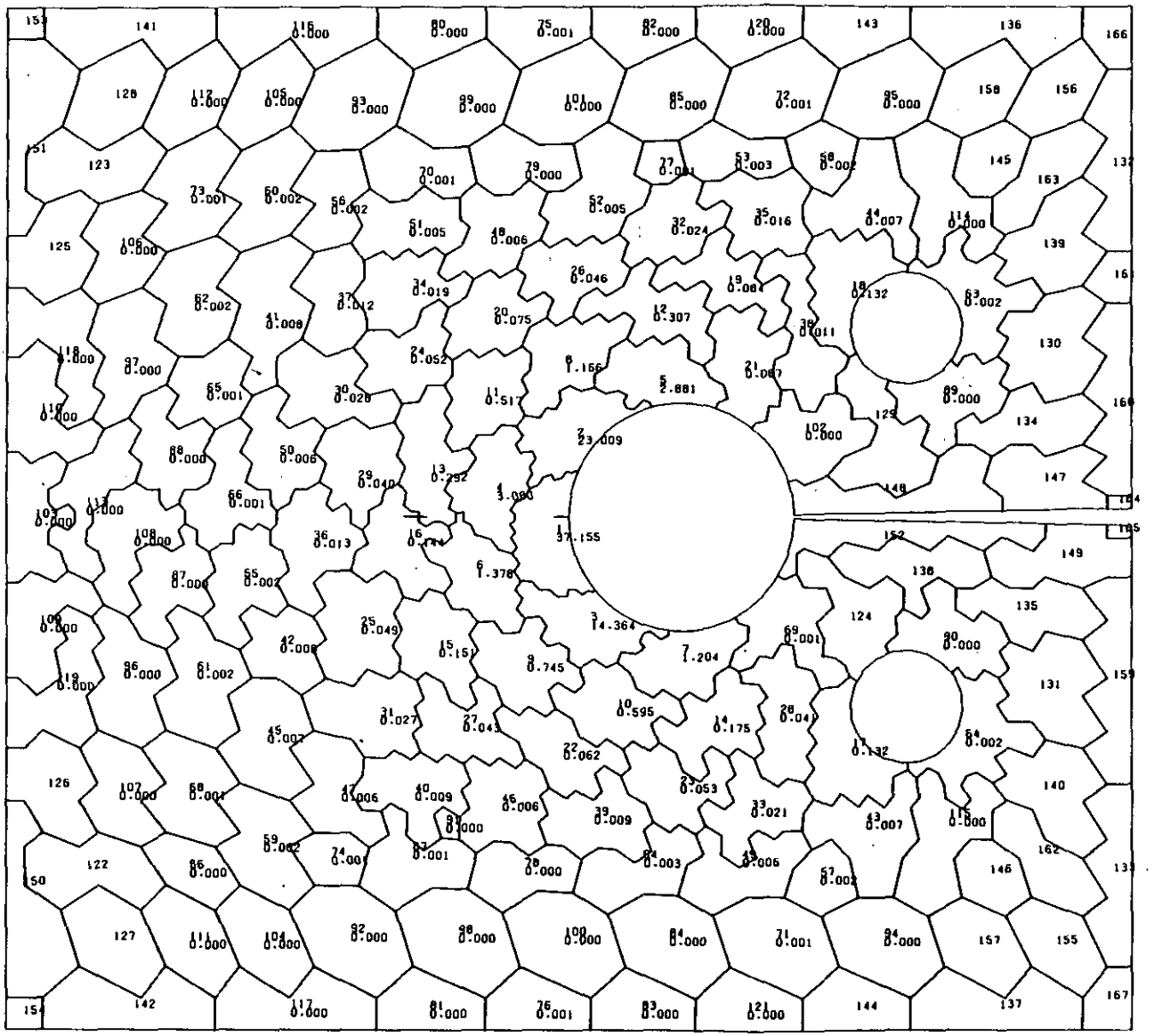

Fig.33: Partitioning into Statistical Cells of Size $\Delta F = 110\,mm^2$
Specimen Type Id $n_{eff} = 5{,}40$ Graphite Grade AS2-F-500

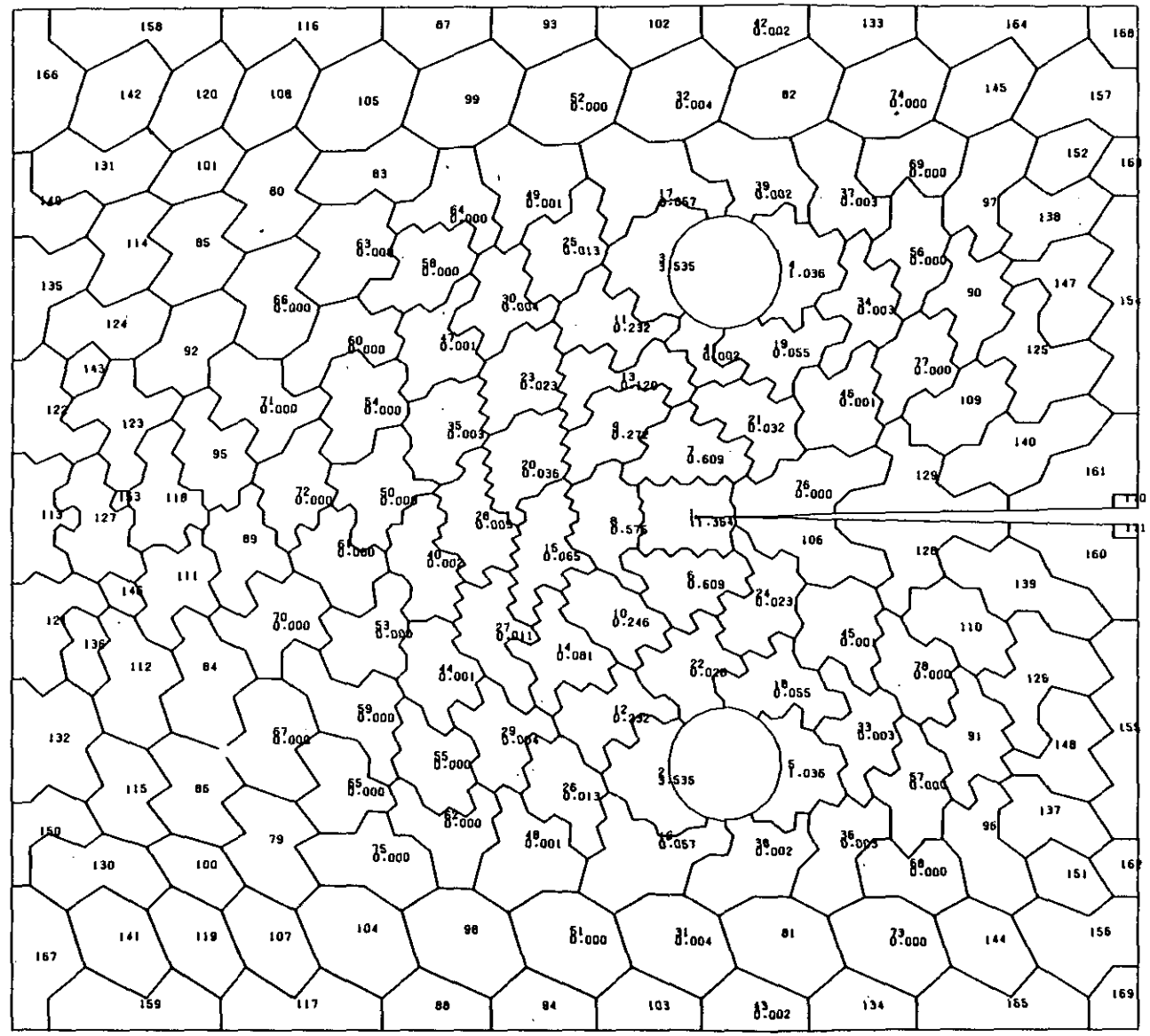

Fig.34 Partitioning into Statistical Cells of Size $\Delta F = 110 mm^2$
Specimen Type IIa $n_{eff} = 5,56$ Graphite Grade AS2-F-500

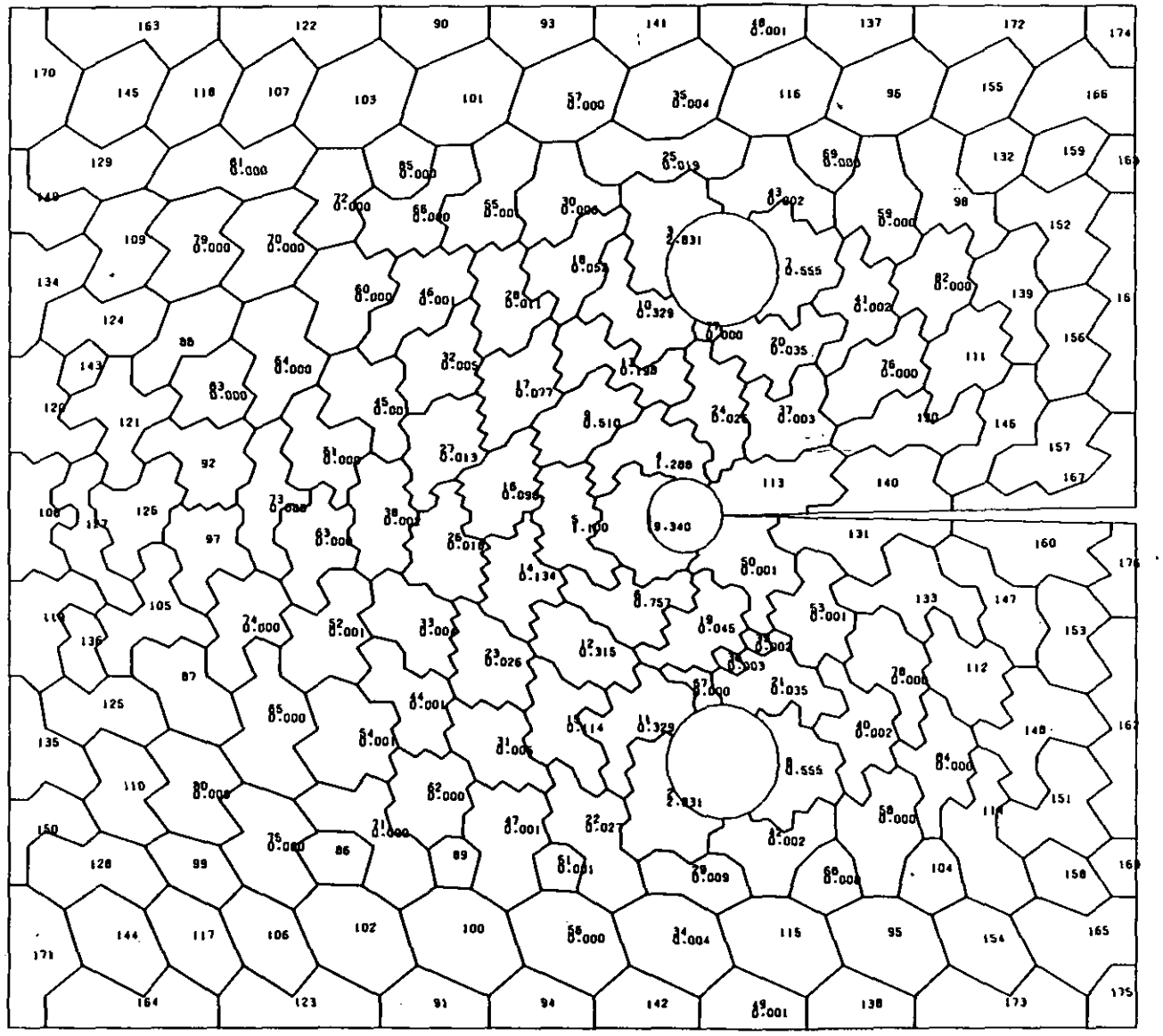

Fig.35: Partitioning into Statistical Cells of Size $\Delta F = 110\,mm^2$
Specimen Type IIb $n_{eff} = 5{,}30$ Graphite Grade AS2-F-500

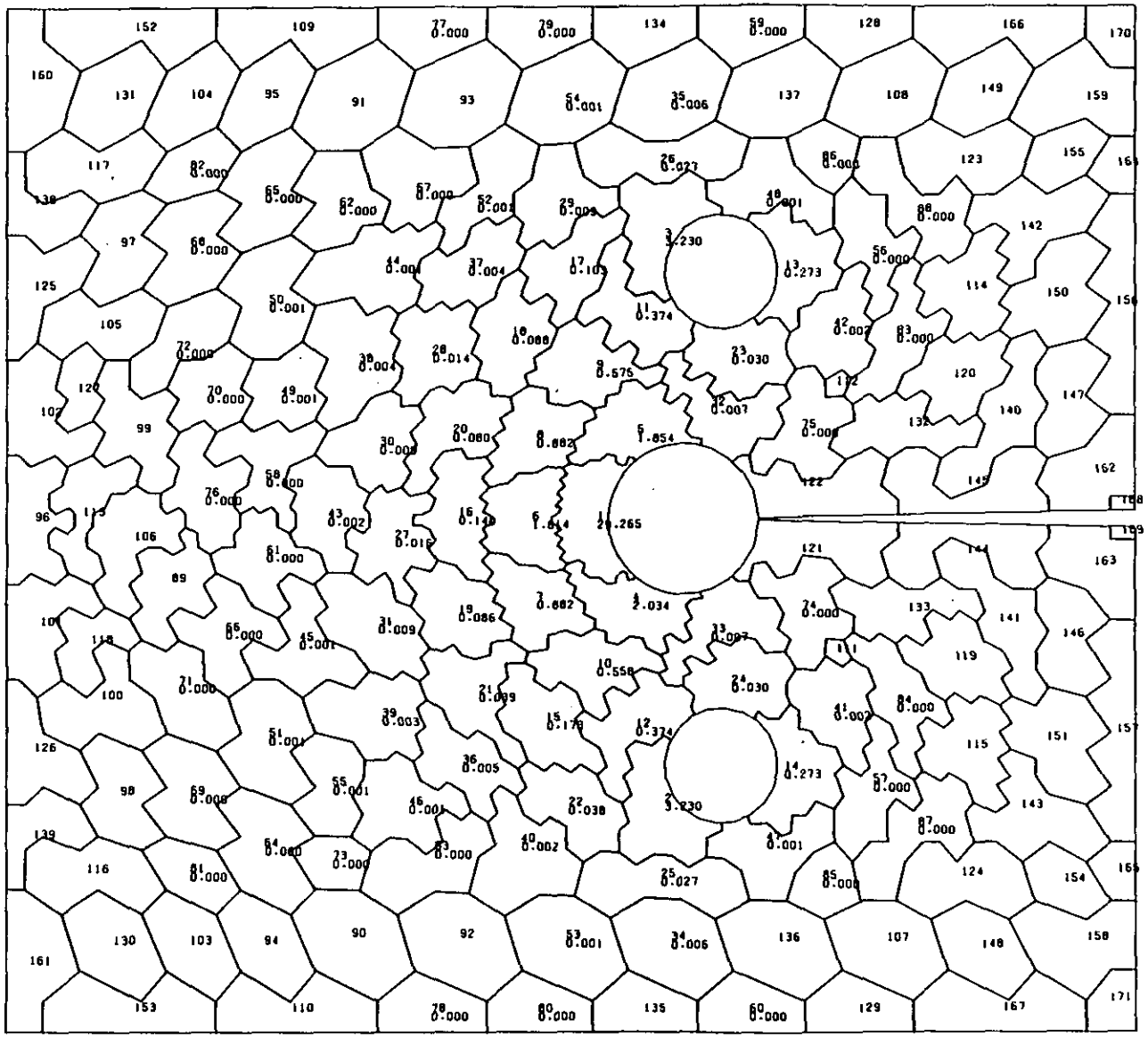

Fig.36: Partitioning into Statistical Cells of Size $\Delta F = 110 mm^2$
Specimen Type IIc $n_{eff} = 5{,}70$ Graphite Grade AS2-F-500

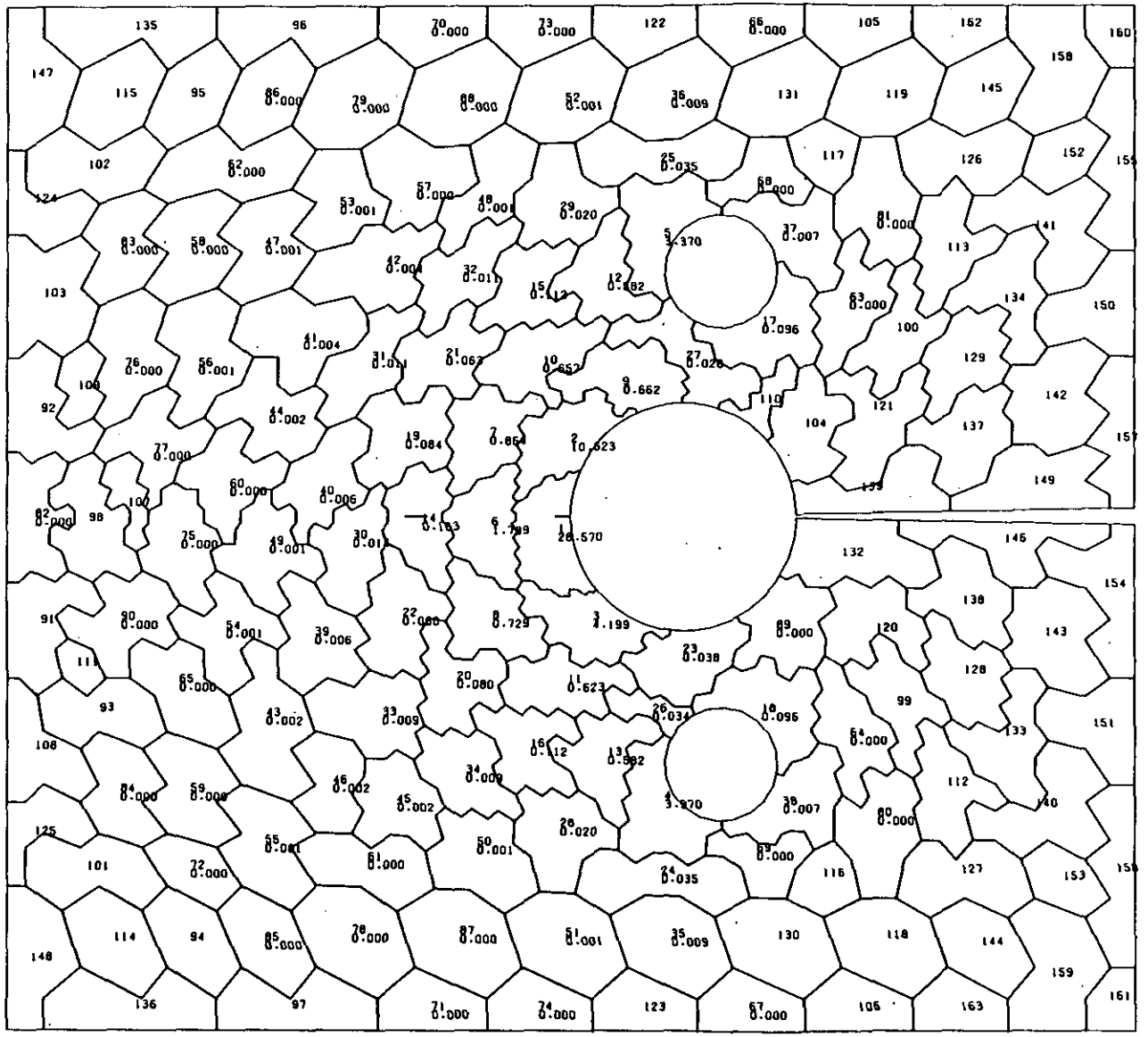

Fig.37: Partitioning into Statistical Cells of Size $\Delta F = 110 mm^2$
Specimen Type IId $n_{eff} = 5{,}90$ Graphite Grade AS2-F-500

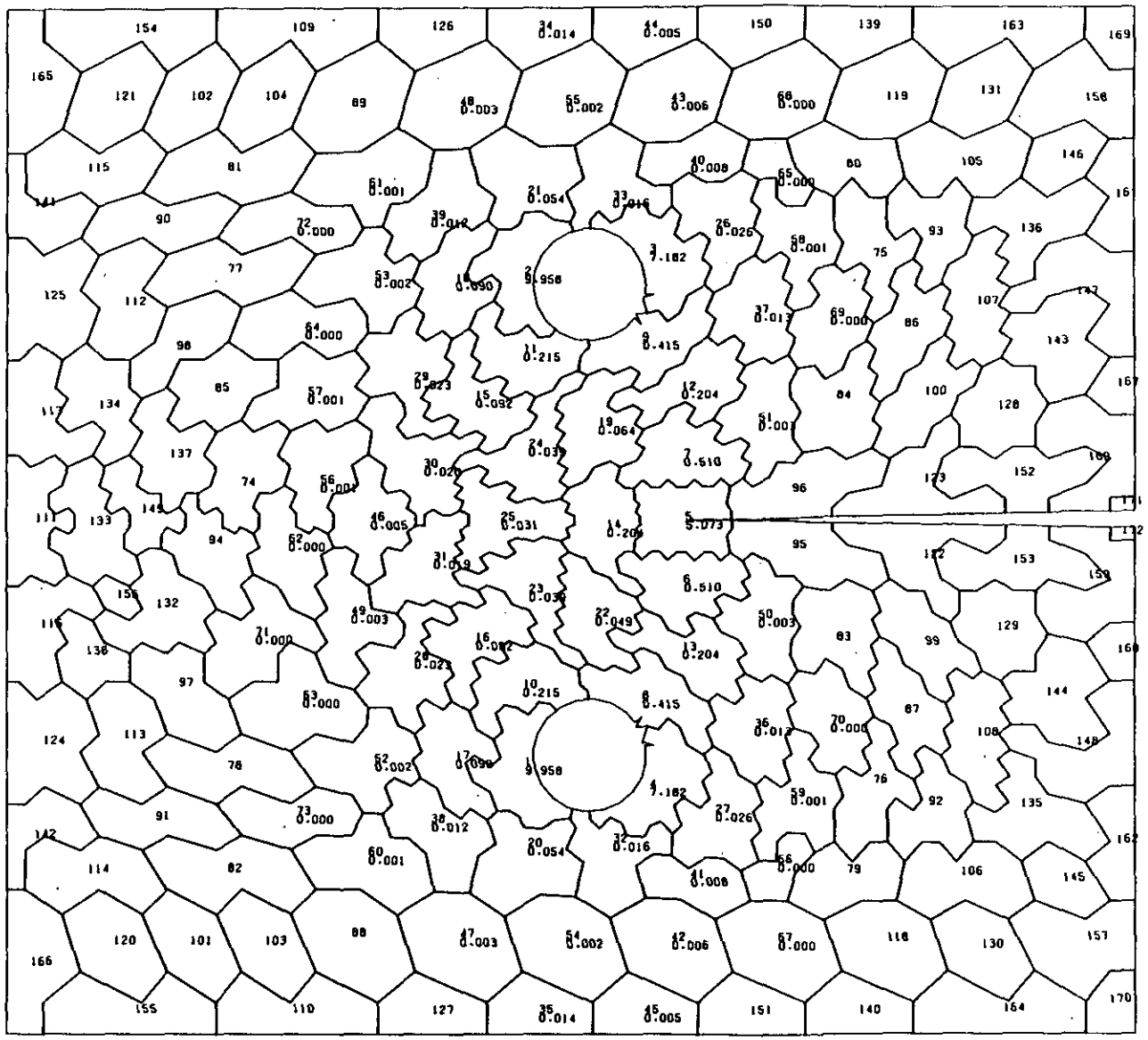

Fig.38: Partitioning into Statistical Cells of Size $\Delta F = 110\,mm^2$
Specimen Type IIIa $n_{eff} = 6,50$ Graphite Grade AS2-F-500

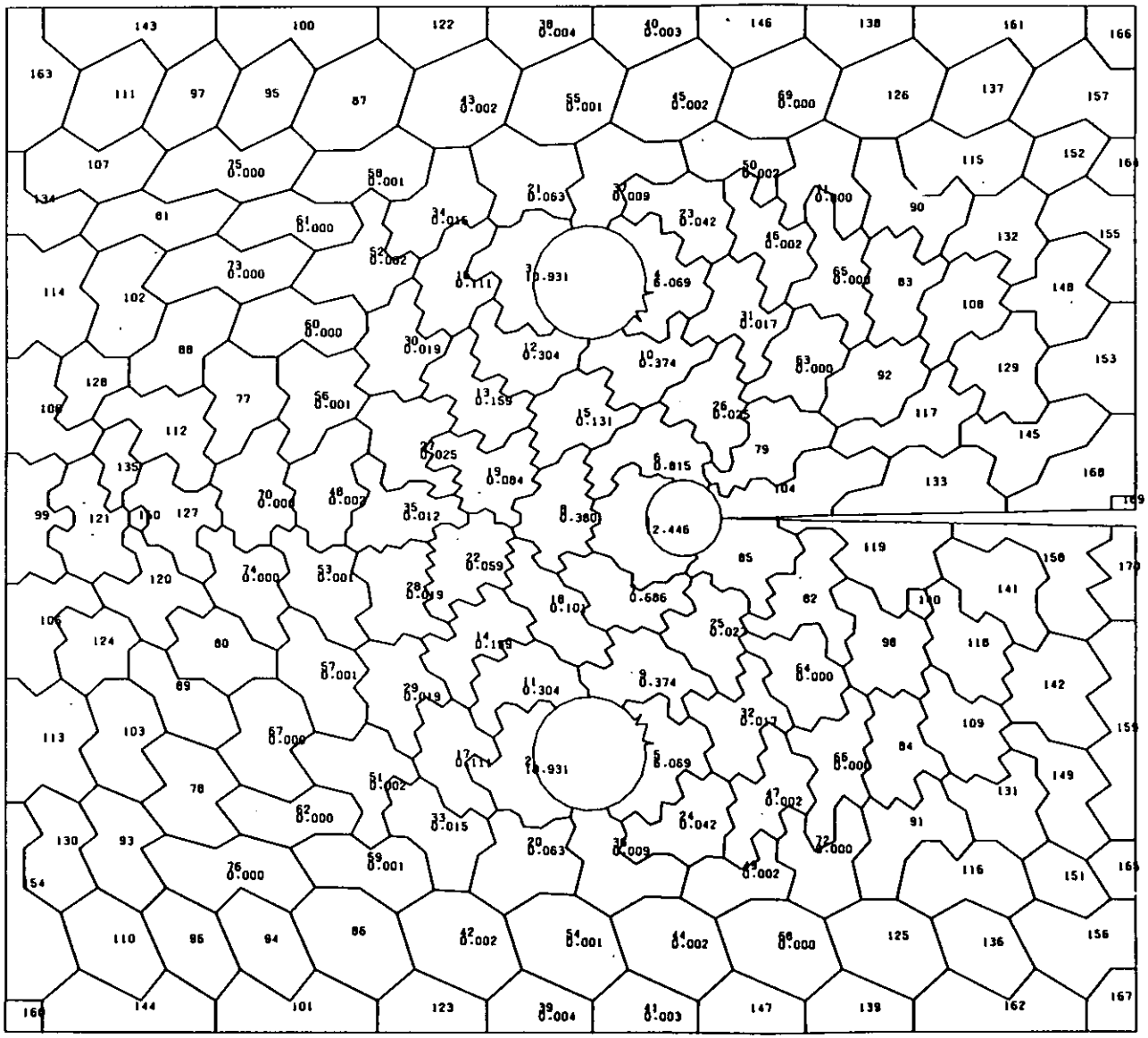

Fig.39: Partitioning into Statistical Cells of Size $\Delta F = 110\,mm^2$
Specimen Type IIIb $n_{eff} = 6{,}24$ Graphite Grade AS2-F-500

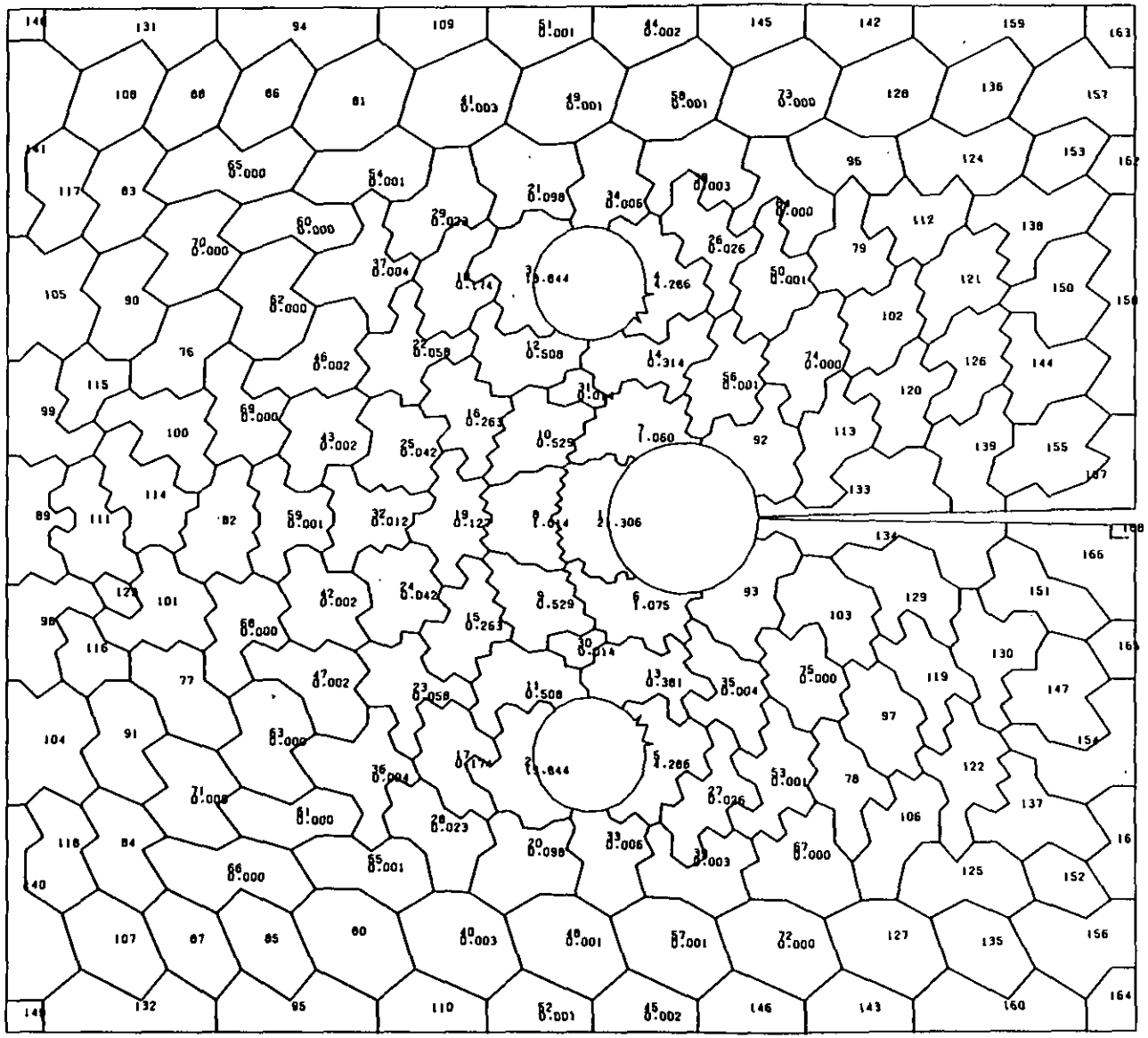

Fig.40: Partitioning into Statistical Cells of Size $\Delta F = 110 mm^2$
Specimen Type IIIc $n_{eff} = 6,19$ Graphite Grade AS2-F-500

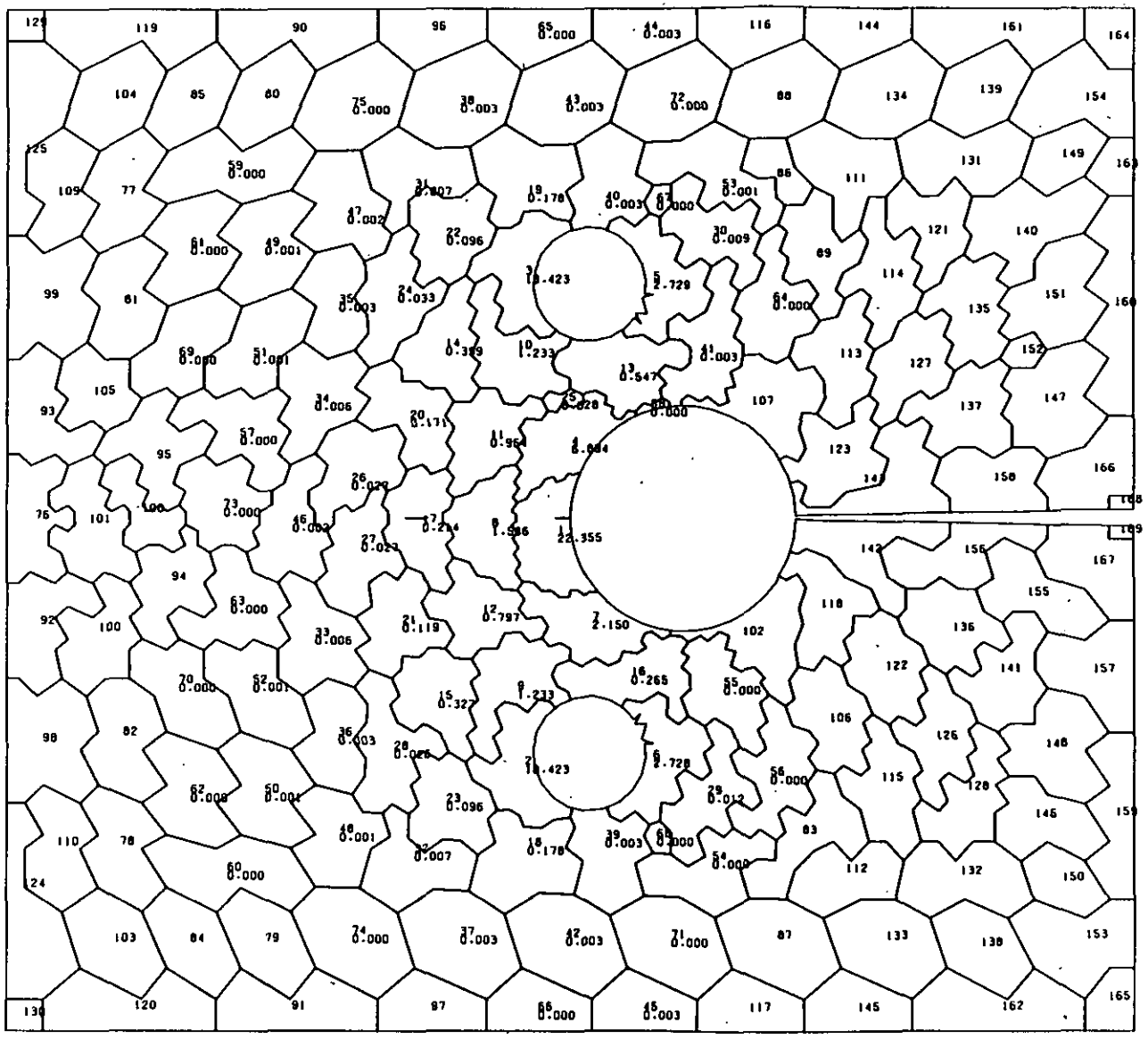

Fig.41: Partitioning into Statistical Cells of Size $\Delta F = 110\,mm^2$
Specimen Type IIId $n_{eff} = 6{,}92$ Graphite Grade AS2 -F-500

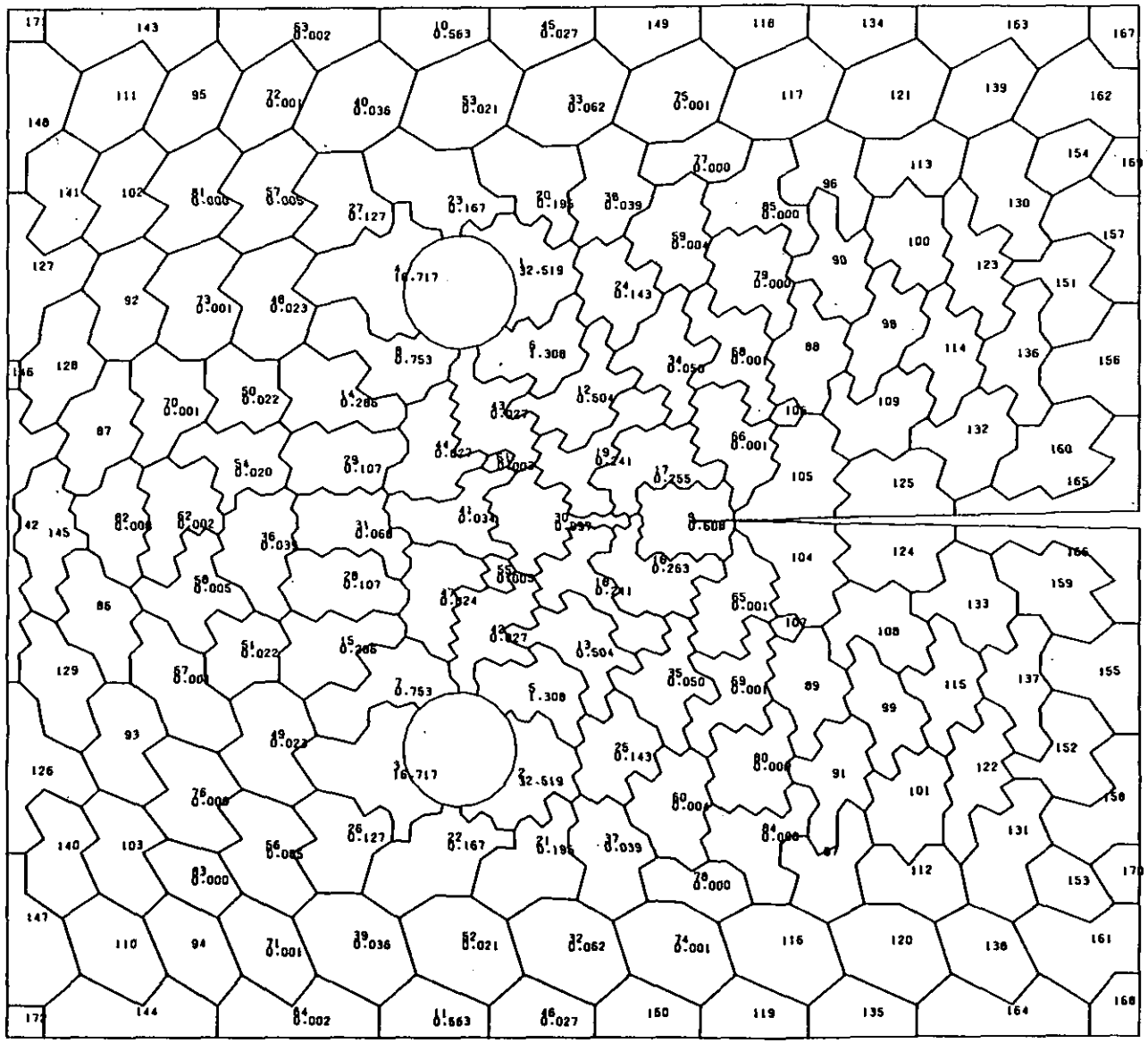

Fig.42: Partitioning into Statistical Cells of Size $\Delta F = 110 mm^2$
Specimen Type IVa $n_{eff} = 7{,}07$ · Graphite Grade AS2-F-500

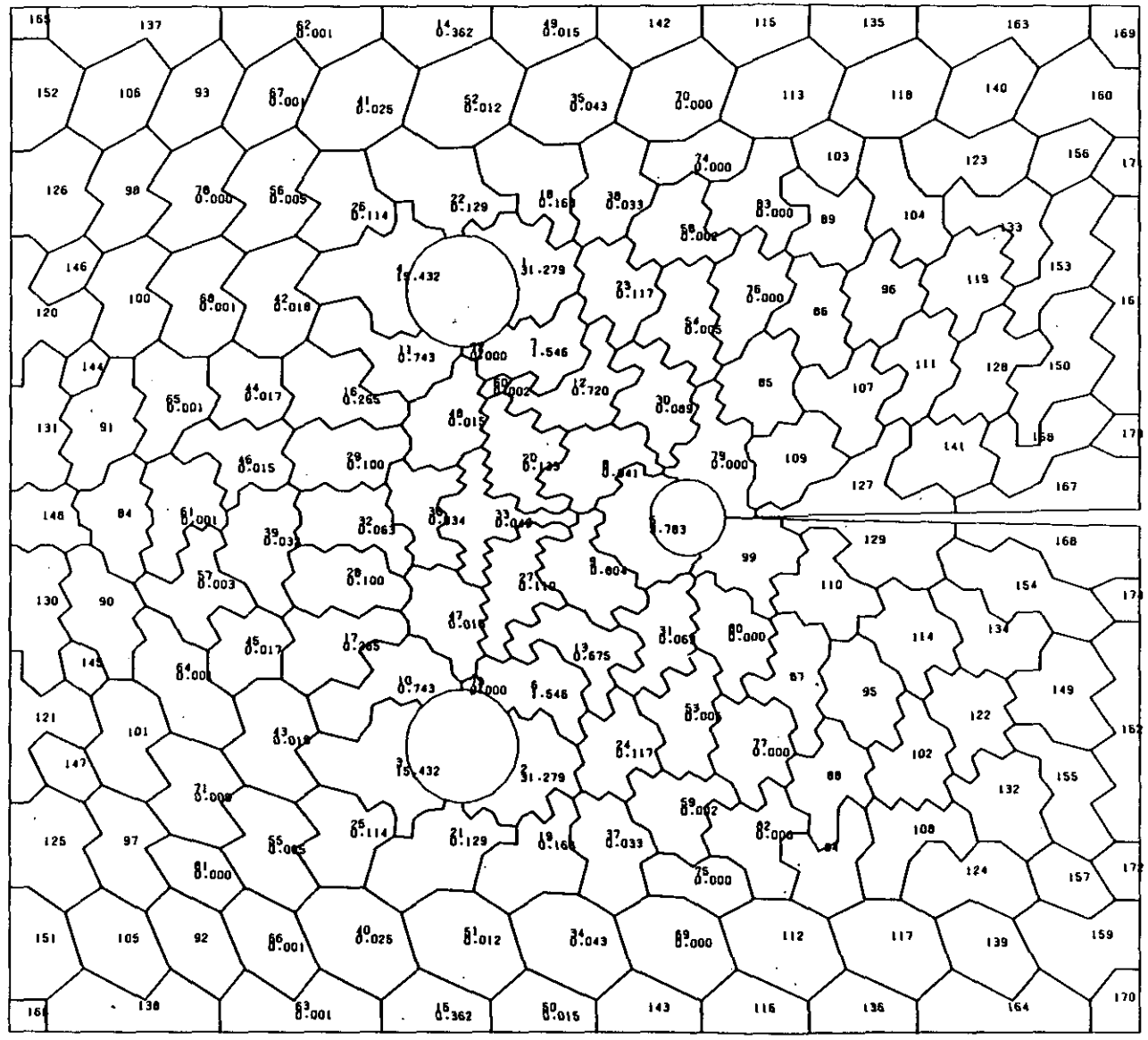

Fig.43: Partitioning into Statistical Cells of Size $\Delta F = 110\,mm^2$
Specimen Type IVb $n_{eff} = 7{,}01$ Graphite Grade AS2-F-500

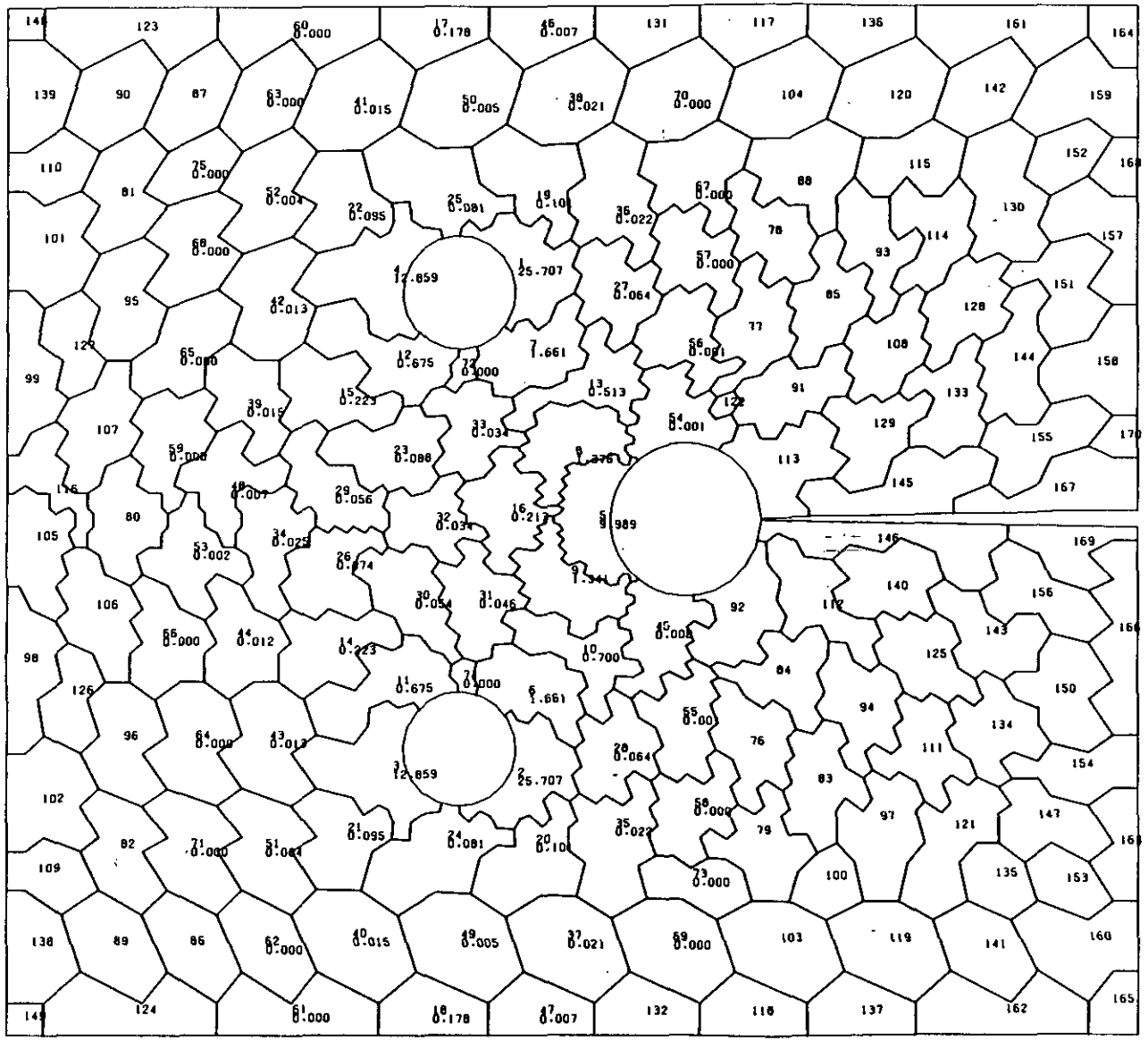

Fig.44: Partitioning into Statistical Cells of Size $\Delta F = 110\,mm^2$
Specimen Type IVc $n_{eff} = 6{,}84$ Graphite Grade AS2-F-500

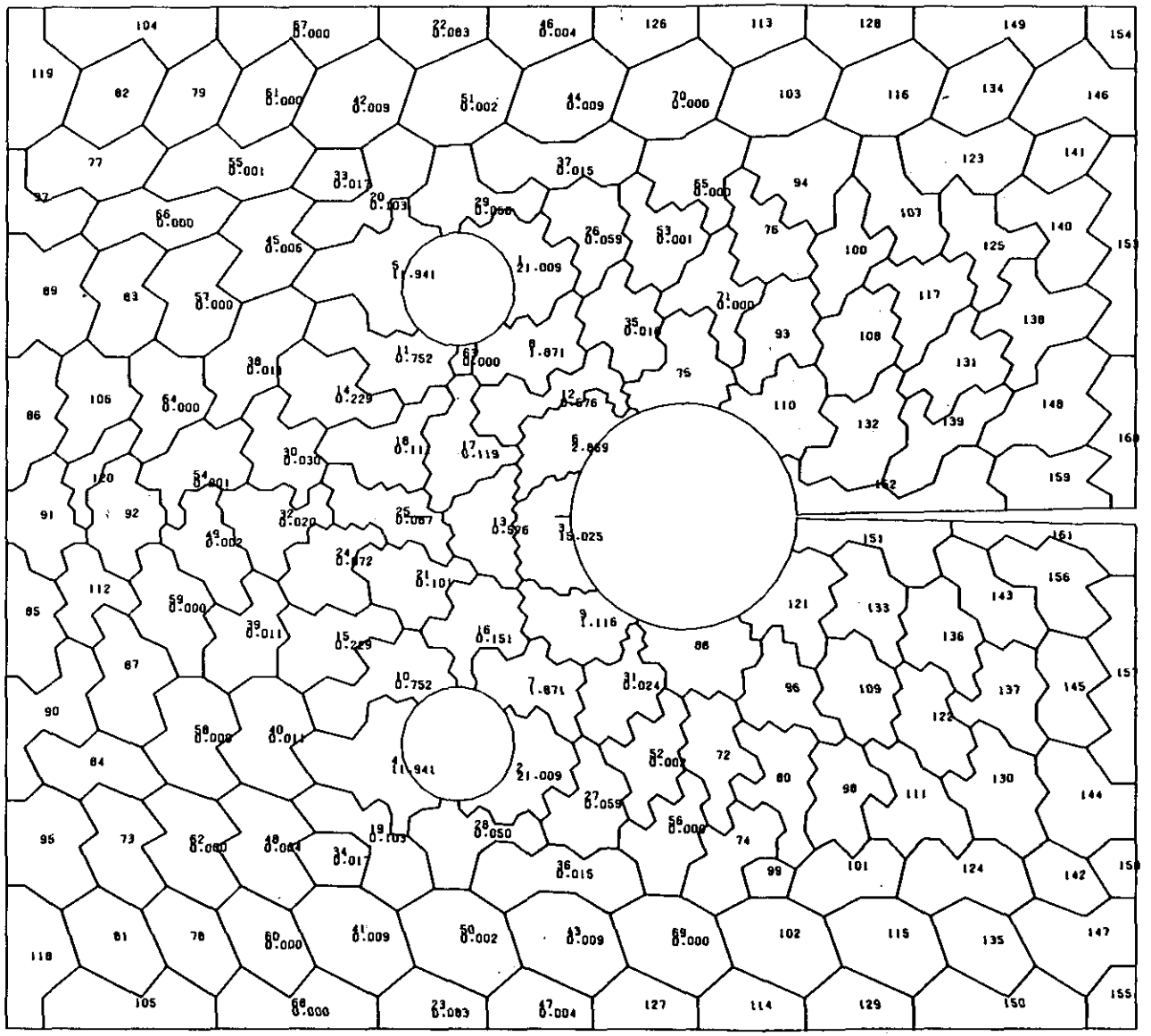

Fig.45: Partitioning into Statistical Cells of Size $\Delta F = 110\,mm^2$
Specimen Type IVd $n_{eff} = 7{,}00$ Graphite Grade AS2-F-500

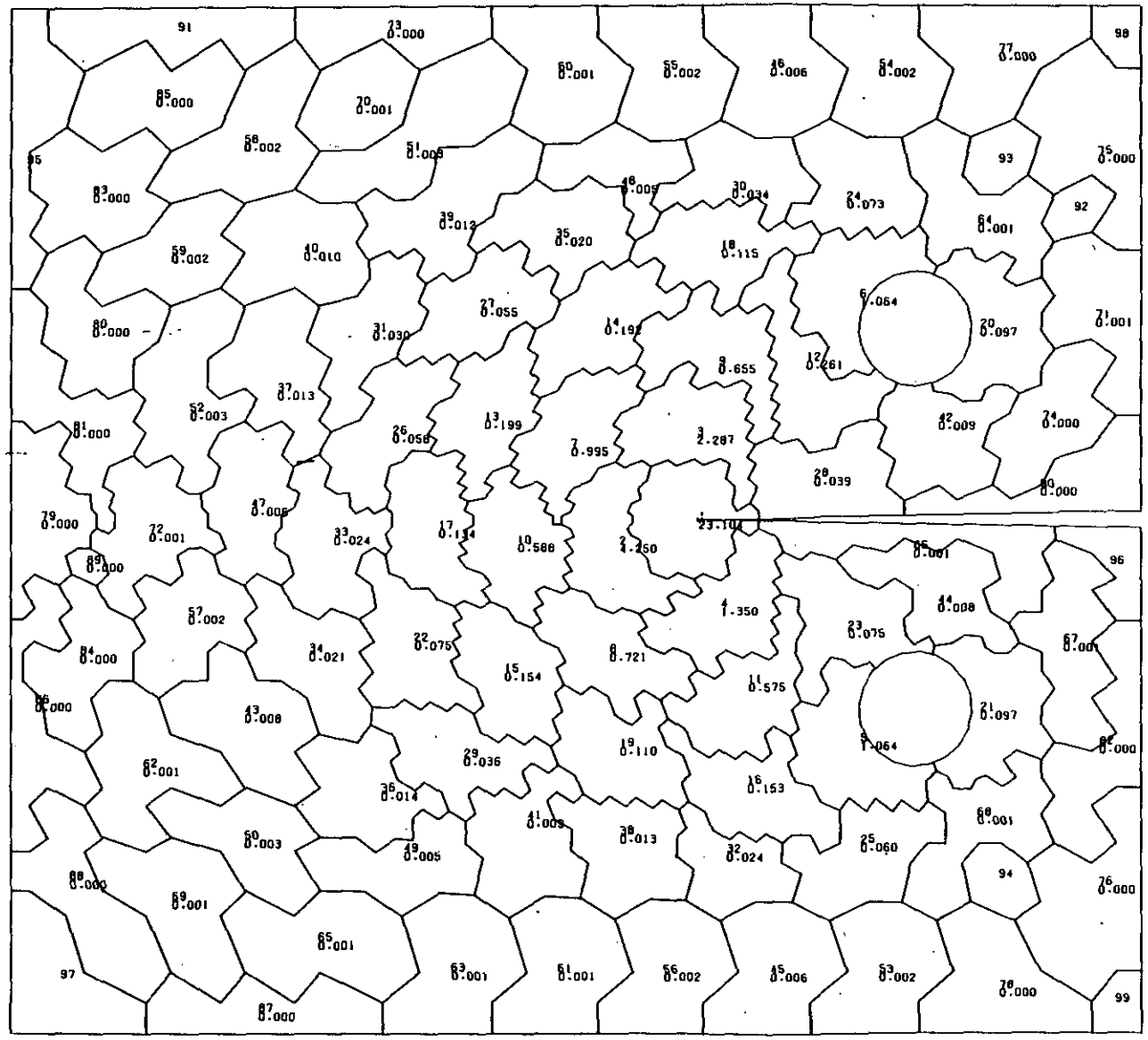

Fig.46: Partitioning into Statistical Cells of Size $\Delta F = 190\,mm^2$
Specimen Type Ia $n_{eff} = 8{,}44$ Graphite Grade M 2190

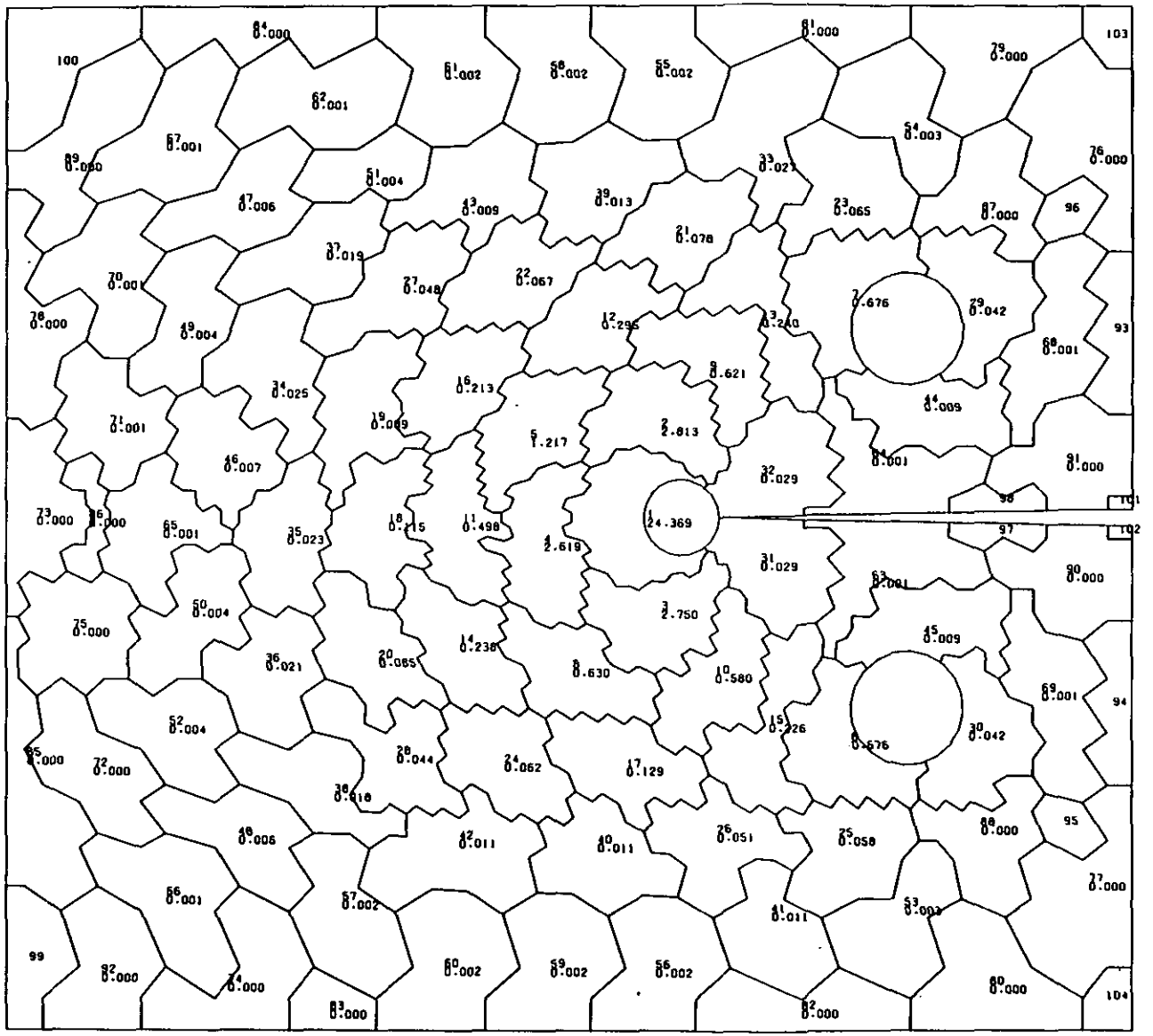

Fig.47: Partitioning into Statistical Cells of Size $\Delta F = 190\,mm^2$
Specimen Type Ib $n_{eff} = 8{,}67$ Graphite Grade M 2190

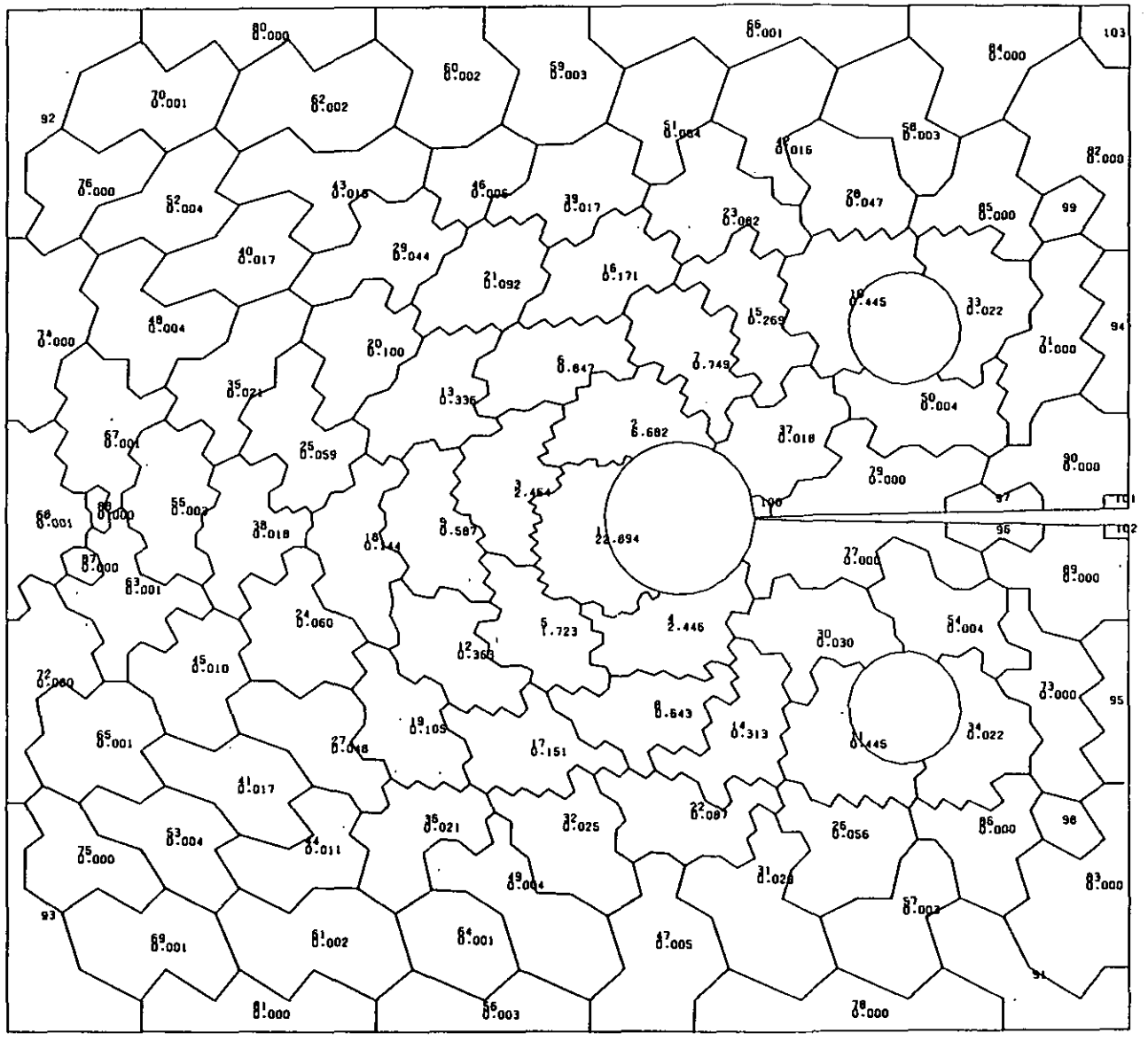

Fig.48: Partitioning into Statistical Cells of Size $\Delta F = 190\,mm^2$
Specimen Type Ic $n_{eff} = 8,44$ Graphite Grade M 2190

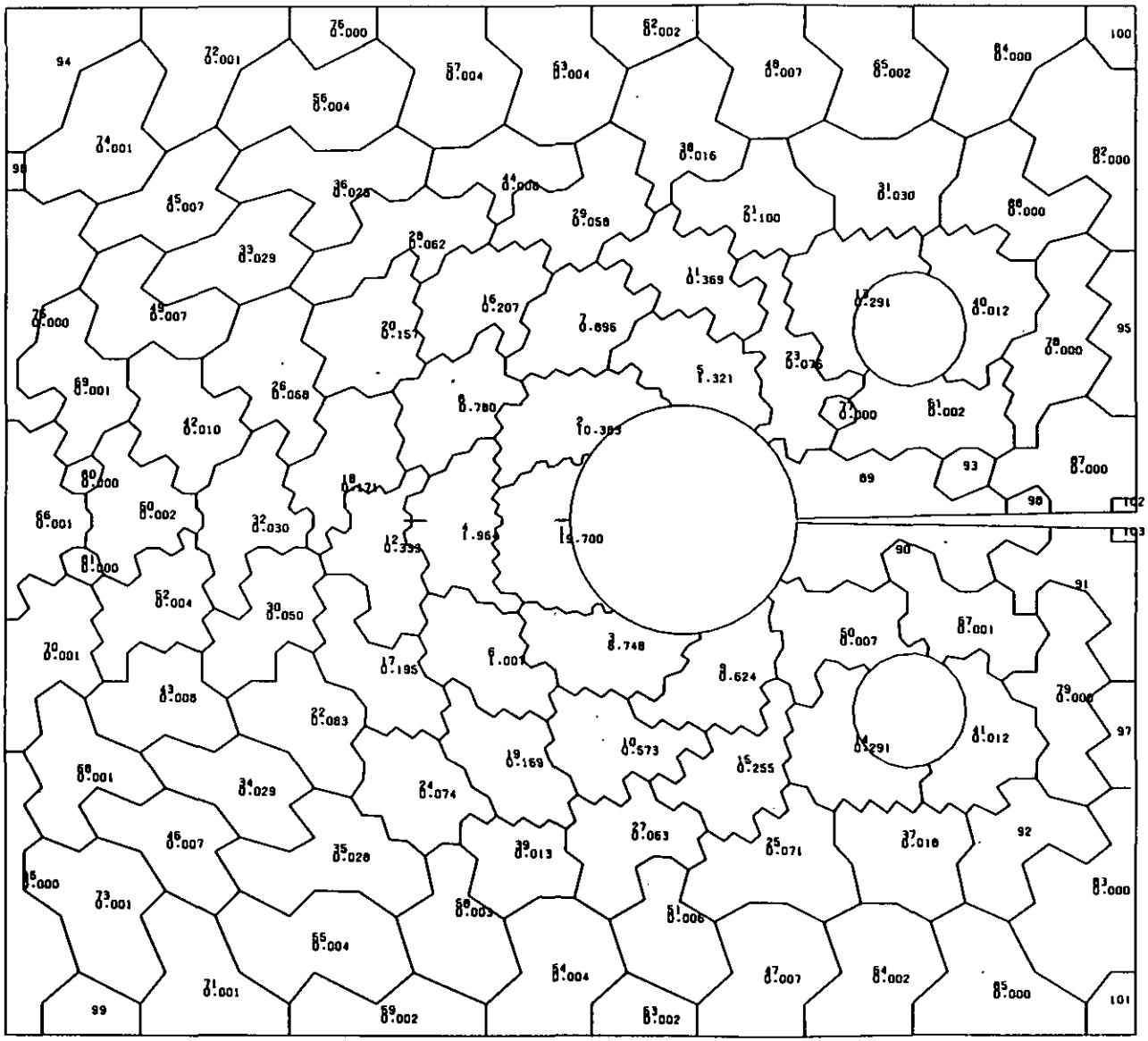

Fig.49: Partitioning into Statistical Cells of Size $\Delta F = 190\,mm^2$
Specimen Type Id $n_{eff} = 8.28$ Graphite Grade M 2190

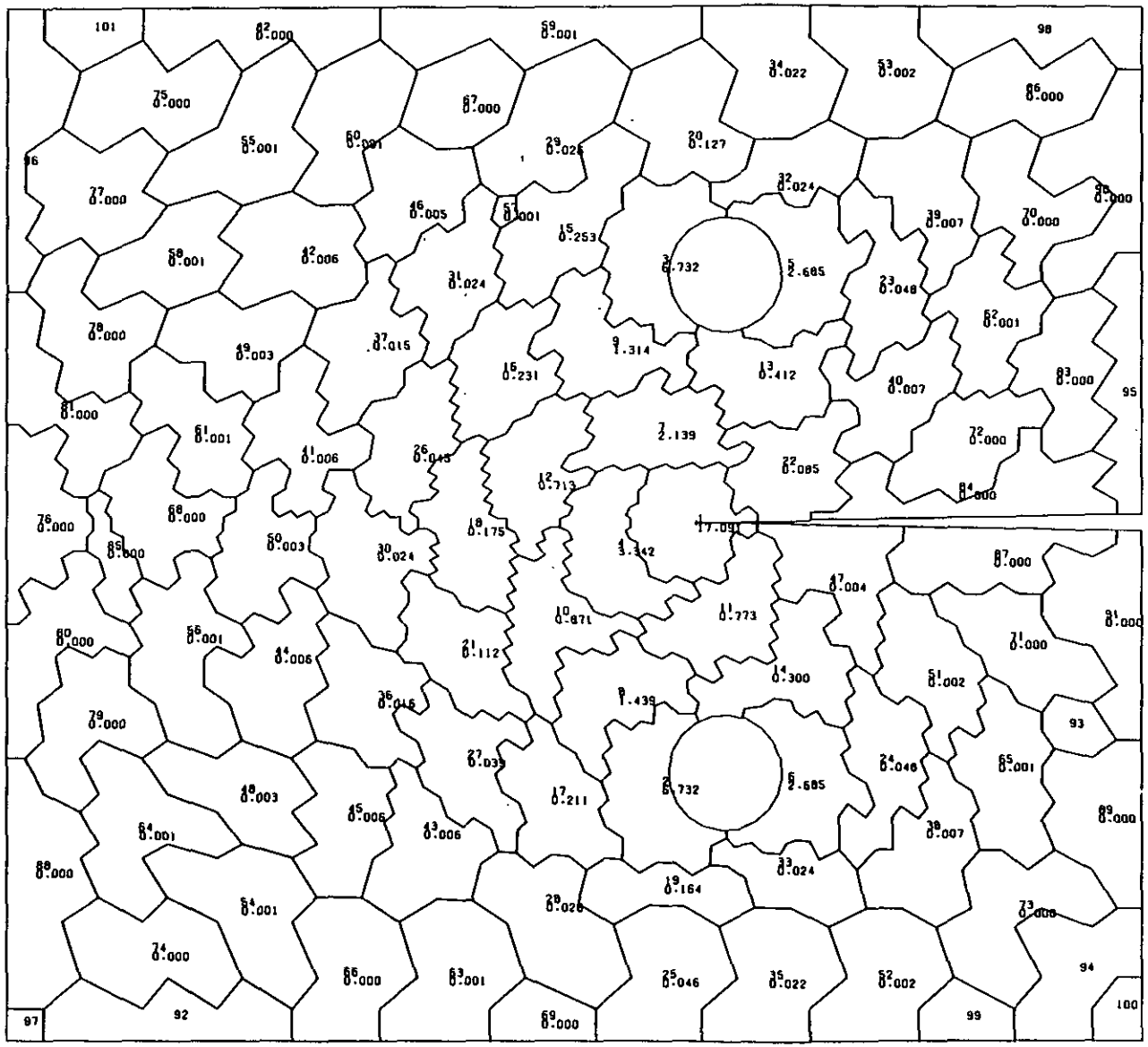

Fig.50: Partitioning into Statistical Cells of Size $\Delta F = 190\,mm^2$
Specimen Type IIa $n_{eff} = 9,20$ Graphite Grade M 2190

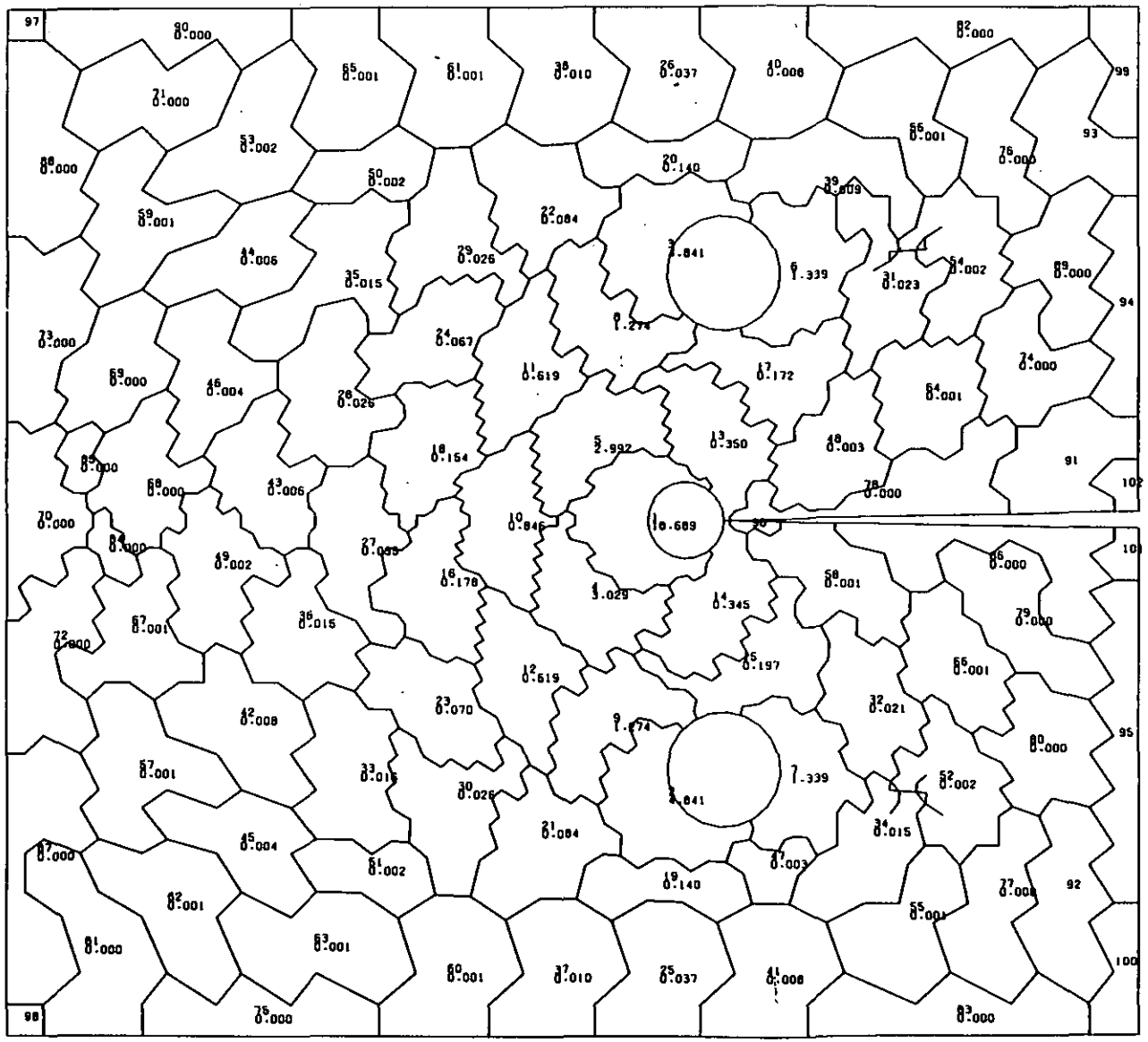

Fig.51: Partitioning into Statistical Cells of Size $\Delta F = 190\,mm^2$
Specimen Type IIb $n_{eff} = 9{,}01$ Graphite Grade M2190

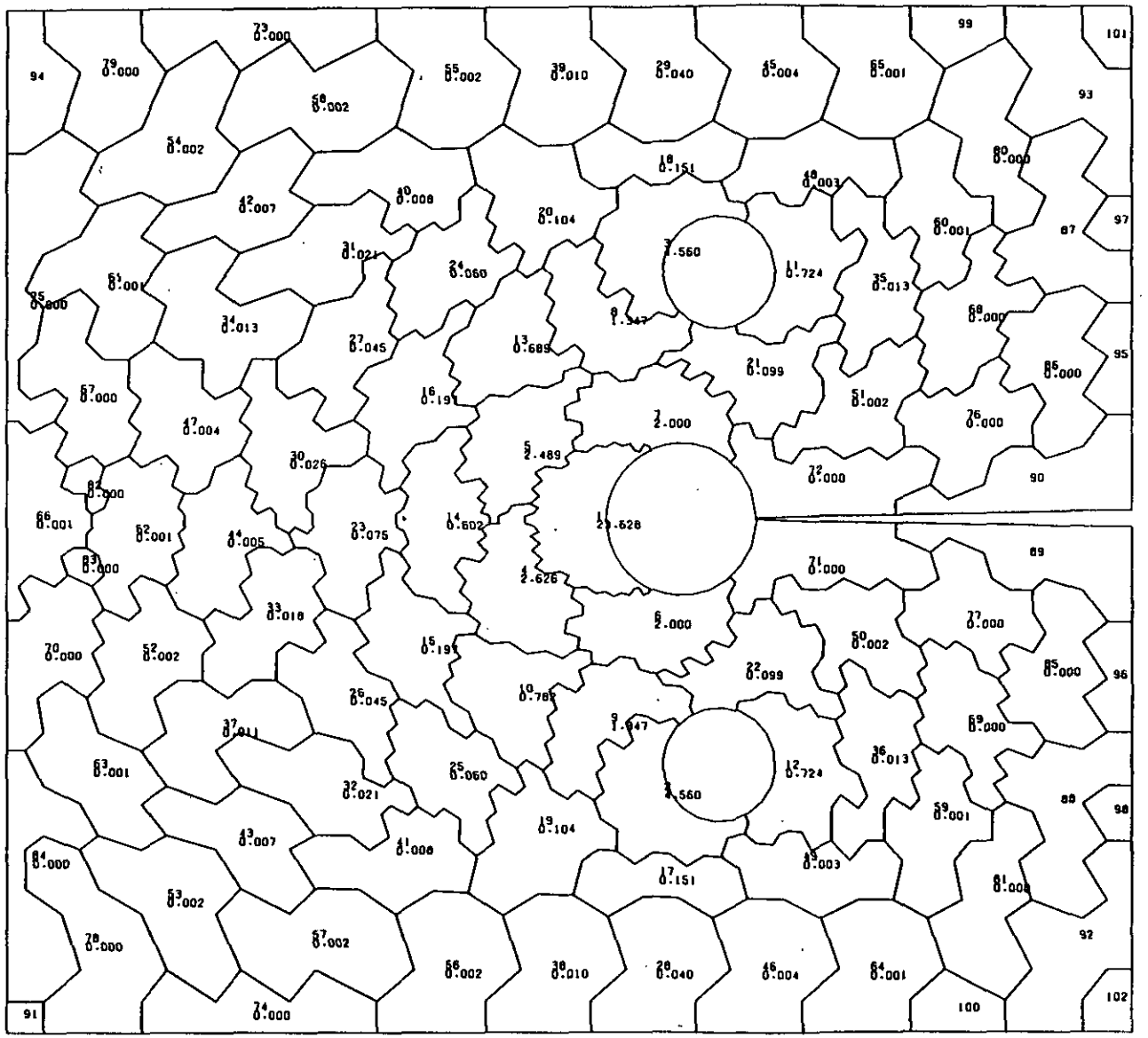

Fig. 52: Partitioning into Statistical Cells of Size $\Delta F = 190\,mm^2$
Specimen Type IIc $n_{eff} = 9.58$ Graphite Grade M 2190

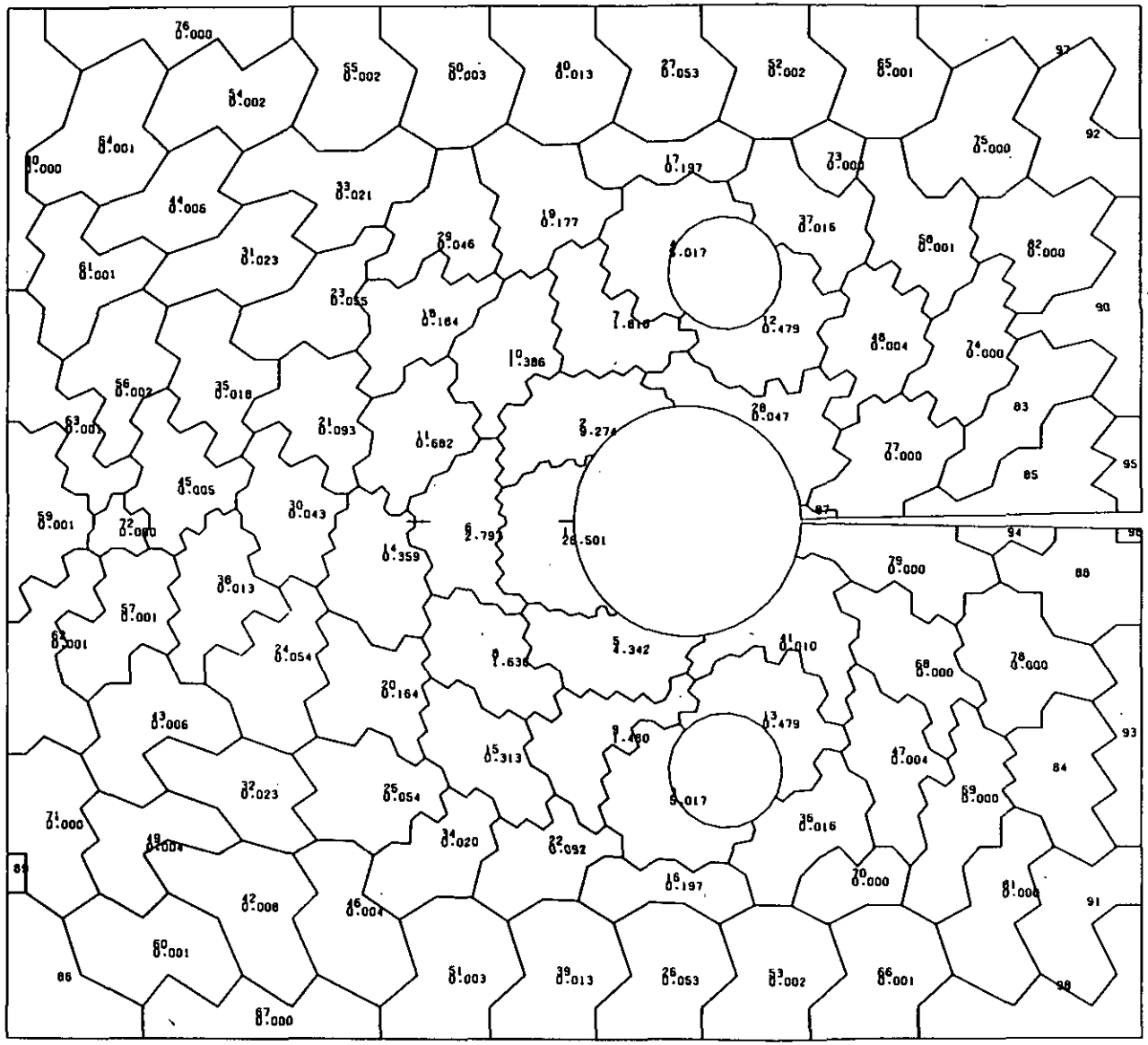

Fig. 53: Partitioning into Statistical Cells of Size $\Delta F = 190\,mm^2$
Specimen Type IId $n_{eff} = 9{,}06$ Graphite Grade M 2190

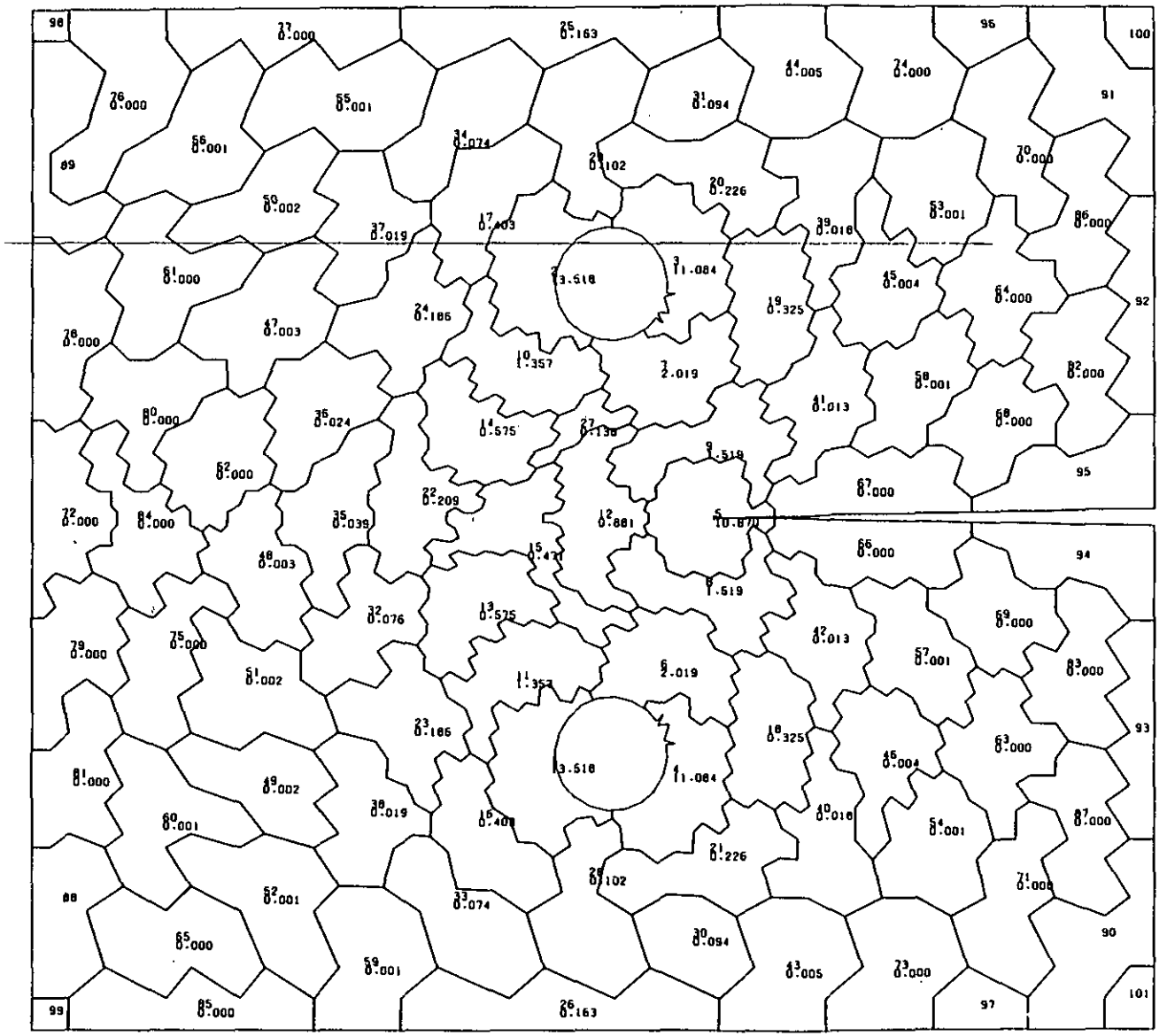

Fig.54: Partitioning into Statistical Cells of Size $\Delta F = 190 mm^2$
Specimen Type IIIa neff = 10.98 Graphite Grade M 2190

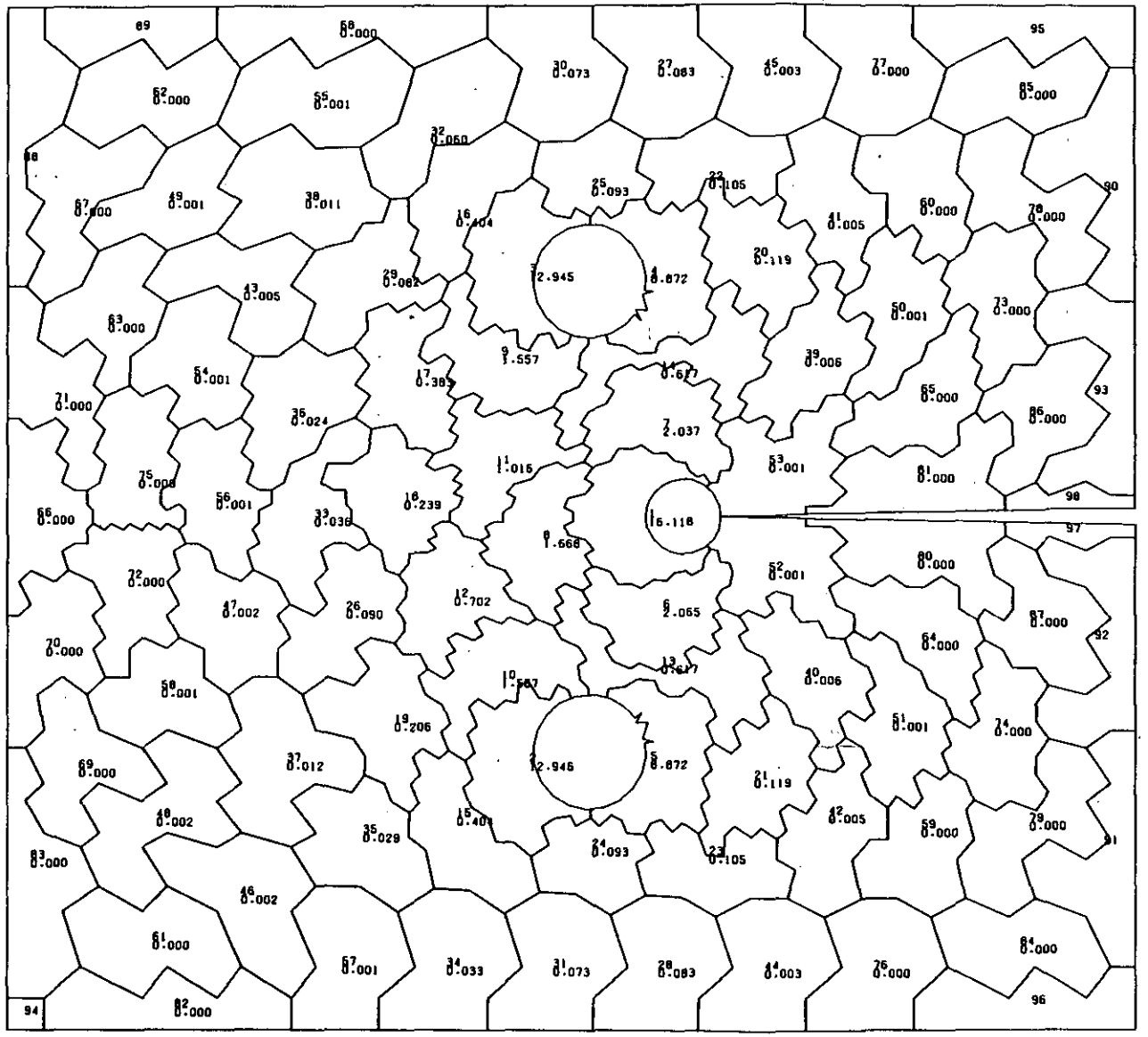

Fig. 55: Partitioning into Statistical Cells of Size $\Delta F = 190 mm^2$
Specimen Type IIIb $n_{eff} = 9{,}72$ Graphite Grade M 2190

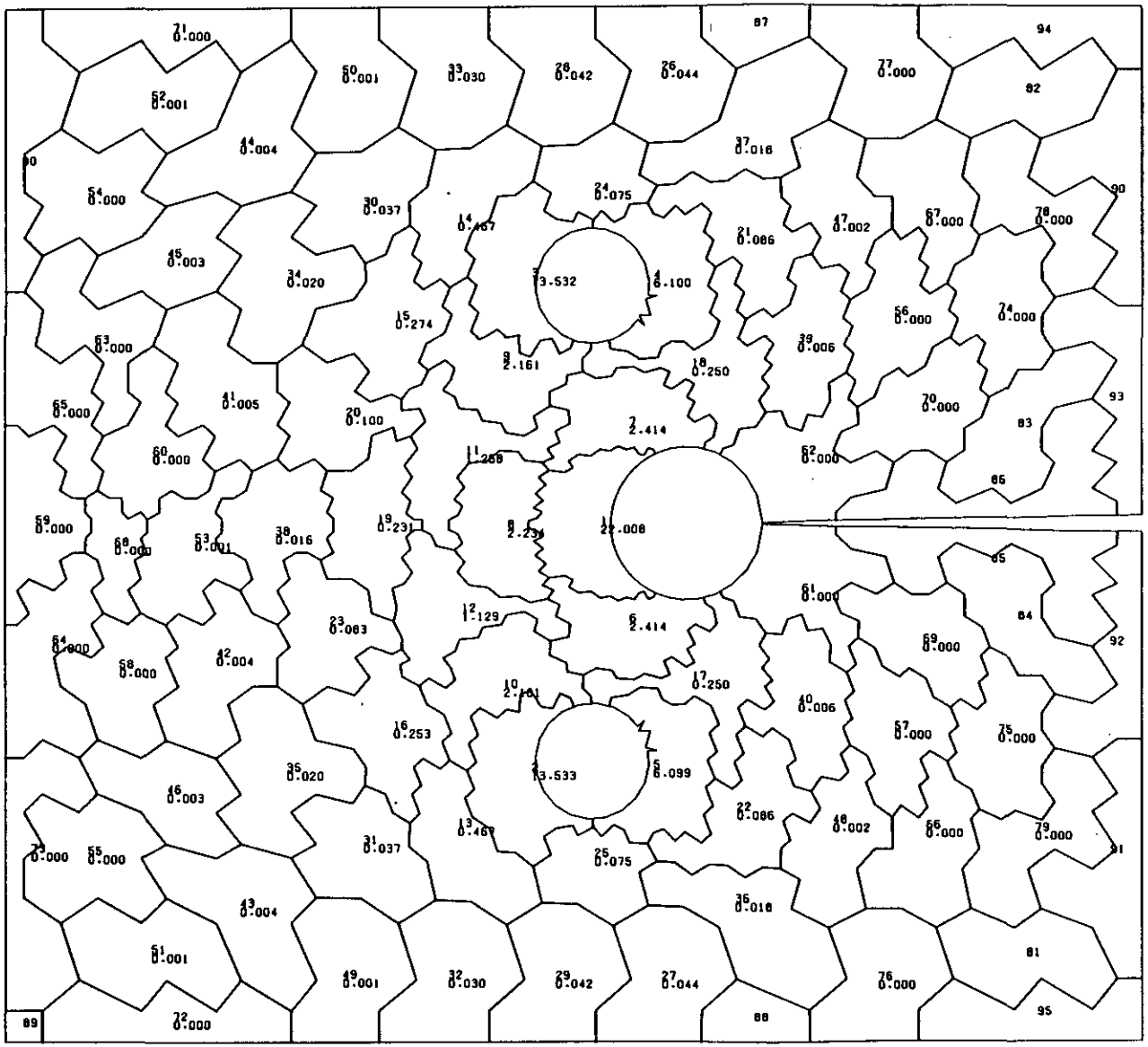

Fig.56: Partitioning into Statistical Cells of Size $\Delta F = 190 mm^2$
Specimen Type IIIc neff = 9.33 Graphite Grade M2190

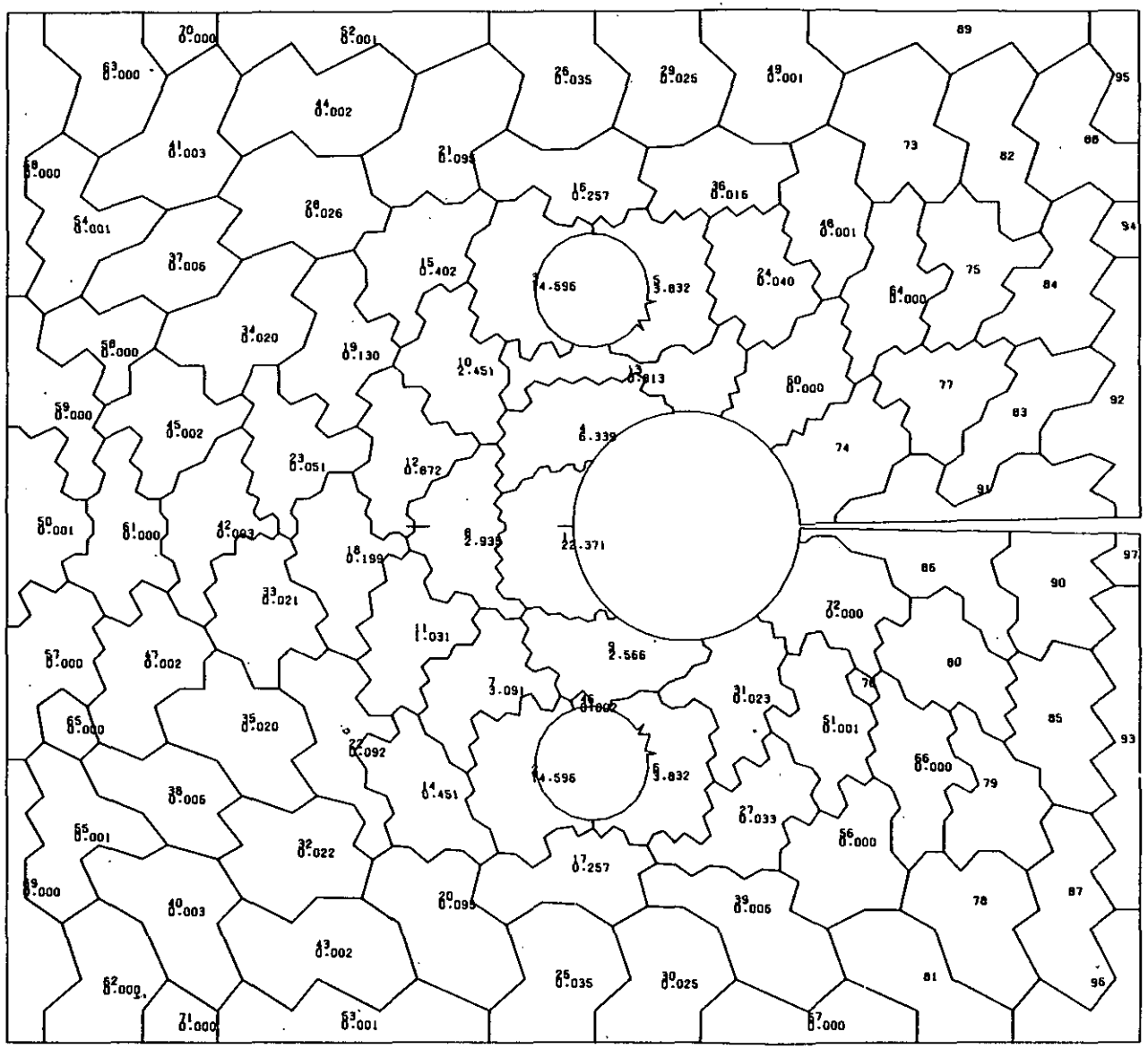

Fig.57: Partitioning into Statistical Cells of Size $\Delta F = 190 mm^2$
Specimen Type IIId $n_{eff} = 9,06$ Graphite Grade M 2190

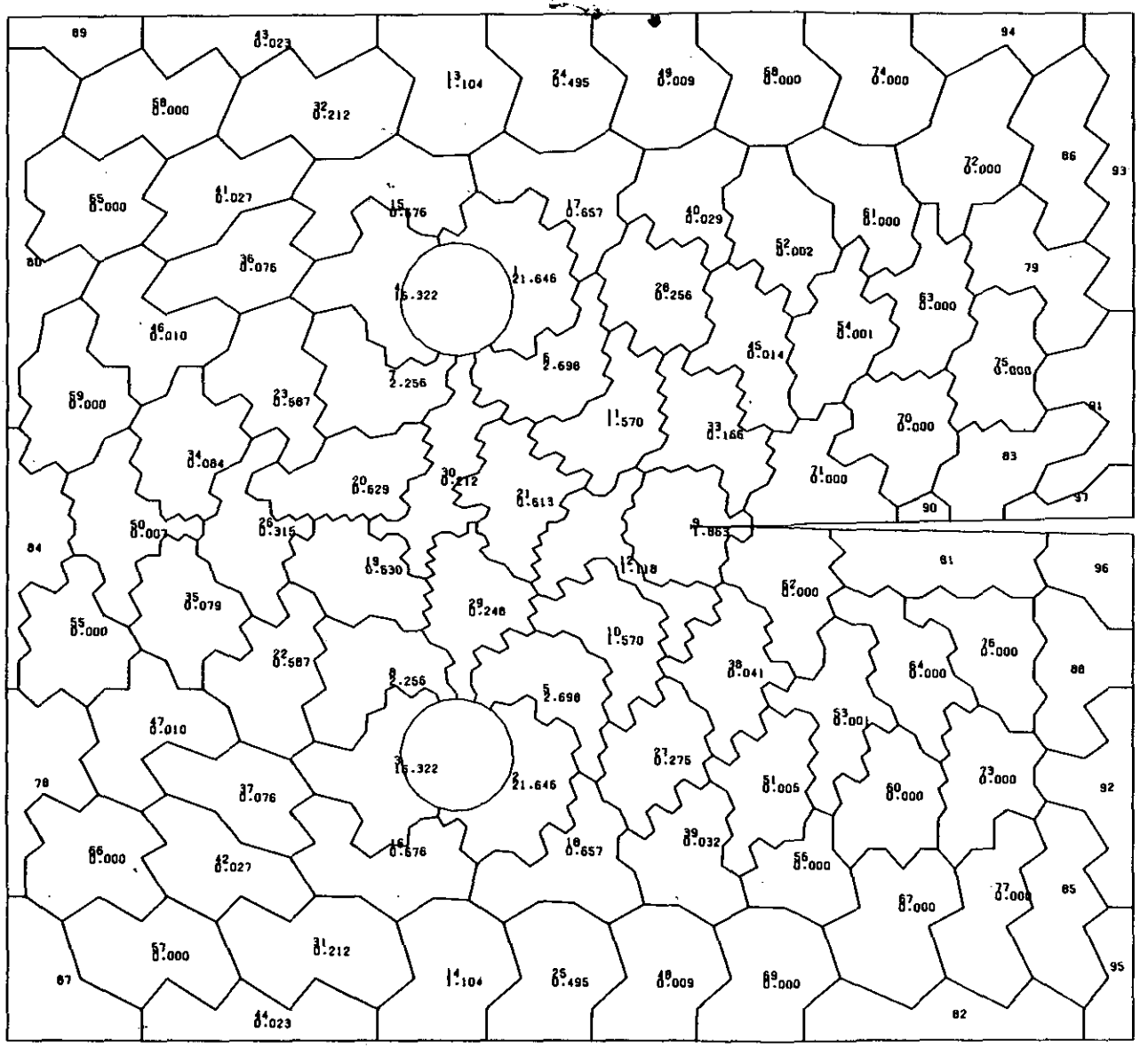

Fig.58: Partitioning into Statistical Cells of Size $\Delta F = 190 mm^2$
Specimen Type IVa $n_{eff} = 15,44$ Graphite Grade M2190

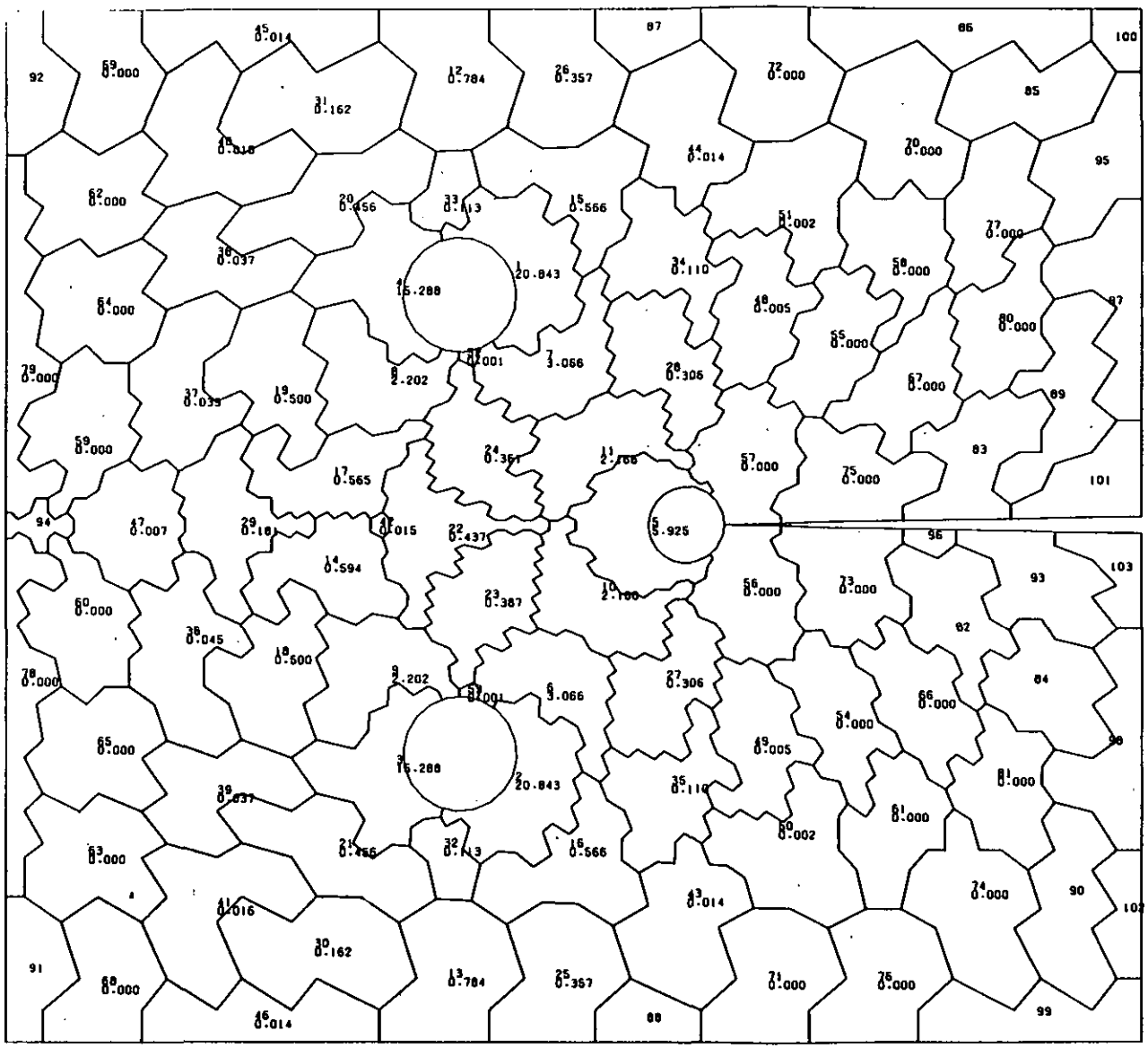

Fig. 59: Partitioning into Statistical Cells of Size $\Delta F = 190\,mm^2$
Specimen Type IVb $n_{eff} = 13.50$ Graphite Grade M 2190

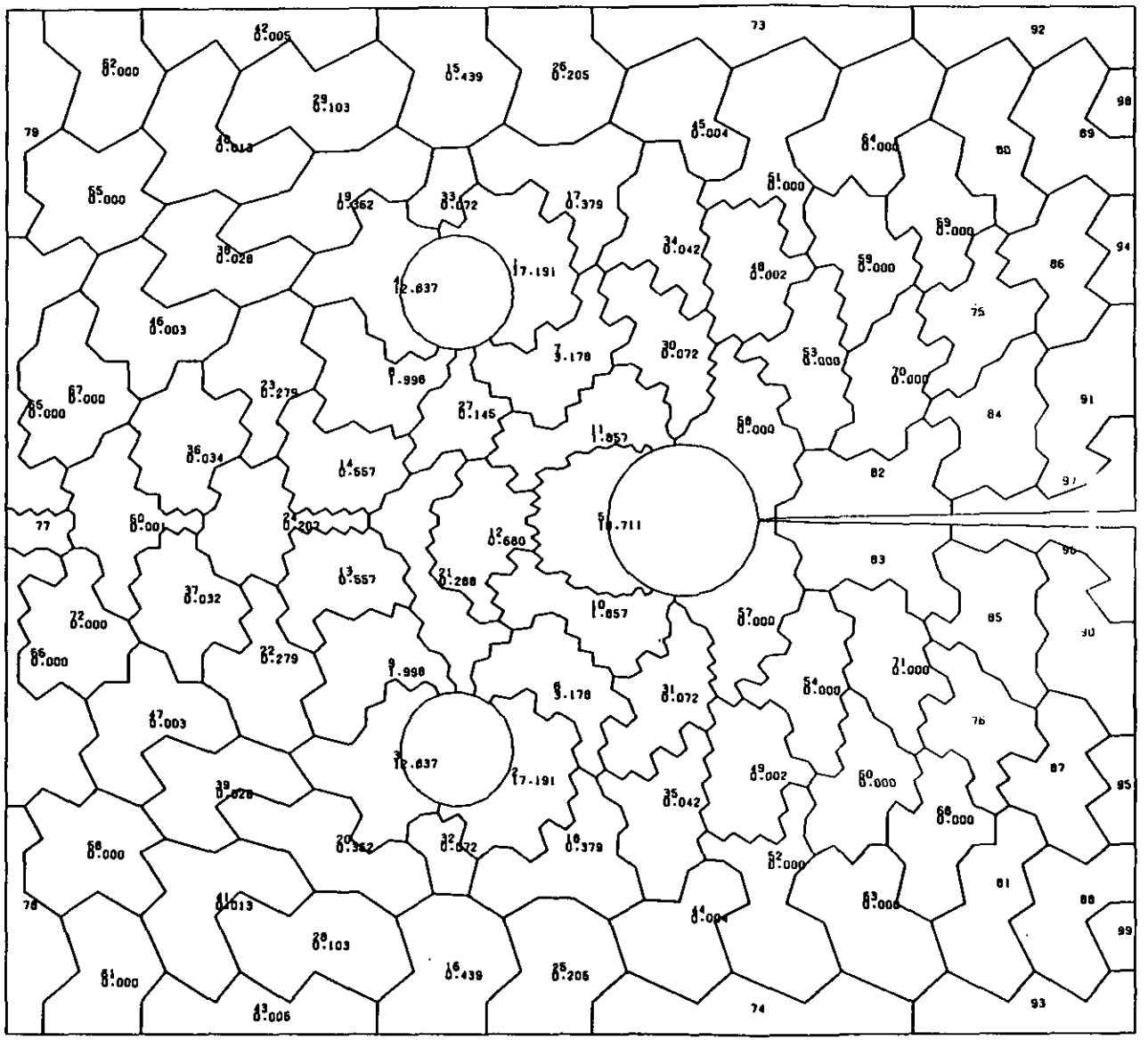

Fig.60: Partitioning into Statistical Cells of Size $\Delta F = 190\,mm^2$
Specimen Type IVc $n_{eff} = 11,18$ Graphite Grade M 2190

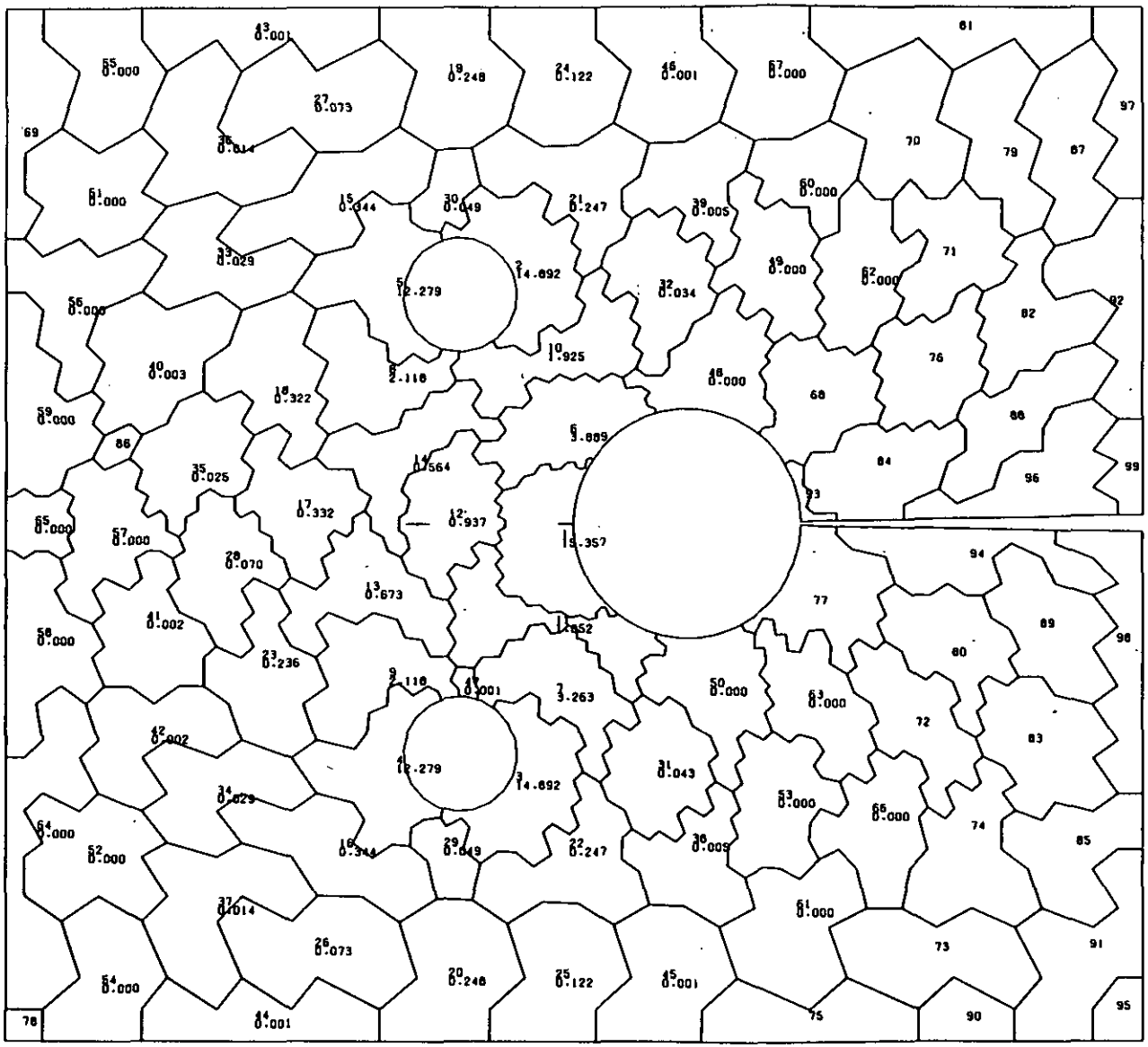

Fig.61: Partitioning into Statistical Cells of Size $\Delta F = 190 mm^2$
Specimen Type IVd $n_{eff} = 10,04$ Graphite Grade M2190

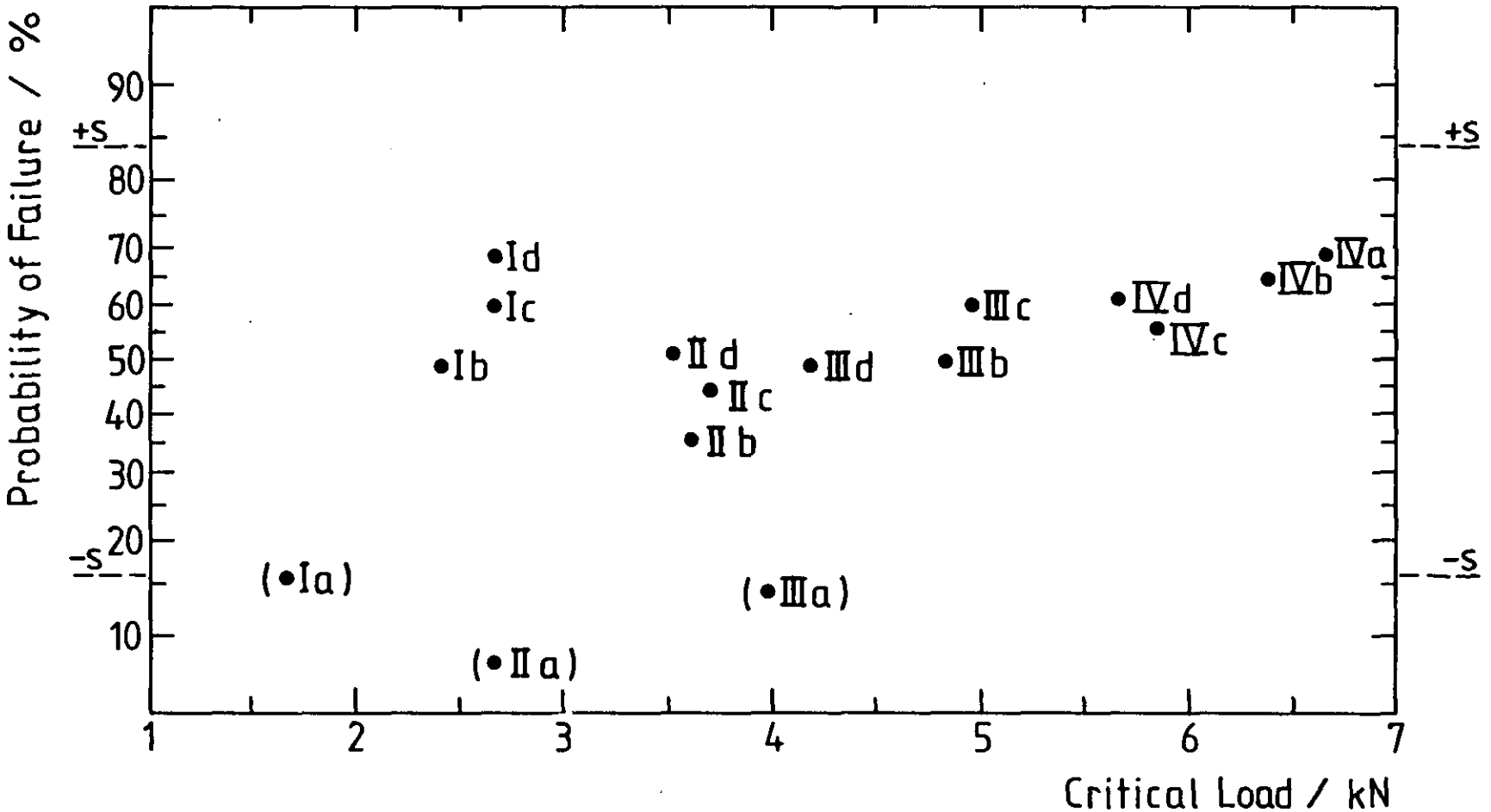

Fig. 62 : Probabilities of Failure Calculated from Experimentally Found Averaged Critical Loads for Graphite Grade V483T

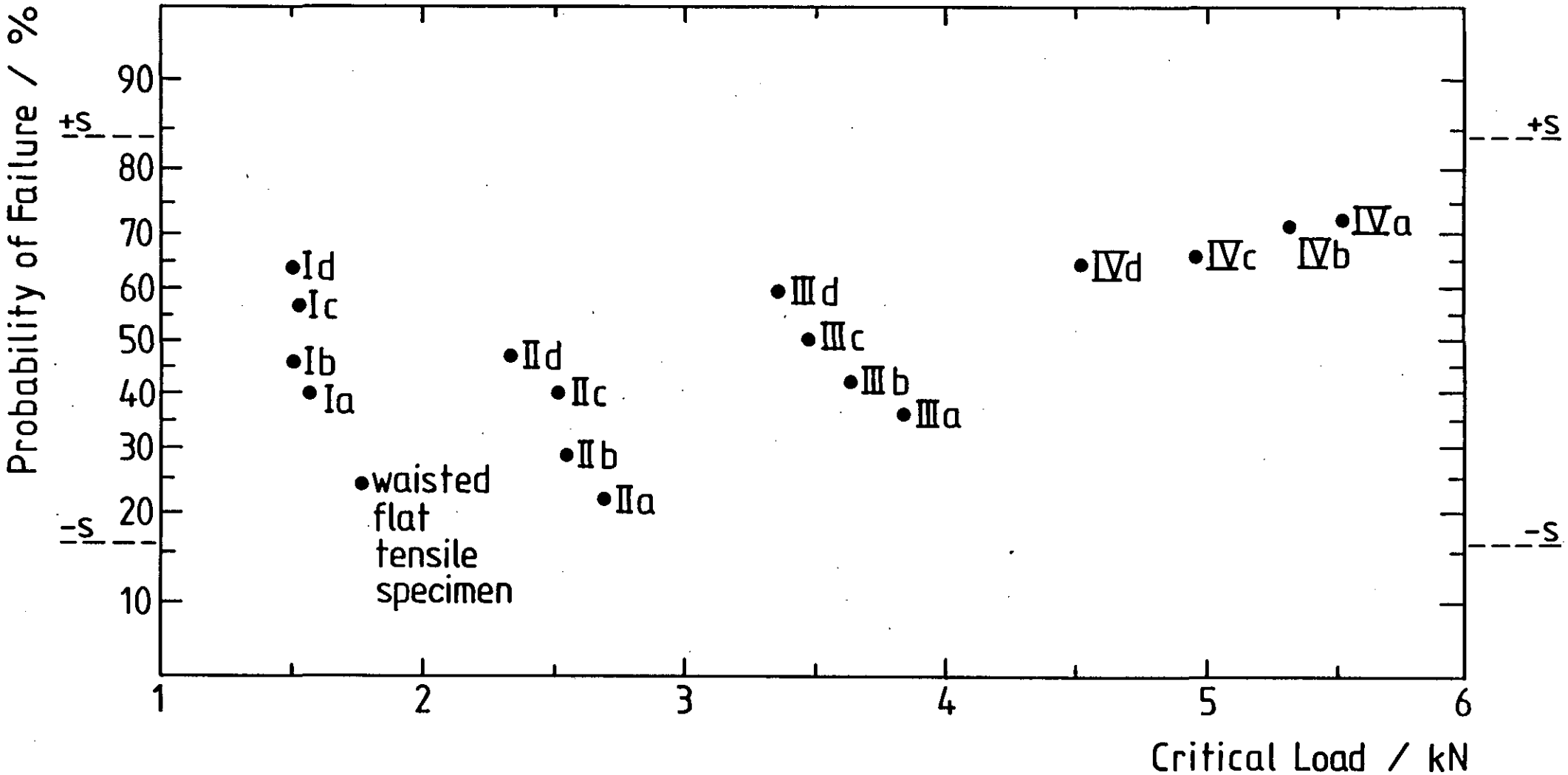

Fig. 63 : Probabilities of Failure Calculated from Experimentally Found Averaged Critical Load for Graphite Grade AS2-F-500

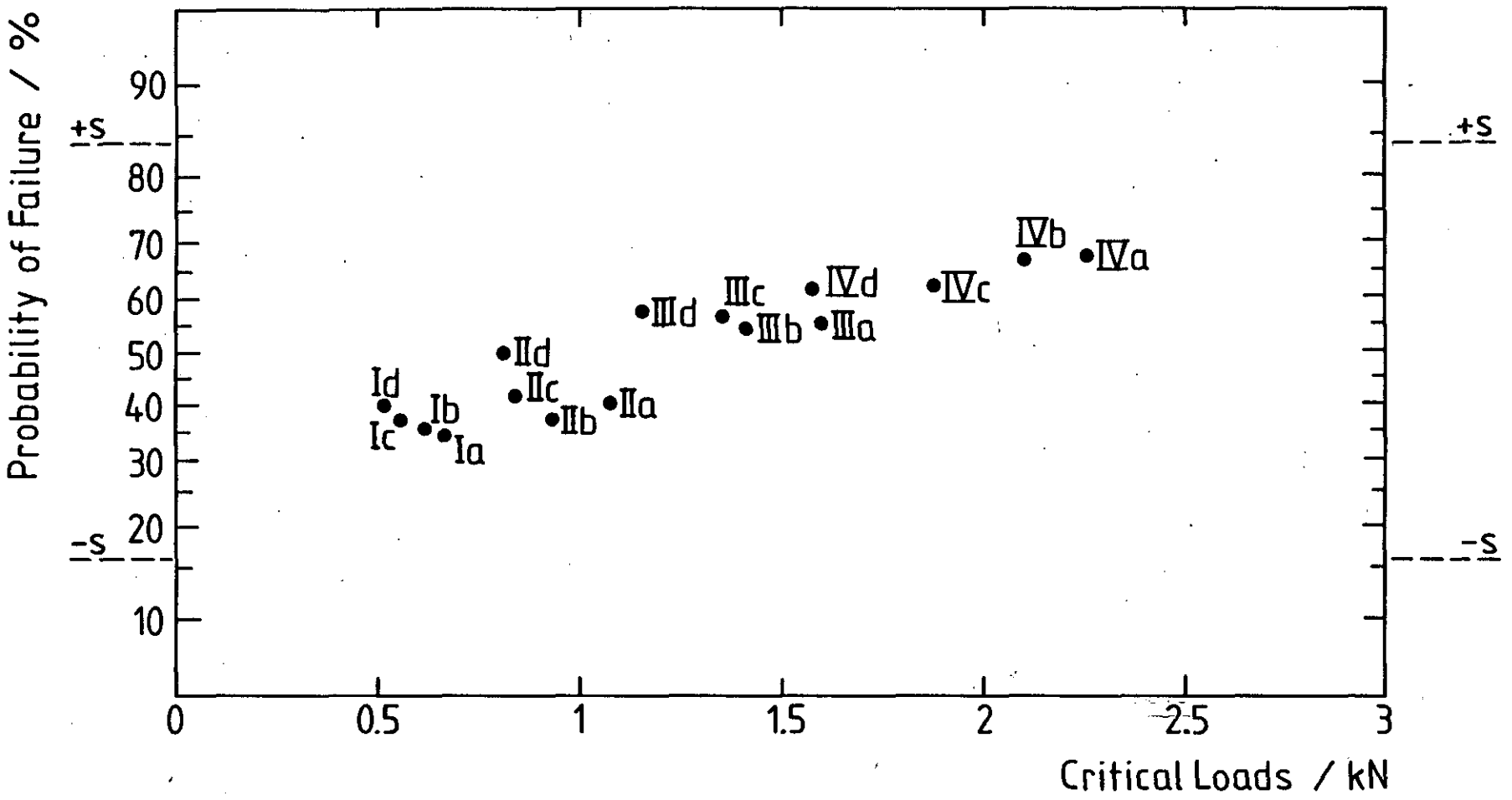

Fig. 64: Probabilities of Failure Calculated from Experimentally Found Averaged Critical Loads for Graphite Grade M 2190